

AN INVESTIGATION OF
COLLISIONLESS PLASMA BEAM INTERACTION
WITH A NONHOMOGENEOUS MAGNETIC FIELD

Thesis by
Peter Hoong-Yee Lee

In Partial Fulfillment of the Requirements
for the Degree of
Doctor of Philosophy

California Institute of Technology
Pasadena, California

1973

(Submitted May 18, 1973)

ACKNOWLEDGMENTS

I would like to express my deepest appreciation to Professor Toshi Kubota for his patient guidance, his continued interest, and the enormous amount of hours of stimulating discussions which he contributed throughout the course of this research.

I would also like to express my appreciation to Dr. Miklos Sajben, now at McDonnell Douglas Corporation, St. Louis, and to Professor Lester Lees for their guidance at the initial phase of this work; and to Professors Hans W. Liepmann and Roy W. Gould for some invaluable suggestions during the course of this work.

I would like to thank the staff of the GALCIT Hypersonic Wind Tunnel, especially Mr. Henry Mazurowski (now retired), and the staff of the Aeronautics Machine Shop for their assistance in the experimental program.

I wish to acknowledge with appreciation the California Institute of Technology who provided me with financial support throughout this endeavor. Acknowledgement is due to the U.S. A. F. Cambridge Research Laboratories who supported the initial part of the experimental program under Contract No. F19628-70-C-0152, and also to Professor Lester Lees who generously provided me with the Alfred P. Sloan Fund for the latter part of the experimental program.

Finally, I would like to thank Mrs. Virginia Conner who did the endless typing of this thesis with patience and skill.

This work is dedicated to my parents, who unselfishly guided me; to all the teachers, who patiently taught and inspired me; and to my wife, Robin, whose loving devotion and constant encouragement made the completion of this task possible.

ABSTRACT

The interaction between a rarefied flowing plasma and an externally imposed nonhomogeneous magnetic field is studied experimentally in a collisionless plasma wind tunnel, where a collisionless plasma beam is directed through a current loop. The collisionless plasma is generated by an electron bombardment engine. Nominal values of ion flow speed, number density, electron temperature and magnetic induction of the loop are $U \sim 10^4$ m/s, $N \sim 5 \times 10^7$ /cc, $kT_e \sim 0.2$ eV and $B \sim 10$ Gauss, respectively.

Due to lack of probe theories in the presence of nonhomogeneous magnetic fields and failure of conventional Langmuir probe methods, a new, simple method of diagnostics is developed. This method employs two probes of different geometry and obtains information on the ion density and flow speed from the ion-saturation region of the probe characteristic.

Radial density profiles in the wake of the current loop mapped by the "two-probe" method indicate annular density "peaks" at certain radial positions.

In order to understand this non-uniform "pinching" process, a theoretical analysis is attempted. It is found that the experimentally observed phenomenon can be qualitatively described by the collisionless two-fluid equations, but turbulent "friction" is required to improve the two-fluid model. A heuristic turbulent model is used, and evidence of turbulence in the flow field is also obtained through measurements of the fluctuating probe currents.

TABLE OF CONTENTS

<u>Part</u>	<u>Title</u>	<u>Page No.</u>
	Acknowledgments	ii
	Abstract	iv
	Table of Contents	v
	List of Figures	ix
	List of Symbols	xii
I.	INTRODUCTION	1
II.	DESCRIPTION OF EXPERIMENTS	6
	1. Test Facilities and Instrumentation	6
	1.1. The Vacuum System	6
	1.2. Plasma Production	7
	1.2.1. The Electron Bombardment Ion Engine	7
	1.2.2. Neutralization of the Ion Beam	9
	2. Instrumentation of Experiments	11
	2.1. The Langmuir Probe	11
	2.1.1. The Conventional Method of Measurement in the Absence of External Magnetic Fields	13
	a. Maxwellian Electrons	13
	b. Non-maxwellian Electrons	18
	2.1.2. Probe Theories in Magnetic Fields	20
	2.1.3. Probe Theories and the Inverse Problem	22
	2.1.4. A Langmuir Probe Method of Density and Velocity Measure- ment of Collisionless Plasma Flows in Non-homogeneous Magnetic Fields	24

Table of Contents (Continued)

<u>Part</u>	<u>Title</u>	<u>Page No.</u>
	2.1.5. Calibration of Probes	27
	a. Thin Sheath	27
	b. Thick Sheath	28
	c. Magnetic Fields	30
	d. The Hybrid Probe	30
	2.2. Model	31
III.	EXPERIMENTAL RESULTS	32
	1. Performance Characteristics of the Plasma Beam Generator	32
	1.1. Effect of the Neutralizer Filament	32
	1.2. The "Optimum" Beam Condition	33
	1.3. Floating Potential	33
	1.4. Effect of Screen Grid	34
	1.5. The Confining Magnetic Field	35
	2. Properties of the Plasma Beam	35
	2.1. General Description	35
	2.2. Source-like Flow	36
	2.3. Beam Spread	37
	2.4. Slow Ions	37
	2.5. Characteristic Length and Time Scales	37
	3. Flow with Magnetic Field	38
	3.1. General Description of the Wake	38
	3.2. Upstream Beam Profiles	39
	3.3. Effects of Magnetic Field Strength	40

Table of Contents (Continued)

<u>Part</u>	<u>Title</u>	<u>Page No.</u>
IV.	THEORETICAL ANALYSIS	42
	1. Preliminaries	43
	2. The Two-Fluid Model	43
	2.1. The Governing Equations	43
	2.2. Assumptions	44
	2.3. System of Reduced Equations	45
	2.4. Nondimensionalization and Further Simplifications	47
	2.5. Results of Computation	49
	3. A Heuristic Model	51
	3.1. A Heuristic Turbulent Two-Fluid Model	51
	3.2. Results of Computation using the "Resistive Dissipation" Model	54
	4. A Posteriori Check on the Turbulent Assumption	56
V.	CONCLUSIONS	58
	APPENDIX A	63
	a. The average speed of Maxwellian particles	
	b. The percentage of Maxwellian particles with energies greater than $\frac{1}{2} kT$	
	APPENDIX B	65
	a. Derivation of the Druyvestyn formula for a flat probe	
	b. The a-c potential perturbation method of Sloane and MacGregor	

Table of Contents (Continued)

<u>Part</u>	<u>Title</u>	<u>Page No.</u>
APPENDIX C		68
	Derivation of the orbital-motion-limited ion current collected by a cylindrical probe	
APPENDIX D		70
	Computation of the Guard Length for the parallel-to-flow collector	
APPENDIX E		73
	Mean free paths and characteristic times of the plasma beam	
APPENDIX F		76
	Discussion of some parameters of the problem	
APPENDIX G		78
	Particle equations of motion	
APPENDIX H		80
	The magnetic field of a circular current loop	
APPENDIX I		82
	Derivation of the turbulent collision term	
APPENDIX J		85
	A posteriori justification of the small R_M assumption	
REFERENCES		87
FIGURES		96

LIST OF FIGURES

<u>Fig. No.</u>	<u>Title</u>	<u>Page No.</u>
2.1	Schematic of the Vacuum System (ref. List of Symbols)	96
2.2	Schematic of the Plasma Source	97
2.3	Schematic of Cathode Filament Holder	98
2.4	Power Circuit Diagram of Plasma Beam Generator	99
2.5	Experimental Configuration and Coordinate System	100
2.6	Schematic of Probe Circuit	
	a. Langmuir Mode - probe characteristic	101
	b. Ion Current Mode - relative measurements	102
2.7	Langmuir Probe Characteristic	103
	a. Characteristic of an idealized plane probe	
	b. Definition of probe currents	
2.8	Schematic of the Probe Potential Field	104
2.9	Ion Current Collection of Langmuir Probes in "Hypersonic" Flowing Plasmas	105
2.10	Comparison of Probe Characteristics in the Thin Sheath Case	106
2.11a	Probe Characteristic of Flat Guarded Probe and Thin Wire Probe ($\phi_{N.F.} = 21V$)	107
2.11b	Thin Wire Probe Ion Current vs. $(\phi_{PL,S} - \phi_{pr})^{\frac{1}{2}}$	108
2.12a	Probe Characteristics of Flat Guarded Probe and Thin Wire Probe ($\phi_{N.F.} = 31V$)	109
2.12b	Thin Wire Probe Ion Current vs. $(\phi_{PL,S} - \phi_{pr})^{\frac{1}{2}}$	110
2.13	Probe Characteristic of Thin Wire Probe for Large Negative Probe Bias	111

List of Figures (Continued)

<u>Fig. No.</u>	<u>Title</u>	<u>Page No.</u>
2.14	Influence of Non-homogeneous Magnetic Field on the Probe Characteristic	112
2.15	The Hybrid Probe	113
2.16	Schematic of the Current Loop	114
2.17	Calibration of Axial Field Strength of Current Loop	115
3.1	Effect of Neutralizer Filament on Probe Characteristic	116
3.2	Condition for "Optimum" Plasma Beam: ($\phi_A - \phi_D \leq \phi_{N.F.}$)	
	a. $\phi_{N.F.} = 21V$	117
	b. $\phi_{N.F.} = 31V$	118
3.3	Effect of Neutralizer Filament Bias on Floating Potential (variable Cathode Filament Current)	119
3.4	Effect of Neutralizer Filament Bias on Floating Potential (variable $\phi_{N.F.}$)	120
3.5	Effect of Source Anode Potential on Beam Ion Current	121
3.6	Axial Field of the Confining Magnet in the Test Section	122
3.7	Radial Profiles of Probe Ion Current	123
3.8	Determination of Effective Origin of Source-like Flow	124
3.9	Source-like Nature of Flow	125
3.10	"Similarity" of Profiles	126
3.11	Effect of Anode Potential on Beam Spread and Blocking Effect of Model	127
3.12	Beam Spread vs. Mach Number	128

List of Figures (Continued)

<u>Fig. No.</u>	<u>Title</u>	<u>Page No.</u>
3.13	Effect of the Magnetic Field on the Wake Profile	129
3.14	Upstream Profiles	130
3.15a	"Pinch" Effect in the Near Wake ($M = 10.35$)	131
3.15b	Position of the Ion Density "peak" ($M = 10.35$)	132
3.16a	"Pinch" Effect in the Near Wake ($M = 9.35$)	133
3.16b	Position of the Ion Density "Peak" ($M = 9.35$)	134
3.17a	"Pinch" Effect in the Near Wake ($M = 8.25$)	135
3.17b	Position of the Ion Density "Peak" ($M = 8.25$)	136
3.18	Wake of a Narrow Beam (no blocking)	137
4.1	Computer Plot of Ion Trajectories (Collisionless Theory)	138
4.2a	Computer Plot of Ion Trajectories ("Resistive Dissipation" Model, F is Constant)	139
4.2b	Computer Plot of Ion Trajectories ("Resistive Dissipation" Model, $F \propto B^2$)	140
4.2c	Computer Plot of Ion Trajectories ("Resistive Dissipation" Model, $F \propto B$)	141
4.3a	Computer Plot of Ion Trajectories ($B_0 = 0$)	142
4.3b	Computer Plot of Ion Current Profiles ($B_0 = 0$, $U = 1.44 \times 10^4$ m/s)	143
4.4	Computer Plot of Ion Current Profiles (based on Fig. 4.2c)	144
4.5	Spectrum of RMS Fluctuating Probe Currents (variable magnetic field)	145
4.6	Spectrum of RMS Fluctuating Probe Currents	146
	a. Variable radial probe position	
	b. Variable axial probe position	

LIST OF SYMBOLS

The following symbols have the general meaning as indicated, unless specifically defined otherwise.

A	area; imposed vector potential of magnetic field
a	induced vector potential of magnetic field
B	imposed magnetic induction
b	induced magnetic induction
c	speed
E	electric field
e	electronic charge (positive number)
F	isotropic speed distribution function; nondimensionalized frequency
f	velocity distribution function
g	relative speed
H	Hall parameter
I	current
J	current density
j	species current density
k	Boltzmann constant
L	length
M	Mach number
m	mass
N	species number density of undisturbed quasineutral plasma
n	species number density
O	order of magnitude

List of Symbols (Continued)

p	pressure
q	species charge
R	coil radius
R_M	magnetic Reynolds number
r	radial distance
S	interaction parameter
T	temperature
t	time
U	nominal axial flow speed
u	velocity, average velocity
V	voltage, peculiar velocity
v	velocity, velocity coordinate
W	peculiar speed
x	space coordinate
Z	axial distance in units of coil radius, also axial distance normalized by coil radius; both have origin at coil plane
z	axial distance from nozzle edge
z_0	position of effective origin (from nozzle edge)
ϵ_0	vacuum permittivity
ζ	distance from effective origin defined as equal to $[(z-z_0)^2 + r^2]^{\frac{1}{2}}$
θ	angle
λ	mean free path (subscripted)
μ	vacuum permeability

List of Symbols (Continued)

ν	collision frequency
ξ	probe size to Debye length ratio
ρ	density
σ	scalar conductivity
τ	characteristic time
Φ	electric potential
φ	azimuthal angle
ω	frequency

Superscripts

'	fluctuating quantity
—	ensemble averaged quantity
·	time derivative
~	dimensionless variable

Subscripts

A	source anode
B	source confining magnet
C. F.	cathode filament
D	discharge (with Φ); Debye (with λ)
e	electrons
fl	floating (with Φ)
G	grid
i	ions
N. F.	neutralizer filament
PL, S	source plasma (with Φ)

List of Symbols (Continued)

pl	plasma (with Φ)
pr	probe (with Φ)
—	vector

Abbreviations (ref. Fig. 2.1)

AGFT	Argon gas feed-through
BV	butterfly valve
C	vacuum chamber
CWFT	cooling water feed-through
DP	diffusion pump
MFT	model feed-through
MIT	miniature ionization tube
MP	mechanical pump
PAFT	probe actuator feed-through
PEFT	probe electrical feed-through
R	refrigeration unit
S	spacer
SEFT	source electrical feed-through
TC	thermocouple gauge
V	valve

I. INTRODUCTION

The purpose of this research is to investigate the flow of rarefied plasmas, in particular the interaction of a collisionless plasma with an externally imposed magnetic field.

The motivation for this work stems from interest in finding a correct model that can adequately predict collisionless plasma flows in the presence of applied magnetic fields in a plasma wind tunnel.

The plasma wind tunnel, a laboratory plasma environment, is a useful apparatus in which experiments can be performed on plasma flows under carefully controlled conditions. On the one hand, it can be used as a simulation device to study space plasma flows and related problems. On the other hand it can be used to study basic problems in plasma dynamics. It is in the latter sense that the investigation has been carried out.

A plasma is described as "collisionless," if collisions, interaction between charged particles in the classical sense, are unimportant. Research on collisionless plasma flows was motivated by the space age. Plasma wind tunnels were constructed to simulate spacecraft motion in the ionospheric plasma, and investigations on streaming plasmas, body-plasma interaction and satellite wakes were performed.⁽¹⁻⁶⁾ Although some approximate analysis on satellite wake structures, which take into account the influence of geomagnetic field have been published,⁽⁷⁻⁹⁾ without exception all collisionless plasma wind tunnel experiments available have been conducted in the absence of an applied magnetic field.*

* Blumenthal⁽⁴⁾ used Helmholtz coils to compensate for the Earth's magnetic field in a localized region; in all the other experiments, the Earth's magnetic field effect was simply neglected.

The present work is an attempt to examine a specific configuration of collisionless plasma flow with applied magnetic fields. It concerns itself with the execution of an experimental program by means of which the interaction (i. e. magnetic field effects on plasma flow) can be observed, and the formulation of a physical model which will explain and predict such interaction. If the latter objective can be satisfactorily achieved, besides gaining some insight into a better understanding of collisionless plasmas, it will establish the dimensionless parameters of this class of problems, and it would lead to important scaling laws which would be of value in designing future laboratory experiments.

In the present investigation some exploratory experiments were performed by applying a magnetic field to the flow of a collisionless plasma in a plasma wind tunnel. Due to the axially symmetric nature of the plasma beam, the simplest experimental configuration involving magnetic fields would be axisymmetric flow through a circular current loop.

Several papers⁽¹⁰⁻¹³⁾ investigating this type of plasma-magnetic-field configuration have been published. However, the type of plasma production devices used in the experimental programs consisted of a pinch tube,⁽¹⁰⁾ coax plasma gun⁽¹¹⁾ and arc jets.^(12, 13) The plasmas produced by these devices have some common characteristics:

i) The charge particle number density is relatively high ($N = 10^{13}/\text{cc} \sim 10^{15}/\text{cc}$). Although one speaks of a "low density" plasma, the plasma gas is still collision dominated.

ii) Because the ionization and acceleration of the plasma are achieved through electrothermal means, the ions and electrons have temperatures of the same order.

iii) Because of the low degree of ionization, collisions between charged particles and neutral atoms are usually not negligible. As a consequence of the ion-neutral momentum transfer collisions, the flow of the neutral background gas is usually important.

Theoretical investigations^(12, 14) using the one-fluid model with generalized Ohm's law were carried out under the assumptions of small magnetic Reynolds number, small interaction parameter, small Hall parameter, and no "slip" between ions and neutrals.

In a collisionless plasma wind tunnel, the plasma is usually produced by an electron bombardment ion engine provided with electron neutralization of the ion beam. The charged particle number density is characteristically low, $N = 10^5/\text{cc} \sim 10^9/\text{cc}$, depending on specific ion source and vacuum pumping facilities. The plasma is "collisionless" in the sense that all the collisional mean free paths are long compared to the tunnel dimension or some other characteristic length of the experiment. Another feature of the electron-bombardment-ion-engine produced plasma is that the electron temperature is usually much higher than the ion temperature. Thus the assumption of "monoenergetic ions and thermal electrons" is an often used simplification.

The nominal values of ion density, ion mean speed, electron temperature and magnetic field in the present experiment are:

$N \sim 5 \times 10^7/\text{cc}$, $U \sim 10^4 \text{ m/s}$, $kT_e \sim 0.2 \text{ eV}$, and $B \sim 10 \text{ Gauss}$.

The test facilities, which include the vacuum system, the plasma production apparatus and the instrumentation of the experiment, are described in Chapter II. Because of the limitations of conventional Langmuir probe diagnostic methods as well as the lack of probe theories in the presence of non-homogeneous magnetic fields, a simple "two-probe" method is henceforth developed to measure ion density and current in a way that circumvents the difficulties of conventional diagnostic methods as well as the complications introduced by a non-homogeneous magnetic field.

The experimental results are contained in Chapter III. The performance characteristics of the plasma source are thoroughly studied, and a standard plasma beam is established as a basis for comparison for the case when magnetic field is applied. The result of a strong interaction can be observed from the fact that the radial profiles of ion current collected by the Langmuir probes display distinct peaks at certain radial positions.

In Chapter IV a theoretical analysis is attempted in order to find a model that can adequately describe the observed phenomena as well as provide us with some further understanding of rarefied plasma flows. With certain assumptions based on physical arguments, the collisionless two-fluid model can provide us with a first-order approximation that can qualitatively describe the experimental observations. It is found that turbulence, hypothesized to result from electron-ion two stream instability, is required to improve the two-fluid model. Although evidence of turbulence is observed in the flow field, the lack of basic understanding limits the use of it to a simple

heuristic model. The turbulence model being used is based on elementary physical arguments, and it is applied in the same spirit as the Prandtl mixing length assumption is used in the turbulence of ordinary fluids.

Chapter V contains a summary of the results of the present investigation, with some discussions and concluding remarks, as well as several suggestions for future research which might resolve the questions raised by the present investigation.

II. DESCRIPTION OF EXPERIMENTS

II.1 Test Facilities and Instrumentation

The plasma wind tunnel is a steady-state flow facility which consists of a vacuum chamber in which a plasma generating source operates, and instrumentation by which the proper functioning of the plasma wind tunnel is controlled or monitored.

II.1.1 The Vacuum System

The stainless steel 50 cm inner diameter vacuum chamber consists of three separate sections (Fig. 2.1) which are bolted together and vacuum-sealed by O-rings.

The first section, hence referred to as C1, houses the plasma production device. C1 is mounted on casters and can easily be moved for plasma engine servicing or to provide access to the second section.

The second section, C2, is the meter long test section. On the top of the test section there are ports for inserting models, fixed probes and ionization tube. On the sides, there are two 6-inch diameter ports and a 1.75-inch diameter port. The larger ports have been used for high electric current feedthroughs and connection to a small diffusion pump. The smaller port is connected to a Welch duo-seal mechanical pump (Model 1397). This is used as a roughing pump and produces an ultimate pressure of 10^{-3} torr.

The third section, C3, is a T-section to which the main vacuum pumps are connected. The main component of the pumping system is an Edwards F1605, 16-inch five stage diffusion pump on which is set an Edwards 16-inch chevron baffle which is cooled by a

Tecumsek (Model No. CAT4CHTK) freon refrigeration unit. A 16-inch stainless steel spacer is set on the chevron baffle on which is set an Edwards 16-inch QSB16 high vacuum quarter swing butterfly valve. The butterfly valve can disconnect the vacuum chamber from the diffusion pump by a quarter swing of a lever. An Edwards ISC 1500 Rotary Piston Vacuum Pump serves as the backing pump of the system, it has a nominal speed of 1415 liters per minute and produces an ultimate vacuum of better than 10^{-2} torr. The diffusion pump has a nominal baffled speed of 3000 liters per second and produces an ultimate vacuum of 10^{-7} torr.

The equipment used for pressure measurements of the vacuum system consists of a CVC Type GIC-110A Ionization Vacuum Gauge which is connected to two CVC Cat. GTC-004 thermocouple gauge tubes for pressure measurements above 10^{-3} torr, and also connected to a CVC GIC-028 miniature ionization tube for pressures below 10^{-3} torr. The locations of the tubes are shown in Fig. 2.1.

II. 1. 2 Plasma Production

The plasma beam is produced by extraction and electrostatic acceleration of argon ions from a plasma source. The ion stream emerging from the source can be neutralized either by an external thermionic emitter immersed in a stream, or by high energy electrons escaping from the source.

II. 1. 2. 1 The Electron Bombardment Ion Engine

The plasma source used in this experiment is a modified version of what is usually known as a Kaufman⁽¹⁵⁾ engine. Variations of this type of ion engine have been used by several authors⁽³⁻⁶⁾ in

collisionless plasma wind tunnel work.

The working principle of this plasma source derives essentially from the classical magnetron discharge. Electrons, emitted by a thermal filament (cathode) at the center of the ionization chamber, are accelerated toward a concentric cylindrical anode, but are prevented from reaching it directly by an externally applied magnetic field, which causes them to spiral axially in the chamber until they collide with a neutral atom. Depending on the collision cross sections of the neutral atom, and the electron energy distribution, some of these collisions produce electron-ion pairs (ionization by electron bombardment!), which themselves may participate in subsequent collisions. The extraction and acceleration of ions is effected by two grids, a screen grid and an ion grid, placed at one end of the ionization chamber. The screen grid and the other end of the chamber wall is kept at cathode potential to prevent axial loss of electrons from the discharge region. Ions which wander close to the screen grid are preferentially extracted and accelerated through the ion grid, which is usually biased at a potential lower than the cathode.

The plasma source of the present experiment is a modification of the plasma source originally built by Blumenthal.⁽⁴⁾ The construction is shown schematically in Fig. 2.2. The ionization chamber is a 22 cm long thin walled (4.75 mm) cylinder with a 25 cm outer diameter. On one end wall of the ionization chamber is a brass cathode filament holder (Fig. 2.3) which supports the electron emitting thermal filaments. On the other end there is a thin (2 mm) circular plate with a 2.5 cm diameter hole at the center. This plate is

fastened on to the ionization chamber by four screws, so that it is easily removed to provide access to the cathode holder. A nozzle is attached over the 2.5 cm diameter hole. This nozzle supports the screen grid, the ion grid, and the neutralizer filament. The nozzle is machined out of Mykroy^{*}. Inside the ionization chamber, a 21.5 cm diameter cylindrical anode is supported from the chamber walls by insulating ceramic spacers. All the cylinders and end walls mentioned above are made of stainless steel, and the grids are cut out of fine mesh (0.186 mm spacing) stainless steel screen. Tungsten wires of 0.25 mm diameter are used for the cathode and neutralizer filaments. The confining magnetic field is produced by two coils of gauge 10 anodized aluminum wire wound around anodized aluminum mandrils which are attached outside the ionization chamber. The ionization chamber is supported from a back plate by ceramic spacers and fastened in place by copper strips which are tightened by turn-buckles. The back plate is securely bolted to the end wall of C1, where all the electric, cooling water and argon gas feedthroughs are located.

II.1.2.2 Neutralization of the Ion Beam

If no provision for neutralization of the ion beam were made, the ion engine would acquire a negative potential at a rate proportional to the emitted ion current and inversely proportional to the capacitance of the ion engine. This charging up of the ion engine

* Mykroy is a glass-bonded mica material classified as a ceramoplastic. It has the qualities of being a machineable insulator, non-outgassing, non-magnetic, and arc resistant.

would eventually stall the beam. Also, the positive space charge potentials within the unneutralized ion beam would cause the beam to reflect upon itself, ^(16, 17) and in a more picturesque description, eventually "explode".

In lab experiments, ion engines are kept at fixed potential relative to ground, hence the beam stalling problem usually does not arise. It is mainly for the sake of obtaining a plasma beam rather than an ion beam, or the fear of an ion beam reflecting upon itself, that neutralization is applied.

In the present case, neutralization is achieved by the thermionic emitter immersed in a beam: the neutralizer filament, a thin tungsten wire, is strung across the diameter of the Mykroy nozzle opening. The typical situation that ensues from such a setup is that while the ion engine emits a beam of ions with little spread in velocity in comparison to their directed motion the thermionic emitter (i. e. neutralizer filament) liberates electrons with a broad distribution of velocities and a mean speed much higher than that of the ion beam. The neutralizer filament is biased positive relative to the ion grid so that thermally emitted electrons do not migrate upstream into the ionization chamber, but are retained in the stream. This mode of operation results in a plasma beam with electron temperature of the order of the neutralizer filament temperature ($T_e \sim 2000-3000^\circ\text{K}$).

A method first used by Hester and Sonin ⁽⁵⁾ to obtain higher electron temperatures in the plasma beam is to draw the electrons from the ionization chamber itself. In this mode of operation, the neutralizer filament is not used, but the source cathode potential is

biased slightly negative with respect to the ion grid so that electrons would escape out of the ionization chamber and hence neutralize the ion beam. The power circuit diagram of the plasma beam generator is shown in Fig. 2.4.

II.2 Instrumentation of Experiments

The electrostatic plasma probe, commonly known as the Langmuir probe, is used as the diagnostic tool for the present experiment. The probe is mounted on a phone plug and is inserted into the socket of the probe actuator, which can move the probe axially, radially, and azimuthally. Fig. 2.5 shows the experimental configuration and the coordinate system. The probe actuator has two sockets and is wired to accommodate at least two probes, so that a comparison of probe characteristics of different types of probes can be made under the same plasma flow conditions. Except for the azimuthal movement of the probe actuator, which requires manual cranking, both the axial and radial motions are powered by electric motors.

The model used in the experiment is a current loop. This loop is located 23.5 cm downstream of the Mykroy nozzle and placed in the plasma beam such that the axis of the loop coincides with the centerline of the plasma beam.

II.2.1 The Langmuir Probe

The electrostatic plasma probe is a piece of metallic electrode, which is immersed in a plasma. The probe is connected across a variable DC power supply to a reference (usually grounded) electrode. The probe circuit is shown schematically in Fig. 2.6. The current flowing to the probe is measured as a function of the applied probe

potential; this current to voltage relation is called the probe "characteristic". Under certain conditions, the plasma parameters, i. e. electron density, electron temperature and plasma potential, can be deduced from the probe characteristic.

Compared to other plasma diagnostic methods such as microwave and spectroscopic techniques, the electrostatic plasma probe is experimentally the simplest to use. It also has the distinct advantage over other plasma diagnostic techniques of being able to make local measurements. Almost all other techniques give information (of plasma parameters) which is averaged over a large volume of plasma*.

In the following the conventional method of obtaining the plasma parameters from the probe characteristic will be briefly reviewed. The objective is to examine the conditions under which the conventional method of measurement is still applicable. The various theories of Langmuir probes will not be described here, since they may be referred to in the original papers by Langmuir and his co-workers,⁽¹⁹⁾ and in the review articles by De Leeuw,⁽²⁰⁾ Chen,⁽²¹⁾ and Schott,⁽²²⁾ A new, simple method is derived to measure plasma parameters when the conventional method fails.

* With the advent of high-intensity lasers, light scattering experiments of plasmas are possible (ref. 18). The 90-degree scattering technique offers a method of measurement with high spatial resolution, since the size of the volume in which the information is averaged is equal to the intersection of the incident and scattered beams.

II. 2. 1. 1 The Conventional Method of Measurement in the
Absence of Magnetic Fields

a. Maxwellian Electrons

For the sake of simplicity, we consider the characteristic of an idealized plane probe (Fig. 2. 7a). Following normal convention, the electron current will be plotted positive on a probe characteristic, and the ion current will be plotted negative (Fig. 2. 7b). When the probe is biased positive beyond the plasma potential (ϕ_{pl}), the region is called the electron-sheathed operation region or the region of saturation electron current (A). If the probe is biased negative relative to the plasma potential, the electrons are collected in a repelling electric field, and the electron current falls off as the probe potential decreases. This is called the retarding-field region (B). Finally, when the probe potential is biased so negative such that all the electrons are repelled, one obtains the ion-sheathed operation region, or the region of ion saturation current (C).

If the electrons are in thermal equilibrium, the electron velocity distribution function is Maxwellian, then the electron density in the retarding-field region is governed by the Boltzmann's law:

$$n_e = N \exp \left[\frac{-e(\phi_{pl} - \phi_{pr})}{k T_e} \right] \quad (1)$$

where N is the electron number density in the undisturbed, quasineutral plasma. The electron current density flowing to the probe is then the random electron current density:

$$\begin{aligned}
 j_e &= \frac{1}{4} n_e e \bar{c} \\
 &= \frac{1}{4} e \bar{c} N \exp \left[\frac{-e(\phi_{pl} - \phi_{pr})}{k T_e} \right]
 \end{aligned} \tag{2}$$

where $\bar{c} = (8kT_e/\pi m_e)^{\frac{1}{2}}$ is the average speed of the electron (see Appendix A). Equation (2) is exact if the plasma has no mean motion relative to the probe collector surface: otherwise, the mean motion would contribute an extra term to the electron current density besides the random current. In most cases, however, the mean motion of the plasma (hence the electrons) U is much smaller than the electron average speed \bar{c} so that equation (2) is usually a very good approximation.

The electron temperature is measured in the following way: assuming that the plasma potential is constant (which is usually true), then taking the logarithm of equation (2) and differentiating with respect to the probe potential ϕ_{pr} , we obtain in the transition region (i. e. $\phi_{pr} < \phi_{pl}$):

$$\frac{d \ln j_e}{d \phi_{pr}} = \frac{e}{k T_e} \tag{3}$$

It is obvious from equation (3) that the slope of a ϕ_{pr} versus $\ln j_e$ plot will yield the electron temperature T_e . If the plasma potential ϕ_{pl} can be found from the probe characteristic, then with T_e and ϕ_{pl} known, we can find the electron density N from equation (2). Hence all the plasma parameters are found.

In order to measure the plasma potential directly, the probe has to be biased to the extent that saturation of electron current occurs. Depending on probe geometry and the ratio of sheath

thickness to probe size, the region of saturation electron current is not always flat⁽²¹⁾ (i. e. j_e still grows with Φ_{pr}), hence the location of the "knee" (i. e. the bend between regions B and A on the probe characteristic) is often quite ambiguous. Therefore, this is not a very accurate method of measuring the plasma potential. The greatest objection in using this method, however, is due to the fact that when the probe is biased above the plasma potential, too many electrons are depleted from the plasma, hence the plasma is essentially disturbed. In a plasma without mean motion, the theoretical value of the ratio of electron saturation current to the ion saturation current is of the order of the square root of the ratio of ion mass to electron mass; for an argon plasma, this ratio is 271. If the plasma is flowing at "hypersonic" speeds (i. e. $U \gg (kT_e/m_i)^{1/2}$, but $U \ll (kT_e/m_e)^{1/2}$), the plasma will be essentially disturbed if too many charged particles of one species are depleted from the plasma. To set a criterion, one compares the current collected by the probe (I) to the current that would ideally be swept up by the probe if only one species were present (i. e. $I_{ideal} = N_0 |e| UA$). An arbitrary upper limit (ten or fifty, say) is then set for this ratio I/I_{ideal} , beyond which the plasma is considered to be essentially disturbed.

It is clear from the above mentioned reasons, that region A of the probe characteristic is seldom used in experimental work. In most cases, even the higher portion of region B (near the plasma potential) has to be avoided.

In order to find the plasma potential from the probe characteristic without biasing the probe past the "knee" into region A, a

commonly used method is to evaluate the plasma potential from the floating potential (ϕ_{fl}) and the electron temperature. This method is based on the fact that, in a stationary plasma of thermal electrons and cold ions, the ions must stream into the sheath boundary with an energy greater than $\frac{1}{2}kT_e$. This is known as the sheath criterion originally discovered by Tonks and Langmuir.^(19c) Refined analysis of Langmuir's results was first carried out by Bohm⁽²³⁾ who found that a minimum ion energy is required for the formation of an ion sheath. Bohm's analysis was extended by Allen, Boyd and Reynolds.⁽²⁴⁾ In both investigations, the method of approximation used a sheath edge. Bernstein and Rabinowitz⁽²⁵⁾ progressed further by reformulating the problem and performing a detailed analysis of the orbits of the attracted particles about the probe; their method was completely self-consistent and required no a priori separation of the plasma into quasineutral and sheath regions. Extensions of Bernstein and Rabinowitz' work were carried out by Lam,⁽²⁶⁾ who performed an asymptotic analysis in the limit of large probe size to Debye length ratio (i. e. $\xi \gg 1$) and assuming mono-energetic ions, and by Laframboise,⁽²⁷⁾ who carried out extensive numerical calculations for a wide variety of probe size to Debye length ratios and poly-energetic, Maxwellian ions. Although in modern probe theories,⁽²⁵⁻²⁷⁾ the ion current was found to be dependent not only on the electron temperature, but also on the ion temperature and the probe potential, all modern approaches prove the qualitative validity of Langmuir and Bohm's sheath criterion.

To understand the physics of the sheath criterion, we consider a probe biased negative relative to plasma potential. Let $V = \phi_{pr} - \phi_{pl}$ denote the relative probe potential. Under the action of the probe electric field, ions will be accelerated toward the probe and electrons will be repelled. For a given temperature of the repelled particles, electrons in this case, the majority of the particles has kinetic energy larger than $\frac{1}{2} kT_e$ (see Appendix A). Therefore, in the "pre-sheath" of the probe potential field where $|V| < \frac{1}{2} \frac{kT_e}{e}$, quasineutrality can still be approximately maintained while the ions are being accelerated and gain kinetic energy. When $|V|$ increases beyond $\frac{1}{2} \frac{kT_e}{e}$, the number of repelled particles will decrease sharply such that charge neutrality is destroyed and an ion sheath is formed. The position where $|V| = \frac{1}{2} \frac{kT_e}{e}$ is interpreted as the sheath edge. In the limit of a very thin sheath (i. e. $\xi \rightarrow \infty$), ions enter the sheath with a kinetic energy of $\frac{1}{2} kT_e$, hence the velocity with which they hit the probe is of order $(kT_e/2m_i)^{\frac{1}{2}}$. A probe potential field with sheath formation is shown schematically in Fig. 2.8.

We will consider a simple example of how the plasma potential is obtained from the floating potential and the electron temperature by using the sheath criterion. Assume that the plasma has no mean motion, the electrons are Maxwellian and the ions are cold. We will use, for the sake of demonstration, the most widely used formula for ion current given by Allen, Boyd and Reynolds:

$$I_i = 0.61 (kT_e/m_i)^{\frac{1}{2}} \quad (4)$$

Note that the ion current is independent of the probe voltage; this

result is a consequence of using the approximation of a sheath edge.

By definition, the floating potential is the probe voltage biased such that the ion current is just equal to the electron current, so that no net current is collected by the probe. Therefore, at the floating potential ϕ_{fl} , we obtain from $I_i = I_e$:

$$0.61 \left(\frac{kT_e}{m_i} \right)^{\frac{1}{2}} = \frac{1}{4} \left(\frac{8kT_e}{m_e} \right)^{\frac{1}{2}} \exp \left[\frac{-e(\phi_{pl} - \phi_{fl})}{kT_e} \right] \quad (5)$$

Taking the logarithm of (5), we obtain, for an argon plasma (i. e. $(m_i/m_e)^{\frac{1}{2}} = 271$):

$$\phi_{pl} = \phi_{fl} + 5.07 \frac{kT_e}{e} \quad (6)$$

In summarizing this section, we point out the fact that in all known probe theories, the electron velocity distribution function is assumed to be Maxwellian. This is therefore the one and only stringent condition under which conventional method of measurement is applicable. Next we note the fact that conventional method of measurement uses the retarding field region and the ion saturation region of the probe characteristic.

b. Non-Maxwellian Electrons

If the electron velocity distribution function is not Maxwellian, none of the Langmuir probe theories are valid, hence the common methods of extracting information of plasma parameters from probe characteristics cease to be useful. This fact was first noted by Druyvesteyn⁽²⁸⁾ in 1930. Consequently, he devised a method to extend the usefulness of Langmuir probes in the case of non-Maxwellian electrons.

Druyvesteyn developed a theory which showed that for planar, cylindrical, and spherical probes, the electron speed distribution function could be obtained from the probe characteristic as follows (see Appendix B. a):

$$F(w) = \frac{4 m_e V}{A e^2} \frac{d^2 I_e}{dV^2} \quad (7)$$

where $F(w)$ is the isotropic speed distribution function (see Appendix A), V is the probe potential relative to plasma, A is the collector area and I_e the probe electron current.

An ingenious technique was devised by Sloane and MacGregor⁽²⁹⁾ in 1934 to circumvent the inherent unreliability of graphical differentiation of the probe characteristic. This method involved superimposing a small a-c voltage on the d-c probe potential, which causes the d-c probe current to increase by an amount which is proportional to the second derivative of the probe characteristic (see Appendix B. b):

$$I_p = I(V) + \frac{V_o^2}{4} \frac{d^2 I_e}{dV^2} \quad (8)$$

where I_p is the d-c probe current with a-c voltage imposed on the d-c probe potential, $I(V)$ is the probe current without a-c voltage perturbation and V_o is the magnitude of the perturbing a-c voltage.

The Druyvesteyn method with some extensions, and variations of the Sloane and MacGregor technique have been used in many experiments.

It has been shown by many investigators,⁽³⁰⁻³⁸⁾ that the electron velocity distribution function, particularly in low pressure plasmas, is commonly not only far from being Maxwellian, but quite

often, not even isotropic.

Although Druyvesteyn's method is an essential progress in probe theory, one should note the following inadequacies:

- i) Since $F(w)$ depends on V (equation 7), the inaccurate determination of the plasma potential (ϕ_{pl}) will shift the $F(w)$ curve in velocity.
- ii) The probe measures total current, hence the ion current has to be subtracted in order to obtain the electron current. If the ion current does not saturate, then the behavior of ion current with respect to probe voltage has to be known a priori in order to use equation (7) correctly.

II. 2. 1. 2 Probe Theories in Magnetic Fields

The presence of a magnetic field modifies the motion of the charged particles, especially in the electric field of the probe. Two main difficulties follow as a consequence:

- i) The presence of \underline{B} introduces an anisotropy in space, hence the problem becomes at least two-dimensional; partial differential equations replace ordinary differential equations.
- (ii) Because only collisions can produce diffusion across lines of force, there is essentially no "collisionless" theory in case $B \neq 0$, even if the plasma is not collision-dominated.

Therefore, it is hardly surprising that very few papers have been published on probe theory when a magnetic field is present. This is in stark contrast to the enormous amount of literature published on probe theory for the case $B = 0$.

In 1936, Spiwak and Reichrudel⁽³⁹⁾ investigated the collection of electrons in a weak magnetic field with cylindrical probes.

One unrealistic assumption of their theory is that the magnetic field beyond a certain radius was set to zero and the velocity distribution at this boundary was assumed known. This is, of course, a different form of the sheath edge approximation.

Bickerton and von Engel⁽⁴⁰⁾ considered the problem of plane probes parallel to \underline{B} using the sheath edge approximation (in the Langmuir sense). The plane was considered infinite so as to avoid the two dimensional difficulty. Bertotti⁽⁴¹⁾ considered the plane probe perpendicular to \underline{B} . He reduced the problem to a one-dimensional one by assuming an unspecified anomalous diffusion process and considered collection only along \underline{B} . His results are in contradiction with all available experimental results.

Prior to Bickerton and von Engel, and Bertotti, Bohm, Burhop and Massey⁽⁴²⁾ developed a satisfactory analysis of probe theory in magnetic fields by establishing transverse and longitudinal fluxes using macroscopic equations. They found in qualitative agreement with experiments a decrease of probe current in the transition region (of the probe characteristic) with increasing \underline{B} . They also observed the effect of magnetic field orientation on the electron current collected by the probe.

Sanmartin⁽⁴³⁾ made significant progress by performing an asymptotic analysis of the Langmuir probe in a strong magnetic field for the probe radius much larger than electron cyclotron radius and Debye length but not larger than either ion cyclotron radius or mean free path. He assumed that both ion and electron species were Maxwellian in the undisturbed plasma and have nearly equal temperatures.

He found that the electric potential, which is not confined to a sheath, controls the diffusion far from the probe; inside the magnetic tube bounded by the probe cross section, the potential overshoots to a large value before decaying to plasma potential. As a consequence, the current at the transition region does not vary exponentially, the magnitude is sharply reduced, and the knee at plasma potential disappears.

In all the probe theories for $\underline{B} \neq 0$, the main emphasis has been on the electron current collected by the probe, i. e. on the transition and electron current saturation regions of the probe characteristic. The ion current has been assumed to be weakly affected by the magnetic field. This is true if the ion cyclotron radius is much larger than the probe size.

II. 2. 1. 3 Probe Theories and the Inverse Problem

It has been noted by many experimentalists that, contrary to the tremendous amount of sophistication applied to the probe theories, the method of measurement is handled in a rather crude fashion. This disparity is due to the fact that all probe theories are treated as "direct problems," i. e. a plasma of known properties is postulated, the plasma parameters (Φ_{pl} , T_e and N) are then freely used to construct the necessary characteristic scales in the normalization scheme; the non-dimensionalized probe characteristics thus calculated contain the plasma parameters in a variety of combinations in all of the dimensionless variables.

The experimentalist faces an "inverse problem" of measuring a dimensional current-voltage characteristic from which he hopes to

deduce the unknown plasma parameters. Because of the free use of plasma parameters in the direct problem and hence its consequences, a comparison with experiment usually involves an extremely tedious process of cross plotting and reduction of dimensionless variables to real variables, for each assumed set of values of the plasma parameters. In some cases, it is not known a priori whether the probe theory is the appropriate one to use or not. In many instances, the numerical solution (e. g. curve fitting) is so complicated that curves other than the ones given (i. e. calculated cases in probe theories) are difficult and expensive to obtain.⁽²¹⁾

It has been demonstrated,⁽⁴⁴⁾ however, that it is possible to apply a comparable degree of sophistication to the inverse problem. The method is to replace the variables of the direct problem with a new, experimentally convenient set of variables (in which each dimensionless quantity contains only one plasma parameter), "inverting" the direct problem, and presenting the results in master plots once and for all. The principle of the inversion is applicable to a wide variety of probe theories. It was also suggested that the "inversion" could be best carried out by the theoretician himself, since he is by far the most familiar with his own theory and is usually also in possession of related computer programs which is necessary to generate required information for the inversion process. It seems that there is much to be gained by the relatively small additional effort of inverting a given theory, since presentations in such experimentally convenient forms will certainly transform the more sophisticated theories into common working tools.

II. 2. 1. 4 A Langmuir Probe Method of Density and Velocity Measurement of Collisionless Plasma Flows in Non-homogeneous Magnetic Fields

In diagnosing the flow field of an electron-bombardment engine generated plasma flowing at hypersonic speeds, the transition region of the probe characteristic is not always reliable, since a low pressure plasma does not necessarily guarantee a Maxwellian, isotropic velocity distribution function for electrons. A non-homogeneous magnetic field is an additional complexity to the problem.

It is shown here that under certain conditions, Langmuir probes can be used to measure density and velocity of a flowing plasma in a non-homogeneous magnetic field. For the obvious reasons given in previous sections, the A and B regions of the probe characteristic cannot be used in the plasma stream, hence one has only the region of saturation ion current to work with.

Assume that the ions are cold and mono-energetic with flow speed much larger than the ion acoustic speed, i. e. $U \gg a_1$, the probe is biased sufficiently negative such that all the electrons are repelled, and the magnetic field is not strong enough to affect region C of the probe characteristic.

For a cylindrical probe with probe radius smaller than the Debye length, the collection of ions with probe axis normal to flow is orbital motion limited^(19, 42) (Fig. 2.9). This means that the ion current is limited by the "absorption radius" and not the sheath thickness, which can be infinitely large. The orbital motion limited current is (see Appendix C):

$$I_{\text{thin-wire}} = NeUA_p \left[1 + \frac{2e(\phi_{pl} - \phi_{pr})}{m_i U^2} \right]^{\frac{1}{2}} \quad (9)$$

where $A_p = 2r_p L$ is the projected probe area.

For a probe with probe size much larger than the Debye length, the collection of ions is simply given by the "swept area" concept (Fig. 2.9) of Clayden.⁽⁴⁵⁾ In the limit of infinitesimally thin sheaths (i. e. $\xi \rightarrow \infty$, where ξ is the probe size to Debye length ratio), and hypersonic flow (i. e. $M \gg 1$, where M is the ratio of the flow speed to ion acoustic speed), the ions collected are simply those that are being swept up by the probe; since the sheath is very thin, all the ions that pass through it are collected. Also because of the hypersonic assumption, the contribution of the ion current due to the "sheath criterion" is negligible. Hence the swept area concept ion collection is given by:

$$I_{\text{flat-guarded}} = NeAU \quad (10)$$

where A is the probe area of the plane probe normal to the flow direction, or the projected probe areas of spherical or cylindrical probes.

If ξ is large but not infinite, then equation (10) should not be used for spherical or cylindrical probes; for plane probes, equation (10) can be used with confidence if guards (Figs. 2.6, 2.9) are provided to eliminate fringing effects of the probe potential field.

In an experimental situation, the probe areas, the probe bias and the currents collected are known. Equations (9) and (10) still contain three unknowns, namely ϕ_{pl} , N and U .

The third equation is supplied by the energy conservation for

ions, i. e. the accelerating potential of the ions (generated in the electron-bombardment ion engine) is the difference between the plasma potential in the source and the local plasma potential in the stream:

$$e\bar{\phi}_{acc} \equiv \frac{1}{2} m_i U^2 = e(\bar{\phi}_{PL,S} - \bar{\phi}_{pl}) \quad (11)$$

It is known that in low pressure discharges, the plasma potential of the discharge $\bar{\phi}_{PL,S}$ is almost equal to the anode potential $\bar{\phi}_A$.^(47, 48) This fact has been used in earlier investigations^(4, 5) where it was assumed that:

$$\bar{\phi}_{PL,S} = \bar{\phi}_A \quad (12)$$

In the present investigation, extensive Langmuir probe measurements were made in the source to determine how the plasma potential varied with the anode potential; it was found that $\bar{\phi}_{PL,S}$ was approximately 8 to 12% lower than $\bar{\phi}_A$ for a wide range of anode potentials; hence, in what follows, the appropriate source plasma potential will be used instead of $\bar{\phi}_A$.

Substituting equation (11) into (9), we have for the orbital motion limited current the following expression:

$$I_{thin-wire} = Ne A_p \left[\frac{2e}{m_i} (\bar{\phi}_{PL,S} - \bar{\phi}_{pr}) \right]^{\frac{1}{2}} \quad (13)$$

Equation (13) now contains only one unknown: the ion number density N . N is also the electron density because of plasma quasi-neutrality in the free stream.

If N is evaluated from equation (13), then upon substitution of this value into equation (10), we can find the flow speed U .

This method is of special value when a weak, non-homogeneous magnetic field is present. Since the trajectories of the electrons are disturbed at weaker magnetic fields than the ions are, the effects of magnetic fields will first be noticed in the electron current to the probe. Therefore, with a least amount of disturbance in the plasma stream (since only region C of the probe characteristic is used), and without relying on the electrons being Maxwellian or isotropic, the density and velocity of a collisionless plasma in hypersonic flow can be measured.

II. 2. 1. 5 Calibration of Probes

a. Thin Sheath

In order to check the swept area concept of ion collection, a comparison of probe characteristics for different probes is made under the same flow conditions. Fig. 2.10 shows that for a flat guarded probe, the ion current changes approximately 4% per 10-Volt probe bias, hence for practical purposes, we can consider that the ion current essentially "saturates"; for the spherical probe, the ion current is seen to grow with increasing negative bias of probe; this is due to the thickening of the sheath with increasing negative bias of probe, and hence, in the lack of guards, collecting more and more particles from the fringing portion of the probe electric field.

The sheath criterion (see II. 2. 1. 1a) is checked in the following way: In order to eliminate the effect of mass motion of the plasma, the collector surface is aligned parallel to flow direction, the collector

is provided with a flush mounted guard to insure that particles do not overshoot the collector. The guard length is computed in Appendix D using the Bohm⁽²³⁾ model. If the sheath criterion were the correct model, then the ion current should saturate to a value given approximately by equation (4). Fig. 2.10 shows that this is not the case because the ion current does not tend to saturate. The consequence of this result is that equation (6) cannot be used to determine the plasma potential in the stream from the floating potential of the probe characteristic.

b. Thick Sheath

The theory of orbital motion limited ion current collection is tested by thin cylindrical probes (usually fine tungsten wires) of large length to diameter ratios: $L/D \sim 0(10^2)$, so that end effects are negligible. Note that end effects become important if the cylinder axis is not perpendicular to flow direction.

If the probe is biased sufficiently negative such that all the electrons are rejected, then the total current collected by the probe is just the ion current given by equation (13), from which the ion density can be evaluated easily.

When the probe is used for relative measurements, i. e. the probe is moved in space but fixed in voltage, it is necessary to know that the bias of the probe is sufficiently negative so that equation (13) is really valid, since equation (13) is, in a sense, an asymptotic theory for large negative bias. How negative is "sufficiently negative"? To answer the question is to find the range of validity of the asymptotic theory. From equation (13), it can be seen that the ion density is

proportional to the slope of the probe current vs. $(\phi_{PL,S} - \phi_{pr})^{\frac{1}{2}}$, which should be a constant.

From region C of a thin wire (i. e. thick sheath) probe characteristic (Fig. 2.11.a), the measured probe current is plotted against the square root of the difference between the source plasma potential and the probe potential in Fig. 2.11.b. The region of validity of equation (13) is found from this plot (Fig. 2.11.b) when the curve asymptotes into a constant slope which passes through the origin. Returning to the probe characteristic in Fig. 2.11.a, we find that for $\phi_{pr} < -15$ volts, the orbital motion limited ion collection theory is valid, hence at any point on the probe characteristic (in the valid region), the ion density can be easily obtained from equation (13).

Figures 2.12.a and b show a similar example, but for a different condition of the plasma generating source: the neutralizer filament bias is increased, which increases the floating potential (see III.1); this has the effect of enlarging the region of validity of equation (13) (compare Figs. 2.11.a and 2.12.a). The probe current vs. $(\phi_{PL,S} - \phi_{pr})^{\frac{1}{2}}$ plot (Fig. 2.12.b) shows an experimental curve which asymptotes well into a straight line passing through the origin (compare with Fig. 2.11.b).

Figure 2.13 shows the result of attempting to enlarge the region of validity of equation (13) by simply biasing the probe to very negative potentials. The result is negative. It is seen that for probe potentials less than about -35 Volts, electrons begin to emit from the collector surface due to ion bombardment. This causes an apparent rise in probe ion current and hence invalidates equation (13).

c. Magnetic Fields

The influence of a non-homogeneous magnetic field on the probe characteristic is shown in Fig. 2.14. Radial traces of ion current are recorded with the flat guarded probe biased at a constant negative potential; trace "a" is taken when the magnetic field is not turned on, trace "b" is taken when $B_0 = 10.9$ Gauss (see next section). As the probe moves radially outward from the centerline of the plasma beam, it moves into a magnetic field of increasing magnitude and changing orientation (\underline{B} is perpendicular to the probe surface at $r = 0$; with increasing radius, the angle between \underline{B} and the probe surface decreases).

In Fig. 2.14, note that the electron current in the transition region of the probe characteristic is reduced; also the qualitative effect of the magnetic field orientation on the electron current⁽⁴²⁾ is observed: the reduction of the electron current is more pronounced when the magnetic field is more parallel to the probe.

However, the region of ion saturation current of the probe characteristic is not affected by the magnetic field at all. This indicates that the method as outlined in II.2.1.4, which requires the use of only region C of the probe characteristic, is truly a suitable method when magnetic fields are present.

d. The Hybrid Probe

Figure 2.15 shows the construction of a hybrid probe: a flat guarded probe for thin sheath ion collection and a thin wire probe for thick sheath ion collection.

The theory outlined in II.2.1.4 can be used for this hybrid probe when the ion cyclotron radius (based on flow speed) is much

larger than the probe radius, and when all the tests performed in the previous sections (a, b, and c) indicate that the method is valid.

The probe is used in either of the two modes:

- i) probe characteristics: in this mode the probe is held in fixed position and the probe voltage is swept.
- ii) relative measurements: in this mode the probe voltage is fixed and the probe is moved in space. The probe bias is usually negative so that ion current is collected; this mode is sometimes called the ion current mode. In what follows, the probe bias in this mode is always within the range of validity of equation (13).

II. 2. 2 Model

The model used in this experiment is a current loop. The construction is shown schematically in Fig. 2.16. It consists of ten turns of 2.54 mm diameter anodized aluminum wire. The coil thickness is about 1 cm and the nominal diameter of the coil is 11.5 cm.

The coil is calibrated by measuring the z-component of magnetic induction (B_z) along the axis of the loop (i. e. $r = 0$) with a Hall effect gaussmeter probe. Such measurements are made for different nominal field strengths B_0 (the value of B_z on the coil plane) and up to three radii along the loop axis.

The results coincide with the theoretically calculated values. This is shown in Fig. 2.17. Note that in this figure the theoretical curve is plotted beyond three radii. Measurements were, however, not made beyond three radii because the magnetic field strengths were of the order or below the earth's magnetic field.

III. EXPERIMENTAL RESULTS

III.1 Performance Characteristics of the Plasma Beam Generator

From the power circuit diagram of the plasma beam generator as shown in Fig. 2.4, it is obvious that the performance of the plasma-beam generator depends upon many variables such as the anode potential (Φ_A), discharge potential (Φ_D), ion grid potential (Φ_G), neutralizer filament current ($I_{N.F.}$), confining magnetic field strength (B_C) and geometry. A theoretical analysis of the performance characteristics is therefore almost impossible.

An experimental study has been carried out, at least to find the main parametric dependences for the operation (and existence) of a plasma beam. This is done by systematically varying one of the above mentioned parameters while keeping the rest of the parameters fixed. The main conclusions are described in the following sections.

III.1.1 Effect of the Neutralizer Filament

i) Without neutralizer filament:

The Hester and Sonin method of neutralizing the ion beam^{*} does not always produce a stable plasma beam for the present source configuration. When a stable beam is produced, the electrons are definitely not Maxwellian; this can be seen from the kinks on the retarding-field region of the Langmuir-probe characteristic (Fig. 3.1).

* The cathode potential is biased slightly negative with respect to the ion grid so that electrons can escape out of the ionization chamber and hence neutralize the ion beam.

- ii) With neutralizer filament on, the electrons appear to be Maxwellian from looking at the probe characteristic (Fig. 3.1); but upon checking a $\ln j_e$ vs. ϕ_{pr} plot, it is found that the curve is not exactly a straight line. However, the "average" slope of the curve is of the order of 0.2 Volts. Hence it will be assumed that the electrons are "nearly" Maxwellian with a temperature of 0.2 eV, which is also approximately the temperature of the neutralizer filament.

III. 1.2 The "Optimum" Beam Condition

With neutralizer filament on, two conditions have to be satisfied for the plasma beam to exist:

- i) $(\phi_A - \phi_D) \leq \phi_{N.F.}$
with beam ion current increasing with $(\phi_A - \phi_D)$ approaching $\phi_{N.F.}$.
When $(\phi_A - \phi_D)$ is larger than $\phi_{N.F.}$, the beam "decays" with increasing $(\phi_A - \phi_D)$ until there is finally no beam at all (Figs. 3.2a,b).
- ii) The neutralizer filament current must be larger than a specific value (depending on $\phi_A, \phi_D, \phi_{N.F.}, I_{C.F.}, B_C$ and geometry). The range of $I_{N.F.}$ is very narrow. An attempt has been made to correlate this with one dimensional theory,^(16, 17) but was unsuccessful.

III. 1.3 Floating Potential

It has been observed that the neutralizer filament bias $\phi_{N.F.}$ affects the floating potential of the probe characteristic ϕ_{fl} directly. As a matter of fact, $\phi_{N.F.} \approx \phi_{fl}$. This can be seen in Fig. 3.1, where the floating potential is approximately 11 volts; in Fig. 3.3, where

ϕ_{fl} is approximately 24 volts; and in Fig. 3.4, where ϕ_{fl} changes with $\phi_{N.F.}$, for all other variables fixed. The fact that $\phi_{fl} \approx \phi_{N.F.}$, even in the presence of external magnetic fields, can be seen in Fig. 2.14.

III. 1.4 Effect of the Screen Grid

The use of a screen grid is optional, since the ion grid, if biased appropriately relative to anode and cathode potentials, can perform the functions of both extracting and accelerating the ions out of the ionization chamber. The reason for having a screen grid was not so much as to screen out the electrons and extract the ions, but rather for the sake of fixing the distance between the ion emitting plane (screen grid) and the plane of the accelerating electrode (ion grid). This distance, z_a , would then be used in predicting the one-dimensional space-charge limited ion current drawn from the source. This space-charge limited ion current is known as Child's law:

$$j_i = \frac{4 \epsilon_0}{9} \left(\frac{2e}{m_i} \right)^{\frac{1}{2}} \frac{(\phi_A - \phi_G)^{\frac{3}{2}}}{z_a^2} \quad (14)$$

Experiments reveal, however, that the screen grid has a large blocking effect such that the ion number density in the test section is reduced by almost an order of magnitude as compared to the case without a screen grid. Furthermore, for definite ranges of anode potential, the ion current (without using screen grid) is observed to be linearly proportional to $(\phi_A - \phi_G)^{\frac{3}{2}}$, hence Child's law is satisfied for that certain range of anode potential; this is shown in Fig. 3.5 for a grounded ion grid.

In case it is of interest, the distance between the effective ion-emitting plane (fictitious "screen-grid" plane) and the ion grid:

z_{a_eff} can be found from equation (14) by noting that:

$$z_{a_eff} \propto \sqrt{\frac{d}{dj_i} (\Phi_A - \Phi_G)^2}^{\frac{3}{2}}$$

III. 1. 5 The Confining Magnetic Field

The axial field of the confining magnet is calibrated along the centerline of the ionization chamber. Fig. 3.6 shows the fringing portion of this field in the test section, for various values of magnet coil current I_M . It is found that I_M has to be larger than 0.3 Amp for a discharge to initiate, and the beam ion current increases with increasing I_M , though not linearly. In operation, I_M is set to be less than 3.5 Amp to keep the fringing portion of the confining field below half a Gauss at model position.

III. 2 Properties of the Plasma Beam

III. 2. 1 General Description

The radial profiles of the beam are recorded with the hybrid probe operating in the ion current mode at different downstream stations. Beam symmetry is checked by taking radial profiles for different azimuthal angles; this symmetry is best achieved with the use of the cathode filament holder as shown in Fig. 2.3.

Upon evaluation of U and N by the method outlined in II. 2. 1. 4, it is found that the ion velocity is practically constant, and the density falls off like one over distance squared, i. e. the beam is source-like, the ion streamlines are straight. The ion stream velocity is of the order of 10^4 m/s and the ion number density at the model position ($z = 23.5$ cm) is approximately 5×10^7 particles/cc. The electron temperature is of the order of 0.2 eV.

III.2.2 Source-like Flow

An example of finding the source-like nature of the beam is shown in Figs. 3.7 to 3.9. Figure 3.7 shows the radial profiles of the ion current, measured at different downstream stations (ref. Fig. 2.2 for exact location of $z = 0$). Since U is found to be constant, the profiles are also density profiles. If the beam is source-like, then the plot of $1/\sqrt{I_0}$ (I_0 is the probe ion current at $r = 0$) vs. z should be a straight line; this is shown to be true in Fig. 3.8, where the effective origin of the source is also determined by extrapolating the straight line down to where $1/\sqrt{I_0} = 0$. If the flow is truly source-like, then the probe ion current should decrease like $1/\zeta^2$ along every ray $\zeta = \sqrt{(z-z_0)^2 + r^2}$ emanating from the effective origin. From the equation of conservation of current, it can be shown that for a source-like flow, the $\zeta^2 I$ vs. $r/(z-z_0)$ plots for different downstream current profiles should all collapse into one curve, provided that the beam spread is not too large so that a profile trace taken along a tangent can approximate the profile trace taken along the arc. This result is shown in Fig. 3.9, where the general tendency of collapse of data points onto a curve is evident and hence source-like flow is indicated. One notes from Fig. 3.9 a very gradual broadening of profiles with increasing z , which is probably due to radial ambipolar diffusion.

It is interesting to note that the beam profiles in Fig. 3.7 are "similar", in the sense that if I is normalized by I_0 , and r is normalized by the half-width of the profile $r_{H.W.}$, then all profiles collapse into a single curve (Fig. 3.10).

The properties of the plasma beam are essentially unchanged with the model inserted into position, except for the fact that the coil sweeps out the portion of the beam that it obstructs, creating a deficit region in its "wake" (Fig. 3.11). If the model was not floated, but biased highly negative relative to plasma, then ion acoustic waves could be created in the wake;^(4, 5) for a floating model, the deficit region remains deficit throughout the wake, being filled in gradually as it progresses downstream.

III. 2. 3 Beam Spread

It is also found that the beam spread, characterized by the beam half-width (H. W.), is inversely proportional to Mach number ($M = U/a_1$). This is shown in Fig. 3.12 where the beam spread angle, defined as $2 \tan^{-1} \left(\frac{H.W.}{z-z_0} \right)$, is plotted against $1/M$. Note that the electron temperature is assumed to be 0.2 eV for the evaluation of the Mach numbers.

III. 2. 4 Slow Ions

Before the plasma beam is turned on, the vacuum system is pumped down to approximately 3×10^{-7} Torr to insure that impurities are kept at a minimum; the plasma beam operates at a background pressure of 1.2×10^{-5} Torr (in any case not more than 2×10^{-5} Torr) so that the background ion density ("slow" ions) is less than 4% of the stream ion density ("fast" ions).⁽⁵⁾

III. 2. 5 Characteristic Length and Time Scales

The characteristic length and time scales, i. e. collision mean free paths and mean free times ($1/\text{collision frequency}$), of the plasma beam are calculated in Appendix E. Maxwellian electrons of

temperature $kT_e = 0.2$ eV and an electron number density of $N = 5 \times 10^7$ particles/cc are assumed for all the calculations. It is found that:

- i) The assumption of "thermal electrons and cold ions" for the plasma is valid throughout the plasma wind-tunnel test section, because the residence time of the plasma in the test section is much shorter than the equipartition time.
- ii) Since electron-ion collision frequency is much larger than the electron-neutral collision frequency, collisions between particles are predominantly Coulombic; hence by definition, the plasma is strongly ionized.
- iii) Since all the collision mean free paths are much larger than the model or test facility, the flow of the plasma is "collisionless" in the sense that the flow is not collision-dominated.

III. 3 Flow with Magnetic Field

III. 3.1 General Description of the Wake

When the magnetic field of the current loop is turned on, the most direct indication that the magnetic field has interacted with the plasma is a noticeable change in the radial profile of the plasma beam, which is observed in the wake of the current loop.

The results are seen in Fig. 3.13, where the traces of radial profiles recorded with both the flat guarded probe and the thin-wire probe are shown. The traces are taken behind the coil at downstream stations separated by one coil radius (5.75 cm) apart. At every station, the beam profile for the case of no magnetic field (broken line) is superimposed on the beam profile with magnetic field turned on (solid line), thus the effect of the magnetic field on the plasma beam

can be easily visualized by comparison of both profiles.

One notes that the profiles recorded by the flat guarded probe are very similar to the profiles recorded by the thin-wire probe, except for a scale factor in the probe current. Since the thin-wire probe measures density and the flat guarded probe measures ion current, which is a quantity proportional to density times flow velocity, the above mentioned similarity of the profiles recorded by different probes means that the effect of the magnetic field on the plasma beam is manifested mainly in a change in the radial distribution of ion density. Also, a 5-15% decrease in flow speed is observed.

The general effect of the magnetic field on the plasma beam is a non-uniform focusing of ions. One notices a slight focusing of ions in the center, which gives rise to wavelike disturbance and decays within two to three radii downstream. The most notable effect is, however, a focusing of ions in an annular region of radius less than the coil radius. This annular "peak" is very long-lived. As can be seen from Fig. 3.13, the solid-line profile ($B_0 \neq 0$) is squeezed in radially as compared to the broken-line profile ($B_0 = 0$), the peak is formed downstream of the coil; as the beam broadens downstream, this peak broadens and decays slowly. Far downstream where the magnetic field of the coil has no effect at all, the beam radial profile tends to a squared shape.

III. 3.2 Upstream Beam Profiles

Beam profiles upstream of the coil have also been recorded. Fig. 3.14 is a representative result. It is seen that the profiles upstream of the coil are hardly perturbed by the presence of a magnetic

field, an "interaction" of plasma and magnetic field is only noticed in the wake of the model, i. e. the above mentioned annular peak forms only after passing the current loop.

III. 3.3 Effects of Magnetic Field Strength

The observations as noted in the preceding sections indicate that there is a "pinching" effect, i. e. an inward deflection of ions, mostly on that part of the plasma close to the current loop, as the plasma flows past the loop.

The effect of the magnetic field strength of the current loop on the "pinching" of the plasma beam is seen in the near wake beam profiles in Fig. 3.15.a. One notes that the ion "peak" gets sharper with increasing field strength. Also, with increasing field strength, the "peak" position is pushed radially inward (note that a "peaklet" outside the coil is pushed radially outward with increasing field strength); this is shown in Fig. 3.15.b.

Figures 3.16 and 3.17 are repetitions of the same experiment, but with different flow speeds.

Comparing Figs. 3.15 to 3.17, one notes that for a given magnetic field strength of the current loop, the "pinching" is stronger (i. e. the peaks are sharper as well as pushed further away from the coil) for the plasma beam with the slower flow speed.

The reason for the peaks being sharper for lower flow speeds can be qualitatively explained: From Fig. 3.12, note that the slower beam has a wider beam spread. This means that a slower beam has more particles at the coil vicinity than a faster narrow beam. Since it is the plasma near the current loop that is deflected the most, it is

obvious that the same "pinch" effect would give rise to a higher density peak if there were more particles to pinch.

To check out the above idea, very narrow beams are produced such that the coil does not block the plasma beam at all. In these cases, no annular peak has been observed. Fig. 3.18 shows a typical result.

What is the mechanism for producing the annular peaks; why are they pushed further away from the current loop at stronger field strengths and/or lower flow speeds? Some analysis is required to answer these questions. This will be the theme of Chapter IV.

IV. THEORETICAL ANALYSIS

IV.1 Preliminaries

The most general approach to treat the dynamics of collisionless plasmas is to use the kinetic equation with self-consistent electric and magnetic fields. However, this approach is usually burdened with formal complications so that it is very difficult to use except in special simple cases.

Macroscopic equations, generated by taking moments of the kinetic equation for each species result in the two-fluid equations; further simplifications of the two-fluid equations result in the one-fluid equation and the generalized Ohm's law (ref. e.g. Spitzer⁽⁴⁹⁾). Fluid equations are frequently used to describe collisionless plasmas, despite the fact that the fluid concept is not easily justified in the absence of collisions.^(50, 51) However, this approach has been found to yield results that are quite reasonable in many respects.⁽⁵²⁻⁵³⁾ The approach using the fluid equations is often known as the "hydrodynamic" approximation.

It should be pointed out, however, that in order for a body of gas particles to be treated as a fluid, the randomizing effects of collisions in the classical sense, or some comparable process, must be important. Collisions in a field-free rarefied plasma are principally accumulated small angle deflections due to distant encounters, rather than single large angle deflections.⁽⁴⁹⁾ If Coulomb collisions were the only important process, then the hydrodynamic approximations should not be valid in describing phenomena with typical length scales much smaller than the collision mean free path.

However, there are other mechanisms present in the plasma that might take the place of randomizing collisions. For example, in the presence of a magnetic field, "collisions" can occur through long-range magnetic forces,⁽⁵⁰⁾ or if turbulence is present, charged particles can be scattered by the fluctuating electromagnetic fields,^(54, 55, 56) giving rise to effective "collisions". The efficiency of such processes, however, is not exactly known.

In the following, the collisionless plasma will be described by the fluid equations, if only as a heuristic means of obtaining qualitative results.

A discussion of some relevant parameters of the present investigation is given in Appendix F. It is also shown in the same Appendix that the one-fluid model together with generalized Ohm's law is not an appropriate approximation for collisionless lab plasmas.

IV.2 The Two-Fluid Model

IV.2.1 The Governing Equations

The plasma in this model is assumed to consist of two species: electrons and singly ionized ions. Each species is represented by its mean density and velocities, the dynamical equations are just the steady-state continuity and momentum equations (subscript indicating species):

$$\nabla \cdot (N_i \underline{U}_i) = 0 \quad (15)$$

$$\nabla \cdot (N_e \underline{U}_e) = 0 \quad (16)$$

$$N_i m_i (\underline{U}_i \cdot \nabla) \underline{U}_i = N_i e (\underline{E} + \underline{U}_i \times \underline{B}) - \nabla \cdot \underline{\psi}_i \quad (17)$$

$$N_e m_e (\underline{U}_e \cdot \nabla) \underline{U}_e = -N_e e (\underline{E} + \underline{U}_e \times \underline{B}) - \nabla \cdot \underline{\psi}_e \quad (18)$$

where $\underline{\psi}$ is the pressure tensor and the electromagnetic fields satisfy the self-consistent steady-state Maxwell equations:

$$\nabla \times \underline{B} = \mu_0 e (N_i \underline{U}_i - N_e \underline{U}_e) \quad (19)$$

$$\nabla \times \underline{E} = 0 \quad (20)$$

$$\nabla \cdot \underline{B} = 0 \quad (21)$$

$$\nabla \cdot \underline{E} = \frac{1}{\epsilon_0} (N_i - N_e) \quad (22)$$

IV.2.2 Assumptions

In order that the above system of equations (15) to (22) be further simplified, the following assumptions are made:

i) Using cylindrical coordinates (z, r, φ) (see Fig. 2.5), it is reasonable to assume azimuthal symmetry, i. e. $\frac{\partial}{\partial \varphi} = 0$, for the given flow configuration.

ii) The plasma is assumed to be quasi-neutral, i. e. $N_i \approx N_e$. This approximation is valid for length scales larger than the Debye length. The quasi-neutrality of the plasma does not preclude the presence of the very small space charges necessary to produce \underline{E} ; however, the condition $\nabla \cdot \underline{E} \approx 0$ is not imposed (ref. Davis, Lüst and Schlüter⁽⁵⁸⁾). We will let N denote the particle density subsequently.

iii) Cold ions and thermal electrons are assumed, i. e. $T_i \ll T_e$. This is a condition that arises as a natural consequence from the type of plasma generator being used (ref. II.1.2.2). As a further simplification, electrons are assumed to be Maxwellian and isotropic, so that the pressure tensor becomes a scalar, and the electron pressure is simply $p_e = NkT_e$.

iv) The magnetic Reynolds number is small, so that the induced magnetic field can be neglected compared to the imposed magnetic field. Although this approximation is usually true for laboratory plasmas, the above assumption can be readily justified a posteriori.

v) The average flow velocities in the z(streamwise) and r(radial) directions are approximately equal for both species, but the azimuthal velocities (swirl) are assumed to be different, i. e.

$$\underline{U}_i = (u_z, u_r, u_{i\varphi})$$

$$\underline{U}_e = (u_z, u_r, u_{e\varphi})$$

It can be seen from the momentum equations, that by assuming equal streamwise and radial velocities for both species, we get

$$\frac{u_{i\varphi}}{u_{e\varphi}} \sim O\left(\frac{m_e}{m_i}\right)$$

as a consequence.

IV.2.3 System of Reduced Equations

Under the assumptions of the previous section, and using the fact that $m_i/m_e \gg 1$ ($m_i/m_e \approx 73,000$ for argon ions), one obtains, from simple order of magnitude arguments, the following system of equations (subscripts z, r, φ denote the respective components in cylindrical coordinates):

Continuity:

$$\frac{\partial}{\partial r} (Nru_r) + \frac{\partial}{\partial z} (Nru_z) = 0 \quad (23)$$

Ion momentum:

$$m_i \left(u_z \frac{\partial u_z}{\partial z} + u_r \frac{\partial u_z}{\partial r} \right) = eE_z \quad (24)$$

$$m_i \left(u_z \frac{\partial u_r}{\partial z} + u_r \frac{\partial u_r}{\partial r} \right) = eE_r \quad (25)$$

Electron momentum:

$$0 = e(E_z - u_{e\varphi} B_r) - \frac{1}{N} \frac{\partial p_e}{\partial z} \quad (26)$$

$$-m_e \frac{u_{e\varphi}^2}{r} = -e(E_r + u_{e\varphi} B_z) - \frac{1}{N} \frac{\partial p_e}{\partial r} \quad (27)$$

$$m_e \left(u_z \frac{\partial u_{e\varphi}}{\partial z} + u_r \frac{\partial u_{e\varphi}}{\partial r} + \frac{u_r u_{e\varphi}}{r} \right) = -e(u_z B_r - u_r B_z) \quad (28)$$

Before proceeding further, one notes that if the plasma were "cold", i. e. $T_e = 0$ (so that the pressure gradient term will be absent), then the above system of equations (24)-(28) can be derived from the Lagrangian of each species. This means that the particle formulation and the fluid formulation are equivalent, in the limit of a cold plasma. This is demonstrated in Appendix G. The important conclusion from this somewhat trivial demonstration is to note that in the cold plasma limit, equation (28), in its integrated form, is simply:

$$u_{e\varphi} = \frac{eA_\varphi}{m_e} \quad (29)$$

where A_φ is the vector potential of the magnetic field. Also from $u_{i\varphi} = -eA_\varphi/m_i$, the conclusion drawn from order of magnitude arguments that $u_{i\varphi}/u_{e\varphi} \sim O(m_e/m_i)$ is found to be correct, and that the neglect of ion momentum in the system of equations is justified as an acceptable

approximation. From equation (29), one gets an idea of how $u_{e\varphi}$ should be scaled.

The system of equations can be physically explained as follows: Far away from the magnetic field, the heavy-particle (ions) motion is modified by the electric field due to the electron pressure only. As the ions stream into the magnetic field region, it does not "see" the field because it is relatively weak. However, the electrons, being "dragged" into this field by the heavy ions, interact strongly with the magnetic field, resulting in a tendency to separate from the ions. This creates a space charge and hence electric field, which in turn modifies the motion of the heavy-particles.

IV. 2. 4 Nondimensionalization and Further Simplification

In order to obtain the parameters of the flow and facilitate computation, the system of equations are non-dimensionalized as follows:

$$\tilde{u}_z = u_z / U \quad (30-1)$$

$$\tilde{u}_r = u_r / U \quad (30-2)$$

$$\tilde{u}_{e\varphi} = u_{e\varphi} / \left(\frac{eB_0}{2m_e} R \right) \quad (30-3)$$

$$\tilde{B}_r = B_r / B_0 \quad (30-4)$$

$$\tilde{B}_z = B_z / B_0 \quad (30-5)$$

$$\tilde{r} = r / R \quad (30-6)$$

$$\tilde{z} = z / R \quad (30-7)$$

$$\tilde{N} = N / N_0 \quad (30-8)$$

where U is the stream speed of the undisturbed plasma,* R is the radius of the current loop, B_0 is the value of the magnetic inductance B_z on the coil plane, and N_0 is the density on the axis at the coil plane.

The normalization of $u_{e\varphi}$ is based on equation (29). Noting that from the definition of the vector potential

$$\oint \underline{A} \cdot d\underline{\ell} = \int \nabla \times \underline{A} \cdot \underline{n} dS = \int_s \underline{B} \cdot \underline{n} dS$$

we have $A_\varphi 2\pi r \sim B\pi r^2$, and hence $A_\varphi \sim \frac{Br}{2}$.

Eliminating E_z and E_r from equations (24) to (27) using the above normalizations (30-1 to 8), and assuming $T_e = \text{const.}$ so that ∇p_e can be written as equal to $kT_e \nabla N$, we get (tildes on normalized quantities are now dropped in the following equations):

$$\frac{\partial}{\partial z} (Nu_z r) + \frac{\partial}{\partial r} (Nu_r r) = 0 \quad (31)$$

$$u_z \frac{\partial u_z}{\partial z} + u_r \frac{\partial u_r}{\partial r} = S u_{e\varphi} B_r - \frac{1}{M^2} \frac{1}{N} \frac{\partial N}{\partial z} \quad (32)$$

$$u_z \frac{\partial u_r}{\partial z} + u_r \frac{\partial u_r}{\partial r} = S u_{e\varphi} \left(\frac{u_{e\varphi}}{2r} - B_z \right) - \frac{1}{M^2} \frac{1}{N} \frac{\partial N}{\partial r} \quad (33)$$

$$u_z \frac{\partial u_{e\varphi}}{\partial z} + u_r \frac{\partial u_{e\varphi}}{\partial r} = - \frac{u_r u_{e\varphi}}{r} - 2(u_z B_r - u_r B_z) \quad (34)$$

where $S = \frac{e^2 B_0^2 R^2}{2 m_e m_i U^2}$ is the interaction parameter, and $M = U/a_i$

is the flow Mach number based on ion acoustic speed.

In the limit of a cold plasma, the pressure gradient terms in

* The reason for placing the model (current loop) sufficiently far away from the source now becomes apparent. If this were not so, the plasma condition would be changed at its source when the magnetic field is turned on. Then there is no way of measuring the stream speed of the undisturbed plasma, since $U_{B=0} \neq U_{B>0}$.

equations (32) and (33) would not be present, and hence the equations of motion are uncoupled from the continuity equation. On the other hand, allowing the electrons to be thermal, but if the flow is hyper-sonic, i. e. $M \gg 1$, the pressure gradient term would be negligibly small, unless the density gradients in (32) and (33) become large to the order of $O(M^2)$.

With $U \sim 10^4$ m/s, $kT_e \sim 0.2$ eV, the Mach number is $M \sim 10$. Hence, in the absence of especially steep density gradients, the pressure gradient term would contribute about 1% to the ion momentum equations, which is negligibly small.

IV.2.5 Results of Computation

The system of equations (31) to (34) is simplified by neglecting the pressure gradient terms. This uncouples the momentum equations from the continuity equation, as noted in the previous section, and the solution of this simplified system would give the ion trajectories (see also Appendix G).

The initial values of the velocity components are given at the plane of the nozzle edge (i. e. $Z = -4.2$, Z is the axial distance from the coil plane, normalized by coil radius). The velocity component on the jet centerline is U , the velocity components of any other position are given by $u_{z_o} = U \cos \theta$ and $u_{r_o} = U \sin \theta$, where θ is the angle between the jet centerline and a vector which has its origin at the effective source point (ref. III.2.2) and passes through the point in consideration at the nozzle-edge plane.

The induced magnetic field is neglected (ref. IV.2.2). The expression for the vector potential of the imposed magnetic field can

be found in Lamb;⁽⁵⁹⁾ and the expressions for the components of the magnetic field B_z and B_r are given in Appendix H.

The system of equations (32) to (34) is numerically integrated on the computer, and a typical computer plot is shown in Fig. 4.1. Only the ion trajectories that stream within the coil (i. e. $r/R < 1$) are plotted. The coordinates are strained, so that the cross section of the coil is oval instead of circular. The ion trajectories upstream of the coil ($Z < 0$) are seen to be hardly affected by the magnetic field, but are strongly deflected inward upon passing the coil, and the "pinching" is the strongest for particles nearest the coil. If one imagines a collector (probe) at say $Z = 0.5$, moving radially outward, then it would register a peak as it hits the envelope of crossing trajectories because particles coming from "other trajectories," so to speak, are also collected; beyond the envelope, the probe moves into a vacuum region and thereby collects nothing. Qualitatively, this describes the observations. It has been experimentally observed that upstream profiles are hardly changed by the magnetic field, radial profiles downstream of the coil have annular density peaks, and there is also a sharp drop of density outside (radially) of the peak. The broadening of these peaks is probably due to diffusion caused by the density gradient; however, since this occurs in thin layers (ref. IV.2.4), it can be neglected as a first approximation. The important fact is that the interaction parameter does describe qualitatively how the plasma is being pinched near the coil edge. Although the trends are correct (i. e. the "pinching" effect is increased for stronger fields and/or smaller plasma slow speeds), the pinching as calculated by

this collisionless model is too strong (compare Fig. 4.1 and the curve for $B_0 = 5.45$ Gauss in Fig. 3.15.b).

It might also be noted that the inclusion of the pressure gradient term would just broaden the density peak, but would not essentially change the position of where the peaks occur.

Inclusion of collisions (electron-ion Coulomb collisions) would lead to some improvement of the situation. Since the collision term in the Boltzmann equation would in effect be a friction term in the electron momentum equation (ref. e.g. Schlüter⁽⁶¹⁾), which in the present case would decrease the swirl velocity of the electrons, and as a consequence diminish the Lorentz force; therefore, the inclusion of a friction term would reduce the interaction (i.e. pinch).

A measure of the importance of this friction is obtained by comparing the collision frequency to the "convection time" defined as R/U (R is the length scale of flow, and U is the characteristic speed; therefore, R/U is a characteristic time scale of the experiment). If $\nu_{ei} R/U \ll 1$, then the collision term becomes negligibly small. In the present case, the flow is approximated to be "collisionless," but actually, $\frac{\nu_{ei} R}{U}$ is of the order of a few percent. However, inclusion of classical Coulomb collisions is not going to change the results too much.

IV.3 A Heuristic Model

IV.3.1 A Heuristic Turbulent Two-Fluid Model

In summarizing the previous sections, it is concluded that a resistivity is required to inhibit the electron currents in the plasma. However, since resistivity is proportional to the collision frequency, the resistivity tends to zero in the limit of a collisionless plasma.

A similar difficulty is encountered in the problem of collisionless plasma shocks, (55, 62, 63) where for a given shock structure the dissipation provided by classical collisions* is less than the dissipation required to make the shock. Here, as in ordinary fluids, where viscosity inhibits the bulk flow and provides the dissipation mechanism, resistivity is required to inhibit electrical current that results from the relative streaming of electrons and ions, and to provide the dissipation mechanism which results in heating the particles. In a collisionless plasma, the "resistivity" or some other equivalent dissipative mechanism is postulated to result not from classical collisions, but from the interaction of plasma particles with the turbulent wave fields.

Turbulent wave fields develop as a result of one or more instabilities of an initial "laminar" state. In the present case, the instability mechanism is most likely to be due to electron-ion two-stream instability, (64-67) since the relative swirl velocity between electrons and ions is very large, i. e. $u_{e\varphi} \gg u_{i\varphi}$.

As with all instabilities, linear analysis does not answer the question of how the system will behave eventually if an unstable situation is brought about. It is therefore conjectured that the streaming particles lose their streaming energy to the turbulent wave field, which in turn scatter the particles in a random fashion and thereby has the effect of heating the particles (crudely, one can say that bulk motion has been converted to random motion).

* By classical collisions, we refer to momentum-transfer collisions between particles, e. g. binary collisions, Coulomb collisions, etc.

The problem of constructing a model for a turbulent friction term (i. e. "resistivity") hinges on understanding the basic mechanisms by which the energy transfers from the streaming particles to the turbulent wave field, and the efficiency of scattering of particles by this field. In the total absence of such knowledge, it seems reasonable to assume in the electron momentum equation, a phenomenological friction between the electron diamagnetic drift and the ions of the following form:

$$-\nu(u_{e\varphi} - u_{i\varphi}) \tag{35}$$

This form is known as the "resistive dissipation" model,⁽⁵⁵⁾ It contains essentially a "collision frequency" due to particle collisions with the turbulent wave field. One notes a striking similarity between equation (35) and the friction term due to classical collisions in the two-fluid equations as derived by Schlüter.⁽⁶¹⁾ However, a classical collision frequency is used in Schlüter's case and the form can be formally derived, whereas in the "resistive dissipation" model used in a collisionless plasma, the "collision frequency" ν is unknown. In actual computation, ν is left as a free parameter adjusted to fit the experimental observations.

A formal derivation of the turbulent "collision" term is given in Appendix I. It is also shown that under certain assumptions, the turbulent collision term gives rise to terms like $\overline{n'E'}$ and $\overline{u' \times B'}$ in the momentum equations, which is analogous to the Reynolds stress ($\overline{u'v'}$ etc.) terms in the turbulent momentum equations of ordinary fluids. Unless the terms $\overline{n'E'}$ etc. are measured and the correlations known,

a simple heuristic model is the only means of providing some qualitative results.

IV. 3. 2 Results of Computation Using the "Resistive Dissipation" Model

The system of equations is essentially the same as before (IV. 2. 5), with the exception that the expression given by (35) is added to the right hand side of equation (28). Since $u_{i\phi} \ll u_{e\phi}$, this simplifies to the following nondimensionalized form (ref. equation (34)):

$$u_z \frac{\partial u_{e\phi}}{\partial z} + u_r \frac{\partial u_{e\phi}}{\partial r} = - \frac{u_r u_{e\phi}}{r} - 2(u_z B_r - u_r B_z) - F u_{e\phi} \quad (36)$$

where $F = \frac{\nu R}{U}$ is the "turbulent collision frequency" ν normalized by the convection time. As mentioned in the previous section, F is a free parameter that can be adjusted to fit the experimental observations. It is found that $F \sim O(1)$ is required, i. e. $\nu_{\text{turbulent}} / \nu_{\text{classical}} \sim O(10^2)$.

Typical results are shown in the computer plots of Figs. 4.2. a to c. When the friction term becomes of the same order as the interaction parameter, the strong "pinching" situation is essentially improved (compare Fig. 4.1 to Fig. 4.2. a). Further slight improvements are made possible by scaling F with the magnitude of the magnetic field; in doing so, it is postulated that the turbulent collision frequency is in some way proportional to the imposed magnetic field, since it is this field which gave rise to the two-stream instability in the first place. The results are shown in Figs. 4.2. b and c.

Density and hence current profiles can be computed from equation (31) when the velocity field is known. This means that the current profiles can be obtained when the ion trajectories have been

computed.

An example of this is shown in Fig. 4.3.a where the ion trajectories are calculated for the case $B_0 = 0$, and the computed current profiles are shown in Fig. 4.3.b. The initial conditions of the current profiles were obtained from the data shown in Fig. 3.15.a ($B_0 = 0$ case). Recalling from Section III.2.2, we know that since the undisturbed flow is source-like and the profiles are "similar" (ref. Fig. 3.10), if we have a profile at any downstream station, we can always compute its shape at the nozzle edge, i. e. at $Z = -4.2$, which is the starting point of the computation.

A typical pinched current profile is obtained for the case of Fig. 4.2.c; the current profiles are computed with the same initial condition as the case above, and the computer plot is shown in Fig. 4.4. As expected, there is a density (current) peak downstream of the coil position where the ion trajectories are pinched close together. A comparison with experimental observations (Fig. 3.15) shows that the correspondence is at best qualitative.

It should be noted that the turbulent model provides us only with a qualitative picture. Although the finer details are lacking, the main features can definitely be identified, and the trends are correct.

In the lack of experimental knowledge of turbulence (e. g. the efficiency of scattering of particles from the turbulent wave fields, etc.), further computer experiments with a heuristic model are not very meaningful, since the results so obtained usually have no general validity. The most one could hope for in using a heuristic model is to

gain some insight and understanding of the macroscopic phenomena. In this sense, the model is somewhat successful.

IV.4 A Posteriori Check on the Turbulent Assumption

Since turbulence has been appealed to in order to obtain a heuristic model, it is necessary to inquire whether there really is any turbulence in the flow at all.

In order to check this assumption, spectrum measurements of the fluctuating probe currents are made with the use of a wave analyzer (Hewlett Packard 3590A).

In Fig. 4.5, the spectrum of the RMS fluctuating probe current is plotted. It can be seen that as the magnetic field is increased, broad-band noise is introduced at higher and higher frequencies.

In Fig. 4.6, the strength of the current coil is held constant at 21.8 Gauss and the position of the probe is varied radially and axially. All lengths in Fig. 4.6 are normalized by the coil radius.

In Fig. 4.6.a when the probe approaches the coil, although the magnitude of the magnetic field is increased, the broad-band noise decreases. This might be explained by noting that the density drops sharply in the radial direction (ref. Fig. 3.13 Thin-Wire Probe Profile). Furthermore, the position at $r = 1$ just behind the coil is the "shadow" region where there are no particles at all. If we recall that the turbulent wave field has to gain its energy from the streaming particles before it can scatter the particles randomly, then we might argue that, as the density of the streaming particles decreases, the turbulent wave field has less particles from which to gain energy, therefore resulting in a "weaker" turbulence.

In Fig. 4.6.b, it can be seen that when the probe approaches the coil from upstream the broad-band noise increases to a maximum at $Z = 0$; when the probe moves downstream away from the coil, the broad-band noise decreases. Since the magnetic field is symmetric (if the induced fields are small, see Appendix J), and the flow is source-like (i. e. the upstream particle density is higher than the downstream particle density), for symmetric positions upstream and downstream of the coil the probe at the upstream station should record more broad-band noise than at the downstream station. However, this is not the case when one compares the curves $Z = -0.5$ to $Z = 0.5$, and also $Z = -1$ to $Z = 1$. This offset can be explained by the fact that since the plasma is flowing, the "turbulence" is convected downstream.

In conclusion, it can be stated that although the brief spectrum survey does not provide us with any further clues as to how a turbulent model should be constructed, it does serve the purpose of proving its existence, and hence justifies the use of turbulence for obtaining a heuristic model.

V. CONCLUSIONS

The main theme of the present investigation is to study the flow of rarefied plasmas, in particular the interaction of a collisionless plasma beam with an externally imposed magnetic field. The simplest experimental configuration is used: an axisymmetric flow through a circular current loop. This has two consequences, first the magnetic field is localized, second the magnetic field is axisymmetric but spatially non-homogeneous.

The localization of the magnetic field in such an experiment is important, since otherwise there would be no "flow at infinity" where the plasma is not affected by the field and hence can be used as a reference. The spatial non-homogeneity is not really desirable, however it is a price paid for having experimental simplicity and "localization" of the magnetic field.

A major obstacle to the diagnostics problem is that conventional Langmuir probe methods fail if the plasma electrons are not Maxwellian, and that there is no adequate probe theory for $B \neq 0$. Both of these difficulties are encountered in the present investigation. To that end, a "two-probe" method is developed to measure ion density and current (thereby velocity can be derived) in the ion-saturation region of the probe characteristic, which is both insensitive to whether the electrons are Maxwellian or not, and also to weak magnetic fields. This method works for "hypersonic" plasma flow with "cold" ions.

Prior to studying the interaction problem, the performance characteristics of the plasma source are thoroughly investigated, and interesting experimental results are discovered, such as optimum

beam condition, floating potential dependence on neutralizer filament bias, beam spread dependence on flow speed, source-like flow and "similarity" profiles, etc. Most of these results have proven to be very valuable information for studying the interaction problem.

Using the "two-probe" method of diagnostics, the flow field is carefully mapped for different flow speeds and magnetic field strengths. It is seen that the interaction manifests itself in a pinching of the plasma particles at certain locations in the near wake of the current loop. A theoretical modeling of the problem is carried out in an attempt to find the governing parameter. The one-fluid theory with the generalized Ohm's law is found to be unsuitable for describing a collisionless laboratory plasma. The two-fluid theory provides us with an interaction parameter which has the correct trends, i. e. the stronger the applied magnetic field and/or the smaller the flow velocity, the stronger the "pinching." It is shown, however, that turbulent friction is required to improve the collisionless two-fluid model. The turbulent friction is represented by a crude resistive dissipation model, which is nevertheless physically plausible and also mathematically simple to use.

Finally, the existence of turbulence in the flow field is also demonstrated from spectrum measurements of the fluctuating probe currents.

The results of the present investigation have raised some interesting questions which may be resolved in future research work.

The foremost question concerns the plasma diagnostics problem. The "two-probe" method developed within the framework

of this research was designed to bypass the difficulties of the conventional Langmuir probe method (ref. II.2.1.1), and therefore no information on the electron temperature* was available. However, since the effect of turbulence is supposed to result in heating up the electrons, it would be beneficial if the electron temperature could in some way be measured. For this purpose, microwave or spectroscopic methods might provide some answers. If experimental simplicity and local measurements are desired, further research in developing probe theories is required.

Another question concerns the failure of the theory to describe the wave-like disturbance in the center part of the beam and the breaking up of the sharper annular "peaks." Both of these phenomena are suspected to be ion acoustic waves,^(4, 5) and they are not described by the simplified theory because the electron pressure gradient term was neglected. The reasons for neglecting ∇p_e are given in IV.2.4. It should be emphasized that a reasonably good first approximation has been achieved by the simplifications, and that finer detailed improvements could be carried out in future research.

From the cursory survey of the spectrum of the fluctuating probe current, it may be concluded that the turbulence level is not only a function of the imposed magnetic field strength, but also a function of the number density of charged particles. The latter is physically reasonable, and has been explained in IV.4. However, in the computed examples of the present investigation, the turbulent friction was assumed to have only B-field dependence, but density

* This is used in a broader sense to mean the energy distribution of electrons.

dependence was not included because of computational convenience (the momentum equations would not be uncoupled from the continuity equation). The main reason, however, is that it would not be meaningful to elaborate too much on a simple heuristic model.

With the experience gained from the present investigation, some ideas for future research are advanced in the following paragraphs.

The problem could be studied over again by employing a cleaner geometry. This can be obtained by using a larger plasma beam, all except the uniform center portion is blocked out, and this uniform beam is allowed to stream through a dimensionally matched current loop. In this way the effect of the interaction could be more clearly visualized and computation of the problem would also be simplified. Further details such as the effect of pressure gradient terms should be included in the computations, and the effect of different temperature ratios (if one could obtain different electron temperatures and measure them in a magnetic field!) should also be investigated. This is important since the temperature ratio essentially determines whether ion-acoustic waves⁽⁶⁷⁾ are damped or not, and also, at least theoretically, determine the critical drift speed (between electrons and ions) for two-stream instability.⁽⁶⁶⁾

A more interesting problem to examine would be that of turbulence, which is, of course, a vast and difficult subject. Theoretical considerations^(54, 68) are mostly confined to the study of "weak" turbulence (loosely described by the situation when the energy density

associated with the turbulent wave field is much smaller than the particle kinetic energy density), which allows for perturbation-theoretic treatments. However, in most practical cases, the turbulence one encounters is not weak but strong. In the lack of systematic methods for describing strong turbulence, it might be beneficial to use the analogy with ordinary fluids and to apply a phenomenological approach. It is essential that fluctuating quantities are measured and correlations obtained, from which some insight might be gained in constructing improved heuristic turbulent models.

APPENDIX A

a. The Average Speed of Maxwellian particles

If f is a Maxwellian velocity distribution function, then the number of particles per unit volume in physical space (hence referred to as the number density) with peculiar velocities \underline{v} in dC (unit volume in velocity space) is:

$$fdC = f W^2 \sin\theta d\theta d\varphi dW \quad (A-1)$$

in spherical coordinates.

The number density with peculiar speeds between W and $W + dW$ is obtained by integrating (A-1) with respect to θ and φ ; this gives:

$$4\pi f W^2 dW = \left(\frac{2}{\pi}\right)^{\frac{1}{2}} N \left(\frac{m}{kT}\right)^{\frac{3}{2}} W^2 \exp\left(-\frac{mW^2}{2kT}\right) dW \quad (A-2)$$

Therefore, the probability of finding a particle with peculiar speed between W and $W + dW$ is:

$$F(W) = 4\pi f W^2 = \left(\frac{2}{\pi}\right)^{\frac{1}{2}} N \left(\frac{m}{kT}\right)^{\frac{3}{2}} W^2 \exp\left(-\frac{mW^2}{2kT}\right) \quad (A-3)$$

$F(W)$ is also known as the isotropic speed distribution function.

The average speed is defined as:

$$\bar{c} \equiv \langle W \rangle \equiv \frac{1}{N} \int_0^{\infty} W (4\pi f W^2) dW \quad (A-4)$$

which, upon evaluation using (A-3) gives:

$$\bar{c} = \left(\frac{8kT}{\pi m}\right)^{\frac{1}{2}} \quad (A-5)$$

b. The percentage of Maxwellian particles with energies greater than $\frac{1}{2} kT$

The total number of particles per unit volume is:

$$N = \int_0^{\infty} F(W) dW \quad (A-6)$$

The number of particles in unit volume with energies greater than $\frac{1}{2} kT$ is, using (A-3):

$$n = \int_{W_{\min}}^{\infty} F(W) dW = \sqrt{\frac{2}{\pi}} N \left(\frac{m}{kT}\right)^{\frac{3}{2}} \int_{W_{\min}}^{\infty} W^2 \exp\left(-\frac{mW^2}{2kT}\right) dW \quad (A-7)$$

where $\frac{1}{2} m W_{\min}^2 = \frac{1}{2} kT$

Normalizing W with $\left(\frac{kT}{m}\right)^{\frac{1}{2}}$ in (A-7) and evaluating:

$$\begin{aligned} n &= 2N \int_1^{\infty} \frac{x^2 e^{-\frac{1}{2}x^2}}{\sqrt{2\pi}} dx \\ &= 0.8014N . \end{aligned}$$

Hence, with $\frac{n}{N} \approx 80\%$, we conclude that the "majority" of the particles have energies greater than $\frac{1}{2} kT$.

APPENDIX B

a. Derivation of the Druyvesteyn⁽²⁸⁾ formula for a flat probe:

If $f(\underline{v})$ is the electron velocity distribution function outside of the sheath edge (i. e. in the undisturbed plasma), the electron current collected by the probe is:

$$I_e = e A \int f \underline{v} \underline{d\underline{v}} \quad (\text{B-1})$$

where A is the probe area.

If $f(\underline{v})$ is isotropic, then writing (B-1) in spherical coordinates, denoting w as the velocity normal to the probe surface and integrating over the azimuthal angle φ from 0 to 2π , we get

$$I_e = e A \int_{w_{\min}}^{\infty} 2\pi w^3 f dw \int_0^{\theta^*} \cos\theta \sin\theta d\theta \quad (\text{B-2})$$

$$\left. \begin{aligned} \text{where } w_{\min} &= \sqrt{\frac{2eV}{m_e}} \quad , \quad V = \phi_{pl} - \phi_{pr} \\ \text{and } \theta^* &\text{ is determined by: } \frac{1}{2} m w^2 \cos^2 \theta^* = eV \quad . \end{aligned} \right\} \quad (\text{B-3})$$

Noting that $4\pi w^2 f$ is the isotropic speed distribution function $F(w)$ and using (B-3), we obtain:

$$I_e = \frac{eA}{4} \int_{\sqrt{\frac{2eV}{m_e}}}^{\infty} F(w) w \left(1 - \frac{1}{w^2} \frac{2eV}{m_e} \right) dw \quad (\text{B-4})$$

Differentiating (B-4) twice with respect to V, we arrived at the Druyvesteyn formula:

$$F\left(\sqrt{\frac{2eV}{m_e}}\right) = \frac{4mV}{A e^2} \frac{d^2 I_e}{d V^2} \quad (\text{B-5})$$

b. The a-c potential perturbation method of Sloane and MacGregor⁽²⁹⁾

In the following, ion current saturation is assumed.

If a small a-c potential is superimposed on the d-c probe potential, then the d-c probe current increases by an amount proportional to the second derivative of the probe current with respect to the relative probe voltage V .

This can be shown as follows:

If the probe voltage is:

$$V_p = V + v \quad (\text{B-6})$$

where V is the d-c probe voltage

$$v = V_o \cos \omega t \text{ is the a-c probe voltage} \quad (\text{B-7})$$

and $V_o \ll V$

then by expanding the probe electron current in the Taylor series, we have:

$$I_p = I(V_p) = I(V+v) = I(V) + vI'(V) + \frac{v^2}{2!} I''(V) + \dots \quad (\text{B-8})$$

where I_p is the total current with a-c potential perturbation and $I(V)$ is the total current without a-c perturbation. Substituting $v = V_o \cos \omega t$ into (B-8), we get:

$$\begin{aligned}
 I_p = & \left[I(V) + \frac{V_o^2}{4} I''(V) + \frac{V_o^4}{64} I''''(V) + \dots \right] \\
 & + [\text{odd derivatives of } I] \cos \omega t \\
 & + [\text{even derivatives of } I] \cos 2\omega t \\
 & + \dots
 \end{aligned}
 \left. \vphantom{\begin{aligned} I_p = \\ & + [\text{odd derivatives of } I] \cos \omega t \\ & + [\text{even derivatives of } I] \cos 2\omega t \\ & + \dots \end{aligned}} \right\} \text{a-c probe current}$$

For sufficiently small V_o such that $I'' \gg \frac{V_o^2}{16} I''''$, the d-c probe current is:

$$I_p = I(V) + \frac{V_o^2}{4} \frac{d^2 I}{dV^2} \tag{B-9}$$

APPENDIX C

Derivation of the orbital motion limited ion current collected by a cylindrical probe

The absorption radius is evaluated from conserving the ion angular momentum and energy:

$$pU = r_p v \quad (C-1)$$

$$\frac{1}{2} m U^2 = \frac{1}{2} m_i v^2 - eV \quad (C-2)$$

where p is the absorption radius, U is the flow speed far away from the probe, r_p is the probe radius, v is the tangential velocity with which the ion hits the probe, and V is the relative probe potential equal to $\phi_{pl} - \phi_{pr}$.

Solving for p from Equations C-1 and C-2:

$$p = r_p \left(1 + \frac{eV}{\frac{1}{2} m U^2} \right)^{\frac{1}{2}} \quad (C-3)$$

The current collected by the probe is

$$I = NeUA$$

where A is now the projected area of the probe which is enlarged by the absorption radius:

$$A = 2 pL \quad (C-5)$$

where L is the length of the probe.

Hence from equations C-3 to C-5, we find

$$I = NeUA_p \left[1 + \frac{2e(\phi_{pl} - \phi_{pr})}{mU^2} \right]^{\frac{1}{2}} \quad (C-6)$$

where $A_p = 2 r_p L$ is the projected area of the probe.

APPENDIX D

Computation of the Guard Length for the parallel-to-flow collector

Consider a one-dimensional model in which the x and y coordinates are parallel and perpendicular, respectively, to the flow.

At the sheath edge, the velocity normal to the collector surface is

$$v(y_s) = \sqrt{\frac{2e\phi_0}{m_i}} \quad (D-1)$$

where $\phi_0 = \frac{1}{2} \frac{kT}{e}$ is assumed (Bohm's sheath criterion).

Inside the sheath, the normal velocity is:

$$v(y) = \sqrt{\frac{2e\phi}{m_i}} \quad , \quad y < y_s, \quad \phi > \phi_0 \quad (D-2)$$

Hence the trajectory of a particle is given by:

$$\frac{dy}{dx} = \frac{v}{U} = \sqrt{\frac{2e}{m_i U^2}} \phi^{\frac{1}{2}} \quad (D-3)$$

The integrated plasma-sheath equation for Maxwellian electrons and space charge limited flow (i. e. $\left. \frac{d\phi}{dy} \right|_{\phi=\phi_0} = 0$) supplies a relation for ϕ as a function of y (ref. Bohm⁽²³⁾):

$$\frac{d\phi}{dy} = 2\sqrt{\frac{Ne}{\epsilon_0}} \phi_0^{\frac{1}{2}} \left\{ (\sqrt{\Phi} - 1) + \frac{1}{2} \frac{1}{\chi} \left[e^{-\chi(\Phi-1)} - 1 \right] \right\}^{\frac{1}{2}} \quad (D-4)$$

where

$$\Phi = \frac{\phi}{\phi_0} \geq 1$$

$$\chi = \frac{e\phi_0}{kT_e} \geq \frac{1}{2}$$

and ϵ_0 is the permittivity of vacuum.

Note that the space charge limited flow condition contradicts the sheath criterion. But it is used by Bohm as an approximate boundary condition.

Multiplying (D-3) and (D-4), inverting, and using the definitions:

$$\sqrt{\frac{Ne^2}{\epsilon_0 m_i}} = \omega_{p_i} \quad \text{ion plasma frequency}$$

$$\sqrt{\frac{kT_e}{m_i}} = a_i \quad \text{ion acoustic speed}$$

$$\frac{a_i}{\omega_{p_i}} = \lambda_D \quad \text{Debye length}$$

$$\frac{U}{a_i} = M \quad \text{mach number}$$

we get the equation

$$\frac{dX}{d\Phi} = 2^{-\frac{3}{2}} [\Phi^{\frac{1}{2}} \cdot F(\Phi, \chi)]^{-1} \quad (D-6)$$

where $X = \frac{\chi}{\lambda_D} \cdot \frac{1}{M}$

and $F(\Phi, \chi) = \left\{ \sqrt{\Phi} - 1 + \frac{1}{2\chi} \left[e^{-\chi(\Phi-1)} - 1 \right] \right\}^{\frac{1}{2}}$

The boundary condition for equation (D-6) is obtained as follows: When the particle has traversed the guard length in the flow direction, it should have dropped to the collector surface, which is at the wall (or collector) potential. Hence the boundary condition:

when $\Phi = \Phi_{\text{wall}}, \quad X = X_{\text{Guard Length}} \quad (D-7)$

The integration of equation (D-6) under the boundary condition (D-7) is carried out on the computer. The actual computation is done backwards by starting from $X = 0$ with $\bar{\Phi} = \bar{\Phi}_{\text{wall}}$, and terminating the numerical integration when $\bar{\Phi} = 1.05$. The absolute value of X at the termination point is taken to be the normalized guard length.

APPENDIX E

Mean Free Paths and Characteristic Times of the Plasma Beam

With a background pressure of 10^{-5} Torr and room temperature of 300°K , the neutral particle number density is:

$$N_n = \frac{p}{kT} = 3.21 \times 10^{17} (\text{m}^{-3}) \quad (\text{E-1})$$

For $kT_e = 0.2(\text{eV})$, assuming the electrons are Maxwellian, the most probable speed of the electrons is

$$g_e = \left(\frac{2kT_e}{m_e} \right)^{\frac{1}{2}} = 2.65 \times 10^5 (\text{m/s}) \quad (\text{E-2})$$

Using $Q_M = 0.3 \times 10^{-20} (\text{m}^2)$ as a collision cross section for Argon,⁽⁴⁸⁾ the electron-neutral collision frequency is:

$$\nu_{en} = N_n Q_M g_e = 2.55 \times 10^2 (\text{sec}^{-1}) \quad (\text{E-3})$$

the electron-neutral mean free path is:

$$\lambda_{en} = 1/(N_n Q_M) = 1.04 \times 10^3 (\text{m}) \quad (\text{E-4})$$

The Debye length for $kT_e = 0.2 (\text{eV})$ and electron (or ion) number density $N = 5 \times 10^7 (1/\text{cc})$ is:

$$\lambda_D = \left(\frac{\epsilon_0 kT_e}{Ne^2} \right)^{\frac{1}{2}} = 0.47 (\text{mm}) \quad (\text{E-5})$$

The impact parameter for a 90° -deflection of Coulomb collision is:

$$p_c = \frac{e^2}{4 \pi \epsilon_0 m_e g_e^2} = 2.69 \times 10^{-9} (\text{m}) \quad (\text{E-6})$$

hence the Coulomb logarithm is

$$\ln(\lambda_D/p_c) = 12.64 \quad (\text{E-7})$$

Using the definition:

$$\Theta = \frac{e^4 \ln(\lambda_D/p_c)}{4 \pi \epsilon_0^2 m_e^2}$$

the electron-ion collision mean free time is:

$$\tau_{ei} = \frac{(3k T_e/m_e)^{\frac{3}{2}}}{1.43 N \Theta} = 4.53 \times 10^{-5} (\text{sec}) \quad (\text{E-8})$$

the electron-ion mean free path is:

$$\lambda_{ei} = g_e \tau_{ei} = 8.58 \text{ (m)} \quad (\text{E-9})$$

With $v_{ei} = 1/\tau_{ei}$ one finds from (E-3) and (E-8) that $(v_{ei}/v_{en}) \gg 1$; this means that the collisions are predominantly Coulombic. Hence by definition, the gas is very strongly ionized. In what follows, the plasma will be considered as fully ionized.

The plasma flow is considered to be "collisionless," in the sense that the collision mean free paths (E-4) and (E-8) are much larger than the dimension of the body it is flowing past (the current coil diameter is 11.5 cm); as a matter of fact, the mean free paths are even much larger than the length of the test section of the plasma wind tunnel, which is 1(m).

With a flow speed of 10^4 (m/s), the residence time of the plasma in the test section is:

$$\tau_R = L/U = 10^{-4}(\text{sec}) \quad (\text{E-10})$$

The equipartition time* for ions assumed to be at room temperature, is:

$$\tau_{\text{eq}} = \frac{\epsilon_0^2 m_e m_i \left(\frac{3kT_e}{m_e} + \frac{3kT_i}{m_i} \right)^{\frac{3}{2}}}{0.219 N e^4 \ln(\lambda_D / p_c)} = 1.2(\text{sec}) \quad (\text{E-11})$$

Comparing (E-10) and (E-11), one concludes that the assumption of thermal electrons and cold ions is valid throughout the test section, since the equipartition time is many orders of magnitude larger than the residence time.

* If electrons and ions in a plasma are both Maxwellian but at different temperatures, then the temperatures approach each other according to the equation:

$$\frac{dT_e}{dt} = \frac{1}{\tau_{\text{eq}}} (T_i - T_e)$$

where τ_{eq} is the characteristic time scale for equipartition of energy.

APPENDIX F

Discussion of Some Parameters of the Problem

The interaction parameter (S), defined as the ratio of Lorentz force to inertial force, is obviously the most important parameter in the present investigation.

The magnetic Reynolds number (R_M), obtained from Ampère's law, is a measure of the induced magnetic field compared to the total magnetic field.⁽⁵⁷⁾ From another point of view, R_M compares the rate of macroscopic motion of the plasma fluid with the rate of magnetic field diffusion. Hence if R_M is very small, the magnetic field diffuses into the plasma in a time much shorter than the characteristic time for the motion of the flow field, diffusion is dominant and an imposed field will hardly be affected by plasma currents. In lab created plasmas, the magnetic Reynolds numbers are usually small.

In the absence of an imposed electric field, and neglecting pressure gradient terms, the steady state generalized Ohm's law is:

$$\underline{J} = \sigma \underline{E}' - H \underline{J} \times \frac{\underline{B}}{|B|} \quad (F-1)$$

where σ is the scalar conductivity, \underline{E}' is the electric field in a co-moving frame (i. e. $\underline{E}' = \underline{U} \times \underline{B}$), and H is the Hall parameter, defined as the ratio of electron cyclotron frequency to electron-ion collision frequency. Using the fact from equation (F-1) that the end point of the \underline{J} vector always lies on a sphere whose south pole coincides with the origin and its north pole with the end point of $\sigma \underline{E}'$, one can easily

see that J scales like $\sigma U B$ for small values of H , and J scales like $\frac{1}{H} \sigma U B$ for large values of H .

$$\text{Since } S \equiv \frac{|\underline{J} \times \underline{B}|}{|\rho \underline{U} \cdot \nabla \underline{U}|} \sim \frac{J B L}{\rho U^2} \quad (\text{F-2})$$

$$\text{and } R_M \equiv \frac{|\underline{b}|}{|\underline{B}|} \sim \frac{\mu J L}{B} \quad (\text{F-3})$$

where L is a characteristic length scale of the plasma, we note that as the collision frequency decreases (all other variables fixed), H becomes very large, and hence J becomes very small. Hence, unless L is sufficiently large (e.g. astrophysical case), S and R_M would tend to zero in the collisionless limit. Therefore, since L is usually small in laboratory situations, the one-fluid model is not a suitable approximation for the description of collisionless lab plasmas.

(*) $\underline{B} = \underline{B}_0 + \underline{b}$, where $\underline{B}_0 =$ impose field, $\underline{b} =$ induced field.

From Ampère's law: $\nabla \times \underline{b} = \mu \underline{J}$, hence $b \sim \mu J L$.

APPENDIX G

Particle Equations of Motion

The Lagrangian of a charged particle in an electromagnetic field is:

$$L = \frac{1}{2} m \underline{u}^2 - q \Phi + q \underline{u} \cdot \underline{A} \quad (G-1)$$

where \underline{u} is the velocity vector, m is the mass and q is the charge of the particle. Φ is the electric potential due to charge separation of electrons and ions and \underline{A} is the vector potential of the magnetic field.

Using cylindrical coordinates, and assuming azimuthal symmetry (i. e. $\frac{\partial}{\partial \varphi} = 0$) for the electromagnetic fields, the Lagrangian becomes:

$$L = \frac{1}{2} m (\dot{r}^2 + \dot{z}^2 + r^2 \dot{\varphi}^2) - q \Phi(z, r) + q r \dot{\varphi} A_{\varphi}(z, r) \quad (G-2)$$

The equations of motion in the z and r directions are readily obtained from the Euler-Lagrange differential equations.

From $\frac{d}{dt} \left(\frac{\partial L}{\partial \dot{z}} \right) = \frac{\partial L}{\partial z}$, noting that $\frac{\partial \Phi}{\partial z} = -E_z$ and $\frac{\partial A_{\varphi}}{\partial z} = -B_r$,

we get:

$$m \frac{d\dot{z}}{dt} = q(E_z - u_{\varphi} B_r) \quad (G-3)$$

From $\frac{d}{dt} \left(\frac{\partial L}{\partial \dot{r}} \right) = \frac{\partial L}{\partial r}$, noting that $\frac{\partial \Phi}{\partial r} = -E_r$ and $\frac{1}{r} \frac{\partial}{\partial r} (r A_{\varphi}) = B_z$,

we get:

$$m \frac{d\dot{r}}{dt} = m \frac{u_{\varphi}^2}{r} + q(E_r + u_{\varphi} B_z) \quad (G-4)$$

In the φ -direction, we obtain an integral of motion because

the Lagrangian is not a function of φ , hence $\frac{\partial L}{\partial \varphi} = 0$, and the Euler-Lagrange equation becomes:

$$\frac{d}{dt} \left(\frac{\partial L}{\partial \dot{\varphi}} \right) = 0 \tag{G-5}$$

Assuming the constant of integration of (G-5) to be zero, i. e. particle has no swirl velocity ($r\dot{\varphi}$) when there is no magnetic field, then from $mr^2\dot{\varphi} + qrA_{\varphi} = 0$, we get:

$$u_{\varphi} = - \frac{qA_{\varphi}}{m} \tag{G-6}$$

If one favors the differential form instead of an integral of motion, equation (28) (ref. IV.2.3) can be easily recovered from (G-5) by writing it out in detail and noting that:

$$\frac{d}{dt} = \frac{\partial}{\partial z} \frac{dz}{dt} + \frac{\partial}{\partial r} \frac{dr}{dt} = u_z \frac{\partial}{\partial z} + u_r \frac{\partial}{\partial r} \tag{G-7}$$

APPENDIX H

The Magnetic Field of a Circular Current Loop

Using the expression given by Lamb,^{(59)*} the vector potential of a circular current loop, normalized by $R B_0 / 2$ (ref. IV.2.4) is:

$$A_\varphi = \psi / r \quad (H-1)$$

with
$$\psi = \frac{1}{\pi} (r_1 + r_2) \{K(X) - E(X)\} \quad (H-2)$$

where
$$r_1^2 = z^2 + (r-1)^2$$

$$r_2^2 = z^2 + (r+1)^2$$

$$X = (r_2 - r_1) / (r_2 + r_1)$$

and K, E are the complete elliptic integrals of the first and second kind.

Since
$$B_z = (\nabla \times A_\varphi)_z = \frac{A_\varphi}{r} + \frac{\partial A_\varphi}{\partial r} = \frac{1}{r} \frac{\partial \psi}{\partial r} \quad (H-3)$$

and
$$B_r = (\nabla \times A_\varphi)_r = -\frac{\partial A_\varphi}{\partial z} = -\frac{1}{r} \frac{\partial \psi}{\partial z} \quad (H-4)$$

it is necessary to evaluate $\partial \psi / \partial r$ and $\partial \psi / \partial z$. Carrying out the differentiations, one obtains:

$$B_z = \frac{1}{\pi} \frac{r_1 + r_2}{r r_1 r_2} \left\{ (r-X)[K(X) - E(X)] + E(X)X(X^2 - 2rX + 1) \frac{1}{1-X^2} \right\} \quad (H-5)$$

$$B_r = \frac{1}{\pi} \frac{r_1 + r_2}{r r_1 r_2} \left[K(X) - \frac{1+X^2}{1-X^2} E(X) \right] \quad (H-6)$$

* The expression given by Lamb is the stream function ψ of a circular line vortex. Because of the difference of his definition of ψ and the definition of the vector potential $\underline{B} = \nabla \times \underline{A}$, the expression for the vector potential is $\underline{A} = \psi / r$.

For very small r , i. e. for values near the axis, A_ϕ , B_z and B_r are obtained from Jackson, ⁽⁶⁰⁾ rewritten in cylindrical coordinates and normalized according to IV. 2. 4, they are:

$$r \ll 1: \left\{ \begin{array}{l} A_\phi = \frac{0.5R}{(1+z^2+r^2+2r)^{3/2}} \quad (H-7) \\ B_z = \frac{2+(2z^2-r^2)+r}{2(1+z^2+r^2+2r)^{5/2}} \quad (H-8) \\ B_r = \frac{1.5 zr}{(1+z^2+r^2+2r)^{5/2}} \quad (H-9) \end{array} \right.$$

APPENDIX I

Derivation of the Turbulent Collision Term

Using a statistical approach, we start with the Boltzmann-Vlasov (i. e. collisionless) equation (steady state is assumed without loss of generality):

$$\underline{v} \cdot \frac{\partial f}{\partial \underline{x}} + \frac{q}{m} (\underline{E} + \underline{v} \times \underline{B}) \cdot \frac{\partial f}{\partial \underline{v}} = 0 \quad (\text{I-1})$$

where f is the species velocity distribution function, q is the charge and m is the mass of the species particle, and \underline{E} , \underline{B} are the electric and magnetic fields which satisfy the self-consistent Maxwell equations. Defining f to consist of an ensemble averaged* quantity and a quantity which fluctuates about the average, likewise for \underline{E} and \underline{B} , we get:

$$f = \bar{f} + f', \quad \underline{E} = \bar{\underline{E}} + \underline{E}', \quad \underline{B} = \bar{\underline{B}} + \underline{B}' \quad (\text{I-2})$$

Substituting (I-2) in (I-1), ensemble averaging the equation, we get:

$$\underline{v} \cdot \frac{\partial \bar{f}}{\partial \underline{x}} + \frac{q}{m} (\bar{\underline{E}} + \underline{v} \times \bar{\underline{B}}) \cdot \frac{\partial \bar{f}}{\partial \underline{v}} = \left(\frac{\partial f}{\partial t} \right)_{\text{turb. coll.}} \quad (\text{I-3})$$

where the turbulent collision term is defined as:

$$\left(\frac{\partial f}{\partial t} \right)_{\text{t. c.}} = - \frac{q}{m} \overline{(\underline{E}' + \underline{v} \times \underline{B}') \cdot \frac{\partial f'}{\partial \underline{v}}} \quad (\text{I-4})$$

* The turbulence is assumed to be stationary, the ensemble average of a quantity is defined as:

$$\bar{Q} = \lim_{T \rightarrow \infty} \int_{-T/2}^{T/2} Q \, dt \quad .$$

The turbulent collision term is different from its classical counterpart in that it allows for momentum and energy transfer back and forth between the fluctuating wave field and the average particle distribution, therefore it does not conserve the local momentum and energy density of the plasma particles; another important property of $\left(\frac{\partial f}{\partial t}\right)_{t.c.}$ is that it does not cause the plasma to relax to a Maxwellian distribution, as does a classical collision term. (55)

Momentum equations, generated from taking moments of first order in velocity of the "turbulent" Boltzmann-Vlasov equation result in the following:

$$\frac{\partial}{\partial x_j} (Nm u_i u_j) = - \frac{\partial}{\partial x_j} p_{ij} + Nq(E_i + \epsilon_{ijk} u_j B_k) + \iiint \left(\frac{\partial f}{\partial t}\right)_{t.c.} m v_i d\underline{v} \quad (I-5)$$

where N , \underline{u} and p_{ij} are the mean density, mean velocity and mean pressure tensor obtained from \bar{f} .

The last term on the right hand side of (I-5) is clearly the "friction" term due to turbulence. It can be readily shown in a formal manner that the electrons are scattered by the turbulent wave field more than ions are because of its small mass (recall $m_i/m_e \approx 73,000$ for argon plasma), so that to a first approximation, the friction term is only important in the electron momentum equations.

The turbulent friction term can be further evaluated. Under the following assumptions:

- i) \underline{E}' and \underline{B}' are not functions of velocity space \underline{v} .
- ii) f' is isotropic
- iii) $\lim_{\underline{v} \rightarrow \infty} f' = 0$ and $\lim_{v \rightarrow \infty} \underline{v} f' = 0$

it can be shown that:

$$\iiint_{t.c.} \left(\frac{\partial f}{\partial t} \right) m v_i d\underline{v} = -q (\overline{n' \underline{E}'} + N \overline{u' \times \underline{B}'}) \quad (\text{I-6})$$

The simplest turbulent model to use is the "resistive dissipation" model⁽⁵⁵⁾ (subscripts denote electrons or ions):

$$\iiint_{t.c.} \left(\frac{\partial f_e}{\partial t} \right) m \underline{v} d\underline{v} = -\nu (\underline{u}_e - \underline{u}_i) \quad (\text{I-7})$$

where ν is an effective "turbulent collision frequency."

APPENDIX J

A Posteriori Justification of the Small R_M Assumption

From the problem under consideration, the only currents are those due to the swirl of electrons:

$$j_\varphi = Ne(u_{i\varphi} - u_{e\varphi}) \doteq -Ne u_{e\varphi} \quad (J-1)$$

since $u_{i\varphi}/u_{e\varphi} \ll 1$.

The induced field has a vector potential a_φ that satisfies

$$\nabla^2 a_\varphi = -\mu j_\varphi \quad (J-2)$$

where μ is the permeability of vacuum.

Since $u_{e\varphi}$ has its largest value in the collisionless case (i. e. no turbulent friction), an upper bound of $u_{e\varphi}$ is given by (ref. G-6):

$$u_{e\varphi} = \frac{eA_\varphi}{m_e} \quad (J-3)$$

where A_φ is the vector potential of the applied magnetic field.

From (J-2), using (J-3) and (J-1), one obtains

$$a_\varphi \sim \frac{\mu R^2 Ne^2}{m_e} A_\varphi$$

where R is the length scale of the experiment (coil radius).

Hence from the definition of the magnetic Reynolds number, one obtains:

$$R_M = \frac{|b|}{|B|} = \frac{a_\varphi}{A_\varphi} \sim \frac{\mu R^2 Ne^2}{m_e} \quad (J-4)$$

With $R = 5.75 \text{ cm}$ and $N = 5 \times 10^7 / \text{cc}$

$$R_M \approx 5.8 \times 10^{-3}$$

Hence the assumption that the induced field can be neglected compared to the imposed field in IV.2.2 (iv) is justified.

References

1. Meckel, B. B., "Experimental Study of the Interaction of a Moving Body with a Plasma," Rarefied Gas Dynamics, Suppl. 1, L. Talbot (Ed.), Academic Press, New York, 1961, pp. 701-714.
2. Hall, D. F., Kemp, R. F., and Sellen, J. M., Jr., "Plasma Vehicle Interaction in a Plasma Stream," AIAA J. 2, 1964, pp. 1032-1039.
3. Clayden, W. A. and Hurdle, C. V., "An Experimental Study of Plasma-Vehicle Interaction," Rarefied Gas Dynamics, Suppl. 4, Vol. II, C. L. Brundin (Ed.), Academic Press, New York, 1967, pp. 1717-1731.
4. Blumenthal, D. L., "Experimental Study of Satellite Wakes in a Simulated Ionospheric Plasma," Ph.D. Thesis, 1970, California Institute of Technology, Pasadena, Calif.
5. Hester, S. D., and Sonin, A. A., "A Laboratory Study of the Wakes of Ionospheric Satellites," AIAA J. 8, 1970, pp. 1090-1098.
6. Pigache, D., "A Laboratory Simulation of the Ionospheric Plasma," Office National D'Étude et de Recherches Aérospatiales, 92 Chatillon, France, T.P. No. 951 (1971).
7. Al'pert, Ya. L., Gurevich, A. V., and Pitaevskii, L. P., Space Physics and Artificial Satellites, Consultants Bureau, New York, 1965.
8. Shea, J. J., "Collision Plasma Flow around a Conducting Sphere in a Magnetic Field," Rarefied Gas Dynamics, Suppl. 4, Vol. II, C. L. Brundin (Ed.), Academic Press, New York, 1967, pp. 1671-1686.

9. Pan, Y. S. and Vaglio-Laurin, R., "Trail of an Ionospheric Satellite I," *AIAA J.*, 5, 1967, pp. 1801-1810; "Trail of an ionospheric Satellite II," Rarefied Gas Dynamics, Suppl. 4, Vol. II, C.L. Brundin (Ed.), Academic Press, New York 1967, pp. 1687-1702.
10. Scott, F. R. and Voorhies, H. G., "Plasma Injection into a Magnetic Field," *Phys. Fluids* 4, 1961, pp. 600-606.
11. Gilleo, M. A., "Flow of low-density high-speed plasma through a magnetic barrier," *Phys. Fluids* 4, 1961, pp. 1399-1406.
12. Otis, D. R., "Computation and measurement of Hall potential and flow-field perturbations in magnetogasdynamic flow of an axisymmetric free jet," *J. Fluid Mech.*, Vol. 24, Part 1, 1966, pp. 41-63.
13. Kuriki, K. and Okada, O., "Experimental Study of a Plasma Flow in a Magnetic Nozzle," *Phys. Fluids*, 13, 1970, pp. 2262-2269.
14. Hasimoto, H., "Swirl of a Conducting Gas due to the Hall Effect," *J. Phys. Soc. Japan*, 19, 1964, pp. 1457-1463.
15. Kaufman, H. R. and Reader, P. D., "Experimental Performance of Ion Rockets Employing Electron Bombardment Ion Sources," AIAA Progress in Astronautics and Rocketry Electrostatic Propulsion, D. B. Langmuir, E. Stuhlinger, and J. M. Sellen, Jr. (Eds.), Vol. 5, Academic Press, N. Y., 1961, pp. 3-20.
16. Seitz, R. N., Shelton, R. and Stuhlinger, E., "Present Status of the Beam Neutralization problem." Same book as (15), pp. 383-422.

17. Pearlstein, L. D., Rosenbluth, M. N. and Stuart, G. W.,
"Neutralization of Ion Beams," AIAA Progress in Astronautics
and Aeronautics: Electric Propulsion Development, E. Stuhlinger,
(Ed.), Vol. 9, Academic Press, N. Y. 1963, pp. 379-406.
18. Ramsden, S. A., "Light Scattering Experiments," Physics of
Hot Plasmas, B. J. Rye and J. C. Taylor (Eds.) Plenum
Press, New York, 1970, pp. 379-403.
19. a. Mott-Smith, H. M. and Langmuir, I., "The Theory of
Collectors in Gaseous Discharges," Phys. Rev. 28, 1926,
pp. 727-763.
b. Langmuir, I., "The interaction of electron and positive
ion space charges in the cathode sheaths," Phys. Rev. 33,
1929, pp. 954-989.
c. Tonks, L. and Langmuir, I., "Motion of positive ions in a
plasma," Phys. Rev. 33, 1929, 1070(A).
d. Tonks, L. and Langmuir, I., "A general theory of the arc
plasma," Phys. Rev. 34, 1929, pp. 876-922.
20. DeLeeuw, J., "Electrostatic Plasma Probes," Physico-
Chemical Diagnostics of Plasmas, T. P. Anderson, R. W.
Springer & R. C. Warder, Jr. (Eds.), Northwestern University
Press, 1963, pp. 65-96.
21. Chen, F., "Electric Probes," Plasma Diagnostic Techniques,
R. H. Huddlestone and S. L. Leonard (Eds.), Academic Press,
1965, pp. 113-200.
22. Schott, L., "Electrical Probes," Plasma Diagnostics, W. Lochte-
Holtgreven (Ed.), North Holland Publishing Co., Amsterdam,

- 1968, pp. 668-731.
23. Bohm, D., "Minimum Ionic Kinetic Energy for a Stable Sheath," Characteristics of Electrical Discharges in Magnetic Fields, A. Guthrie and R. Wakerling (Eds.), McGraw-Hill Inc., New York, 1949, pp. 77-86.
 24. Allen, J. E., Boyd, R. L. F. and Reynolds, P., "The Collection of Positive Ions by a Probe Immersed in a Plasma," Proc. Phys. Soc. 70B, 1957, pp. 297-304.
 25. Bernstein, I. B. and Rabinowitz, I. N., "Theory of Electrostatic Probes in a Low-Density Plasma," Phys. Fluids 2, 1959, pp. 112-121.
 26. Lam, S. H., "Unified Theory for the Langmuir Probe in a Collisionless Plasma," Phys. Fluids 8, 1965, pp. 73-87.
 27. Laframboise, J. G., "Theory of spherical and cylindrical Langmuir Probes in a Collisionless, Maxwellian Plasma at rest," UTIAS Rep. No. 100, June 1966.
 28. Druyvesteyn, M. J., "Der Niedervoltbogen," Z. Phys. 64, 1930, pp. 781-798.
 29. Sloane, R. H. and MacGregor, E. I. R., "An Alternating Current Method for Collector Analysis of Discharge-tubes," Phil. Mag. 18, 1934, pp. 193-207.
 30. Chao, K. T. and Yang, T. Y., "Electron Temperatures in Electrical Discharges," Phys. Rev. 68, 1945, pp. 30-39.
 31. Oleson, N. L. and Found, C. G., "Running Striations and Multiple Electron Temperatures," J. Appl. Phys. 20, 1949, pp. 416-417.

32. Howe, R. M., "Probe Studies of Energy Distributions and Radial Potential Variations in a Low Pressure Mercury Arc," J. Appl. Phys. 24, 1953, pp. 881-894.
33. Boyd, R. L. F. and Twiddy, N. D., "Electron energy distributions in plasmas I," Proc. Roy. Soc. A250, pp. 53-69.
"Electron energy distributions in plasmas II, Hydrogen," Proc. Roy. Soc. A259, 1960, pp. 145-158.
34. Twiddy, N. D., "Electron energy distributions in plasmas III. The cathode regions in helium, neon and argon," Proc. Roy. Soc. A262, 1961, pp. 379-394.
35. Thompson, J. B., "Electron energy distributions in plasmas IV. Oxygen and Nitrogen," Proc. Roy. Soc. A262, 1961, pp. 503-518.
36. Schönhuber, M. J., "Über das Auftreten und Verhalten von Raumladungs-Doppelschichten in Hg-Niederdruckgasentladungen," Z. Angew. Phys. 15, 1963, pp. 454-460.
37. Medicus, G., "Probe Measurements through a double layer," J. Appl. Phys. 36, 1965, pp. 435-442.
38. Bond, R. H. "Directed Electron Velocity Distributions in Rare Gas Discharges using Guard Ring Probes," TR No. 25, Calif. Inst. of Tech., June 1965.
39. Spiwak, G. und Reichrudel, E., "Zur Allgemeinen Theorie der Sondenströme in der Gasentladung," Phys. Z. Sowjetunion 9, 1936, pp. 655-682.

40. Bickerton, R. J. and von Engel, A., "The Positive Column in a Longitudinal Magnetic Field," Proc. Phys. Soc. 69B, 1956, pp. 468-481.
41. Bertotti, B., "Theory of an Electrostatic Probe in a Strong Magnetic Field," Phys. Fluids 4, 1961, pp. 1047-1052.
Phys. Fluids 5, 1962, pp. 1010-1014.
42. Bohm, D., Burhop, E.H.S. and Massey, H.S.W., "The Use of Probes for Plasma Exploration in Strong Magnetic Fields," Characteristics of Electrical Discharges in Magnetic Fields, A. Guthrie and R. Wakerling (Eds.), McGraw-Hill, Inc., New York, 1949, pp. 13-76.
43. Sanmartin, J., "Theory of a Probe in a Strong Magnetic Field," Phys. Fluids 13, 1970, pp. 103-116.
44. Sajben, M. and Lee, P.H.Y, "Inverse Problem for Electrostatic Plasma Probes," J. Applied Phys. 41, 1970, pp. 3433-3439.
45. Clayden, W., "Langmuir Probe Measurements in the RARDE Plasma Jet," Rarefied Gas Dynamics, Suppl. 2, Vol. 2, Academic Press, New York 1963, pp. 435-470.
46. Seeliger, R., Einführung in die Physik der Gasentladungen, Barth Verlag, Leipzig, 1927, pp. 205-218.
47. von Engel, A. und Steenbeck, M., Elektrische Gasentladungen, Vol. 2, Springer Verlag, Berlin, 1934, pp. 57-68.

48. Shkarofsky, I. P., Johnston, T. W. and Bachynski, M. P., The Particle Kinetics of Plasmas, Addison Wesley, Reading, Mass., 1966, p. 185.
49. Spitzer, L. Jr., Physics of Fully Ionized Gases, 2nd Ed., Wiley-Interscience, 1962.
50. Chew, G. F., Goldberger, M. L. and Low, F. E., "The Boltzmann equation and the one-fluid hydromagnetic equations in the absence of particle collisions," *Proc. Roy. Soc.* 236, 1956, pp. 112-118.
51. Volkov, T. F., "Hydrodynamical Description of a Collisionless Plasma," Reviews of Plasma Physics, M. A. Leontovich (Ed.), Vol. 4, Consultants Bureau, N. Y., 1966, pp. 1-21.
52. Parker, E. N., "Fluid-Dynamical Problems Associated with Interplanetary Space," Research Frontiers in Fluid Dynamics, R. J. Seeger and G. Temple (Eds.), Wiley-Interscience, N. Y. 1965, Chap. 20.
53. Spreiter, J. R. and Alksne, A. Y., "Solar-wind flow past objects in the solar system," Annual Review of Fluid Mechanics, M. Van Dyke et al (Co-Eds.), Vol. 2, Annual Reviews, Inc., Palo Alto, 1970, pp. 313-354.
54. Kadomtsev, B. B., Plasma Turbulence, Academic Press London, 1965.
55. Tidman, D. A. and Krall, N. A., Shock Waves in Collisionless Plasmas, Wiley-Interscience, New York, 1971.
56. Jokipii, J. R., "Propagation of Cosmic Rays in the Solar Wind," *Rev. Geophys. and Space Phys.*, 9, Feb. 1971, pp. 27-87.

57. Elsasser, W. M., "Dimensional Relations in Magnetohydrodynamics," *Phys. Rev.*, 95, July 1954, pp. 1-5.
58. Davis, L., Lüst, R. and Schlüter, R., "The Structure of Hydro-magnetic Shock Waves," *Z. Naturforschung* 13a, 1958, pp. 916-936.
59. Lamb, Sir H., Hydrodynamics, 6th Edition, Dover, New York, 1932, pp. 236-237.
60. Jackson, J. D., Classical Electrodynamics, Wiley, New York, 1962, p. 143.
61. Schlüter, A., "The Electrical Conductivity in Interstellar Gas," Gas Dynamics of Cosmic Clouds, J. M. Burgers and H. C. van de Hulst, (Eds.), North Holland Publ. Co., Amsterdam, 1955.
62. Sagdeev, R. Z., "Cooperative Phenomena and Shock Waves in Collisionless Plasmas," Reviews of Plasma Physics, Vol. 4, M. A. Leontovitch (Ed.), Consultants Bureau, N.Y., 1966, pp. 23-91.
63. Friedman, H. W., Linson, L. M., Patrick, R. M. and Petschek, H. E., "Collisionless Shocks in Plasmas," Annual Review of Fluid Mechanics, M. van Dyke et al (Co-Eds.), Vol. 3, Annual Reviews Inc., Palo Alto, 1971, pp. 63-68.
64. Buneman, O., "Dissipation of Currents in Ionized Media," *Phys. Rev.*, 115, 1959, pp. 503-517.
65. Jackson, J. D., "Longitudinal Plasma Oscillations," *J. Nuclear Energy Part C: Plasma Physics*, 1, 1960, pp. 1-18.
66. Jackson, E. A., "Drift Instabilities in a Maxwellian Plasma," *Phys. Fluids* 3, 1960, pp. 786-792.

67. Fried, B. D. and Gould, R. W., "Longitudinal Ion Oscillations in a Hot Plasma," *Phys. Fluids*, 4, 1961, pp. 139-147.
68. Davidson, R. C., Methods in Nonlinear Plasma Theory, Academic Press, New York, 1972.

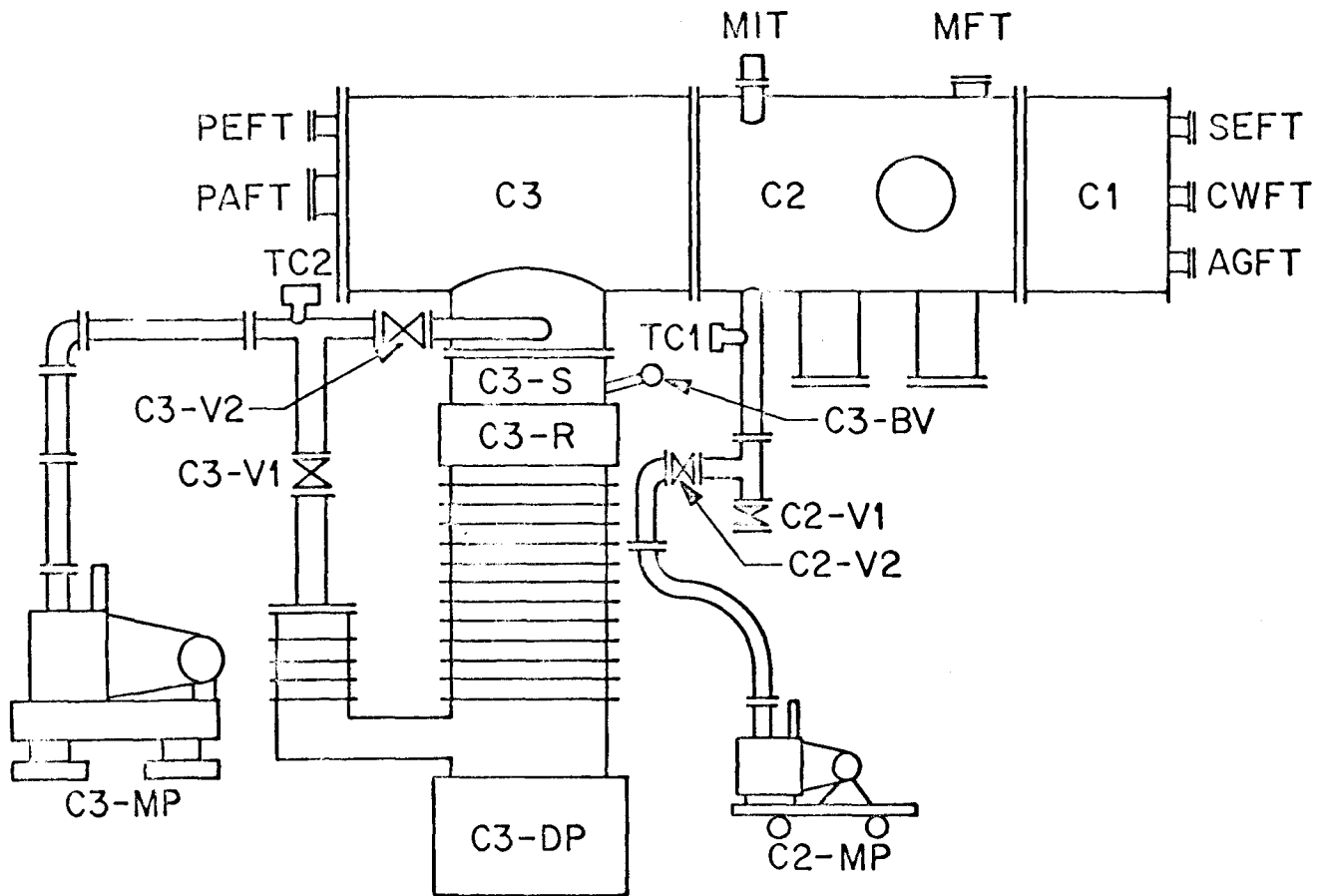


FIG. 2.1 SCHEMATIC OF THE VACUUM SYSTEM (ref. List of Symbols)

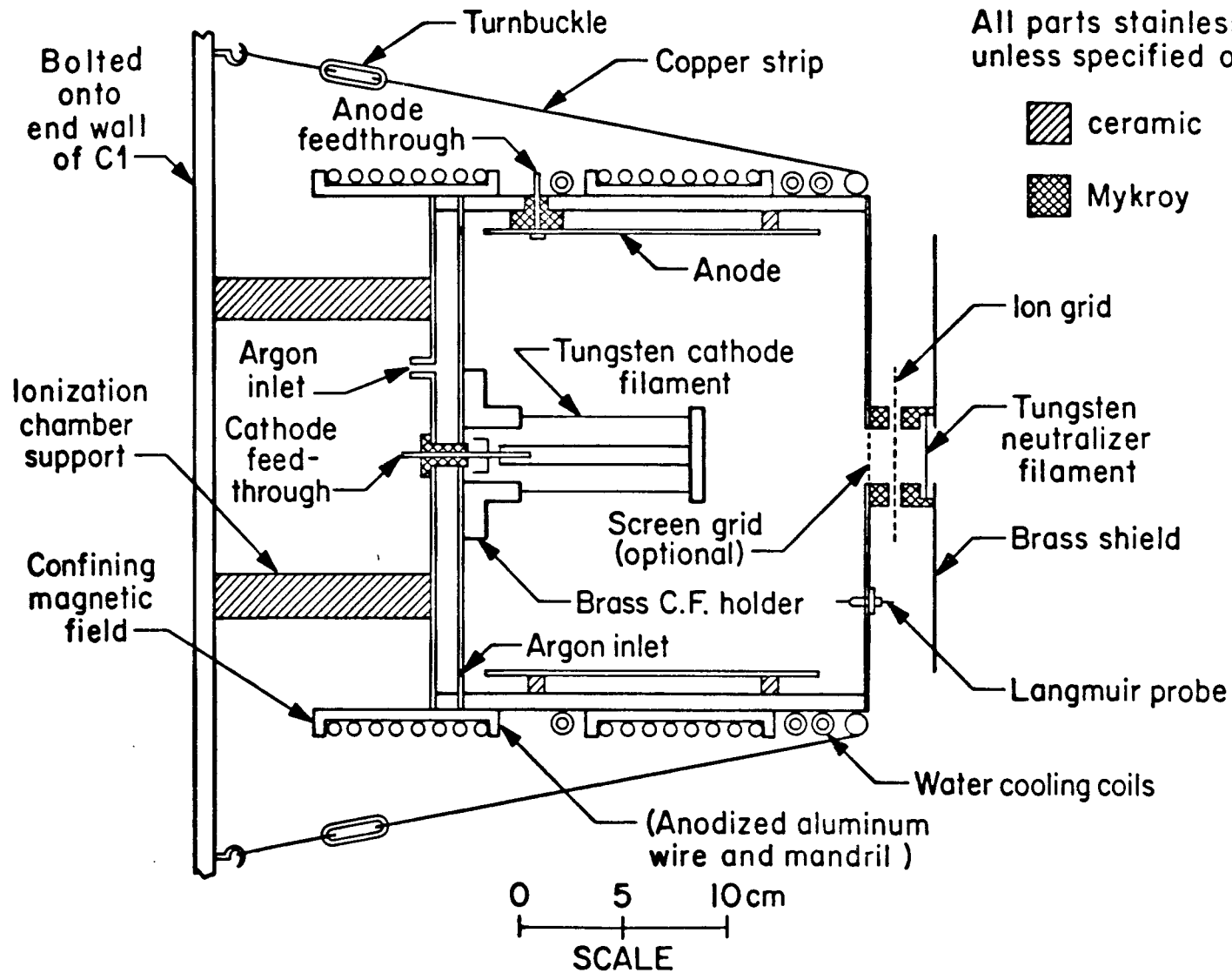


FIG. 2.2 SCHEMATIC OF THE PLASMA SOURCE

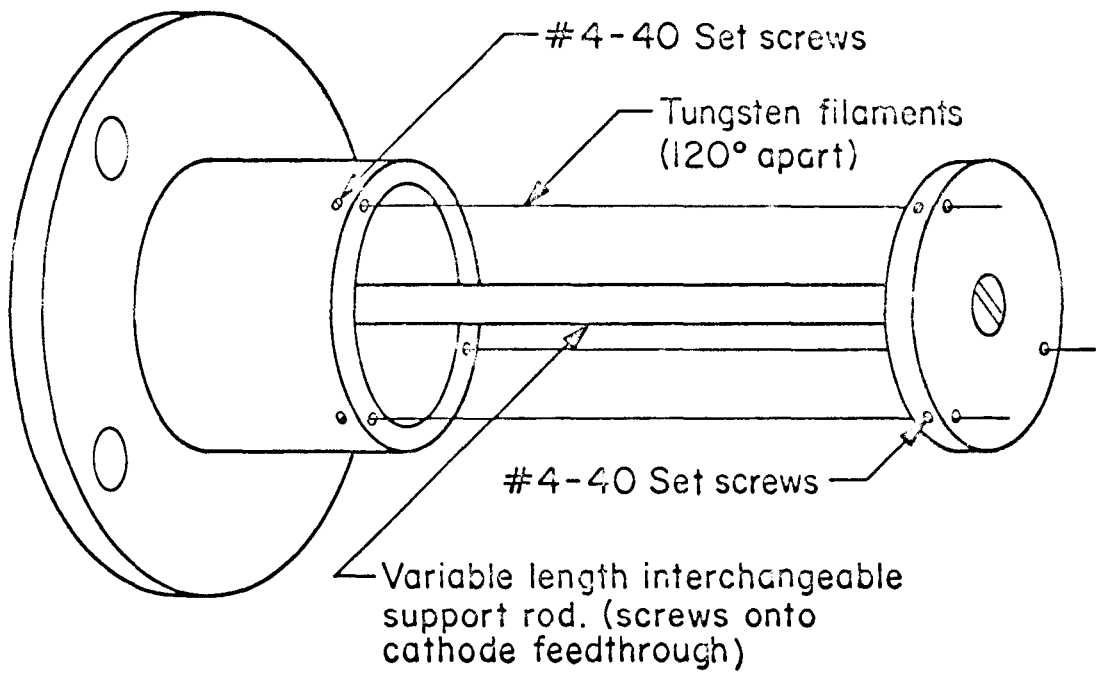


FIG. 2.3 SCHEMATIC OF CATHODE FILAMENT HOLDER

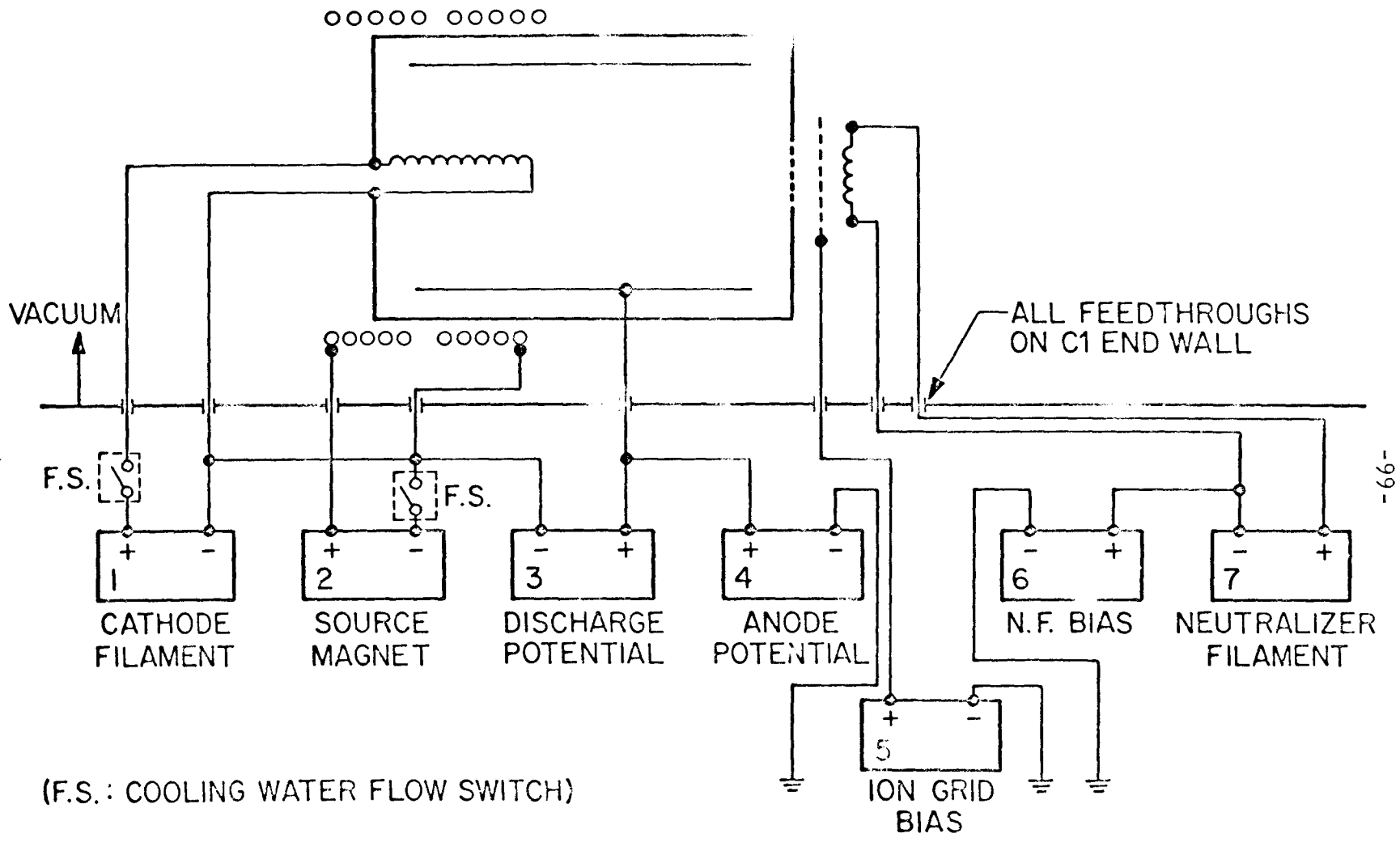


FIG. 2.4 POWER CIRCUIT DIAGRAM OF PLASMA BEAM GENERATOR

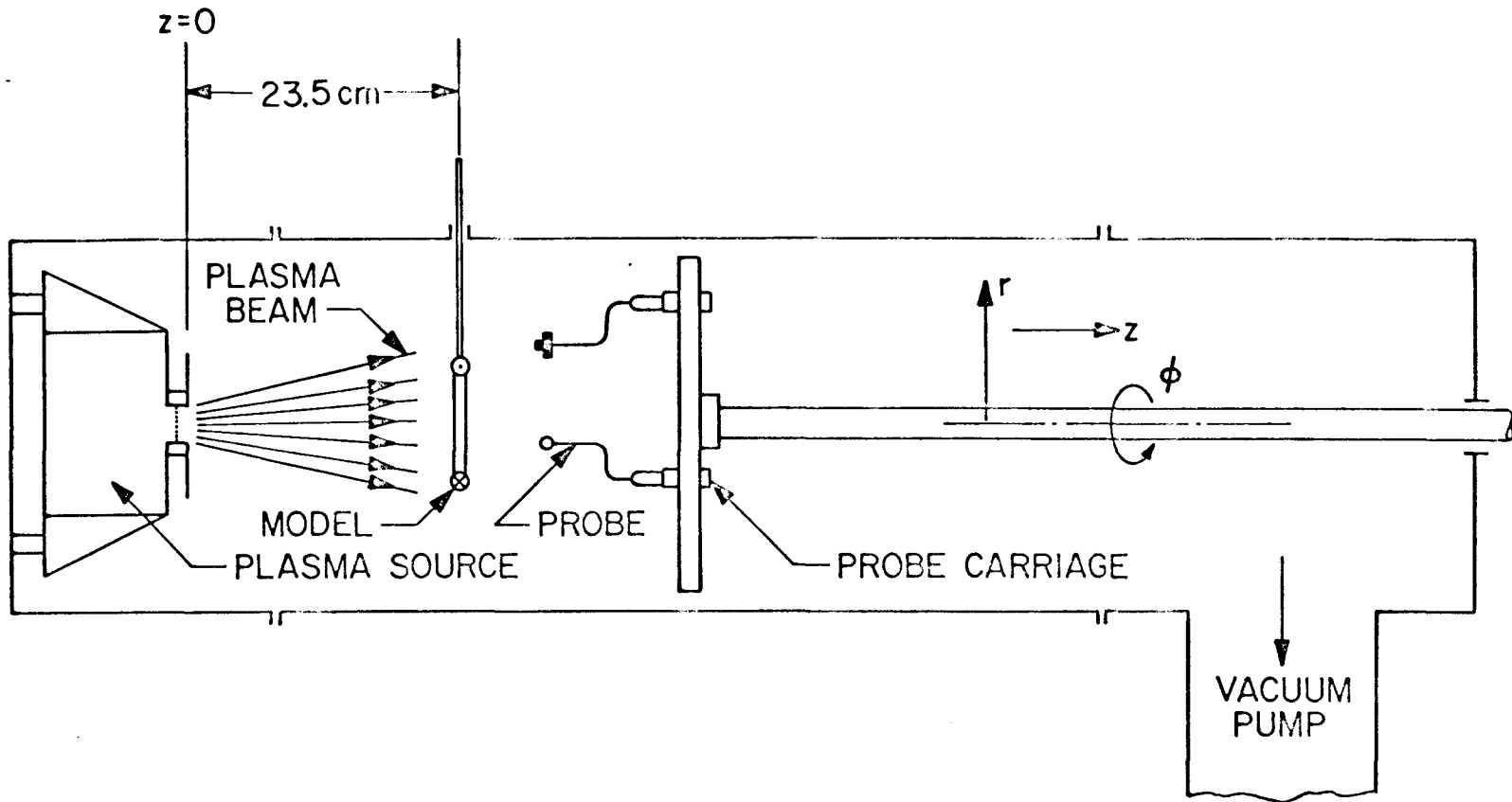
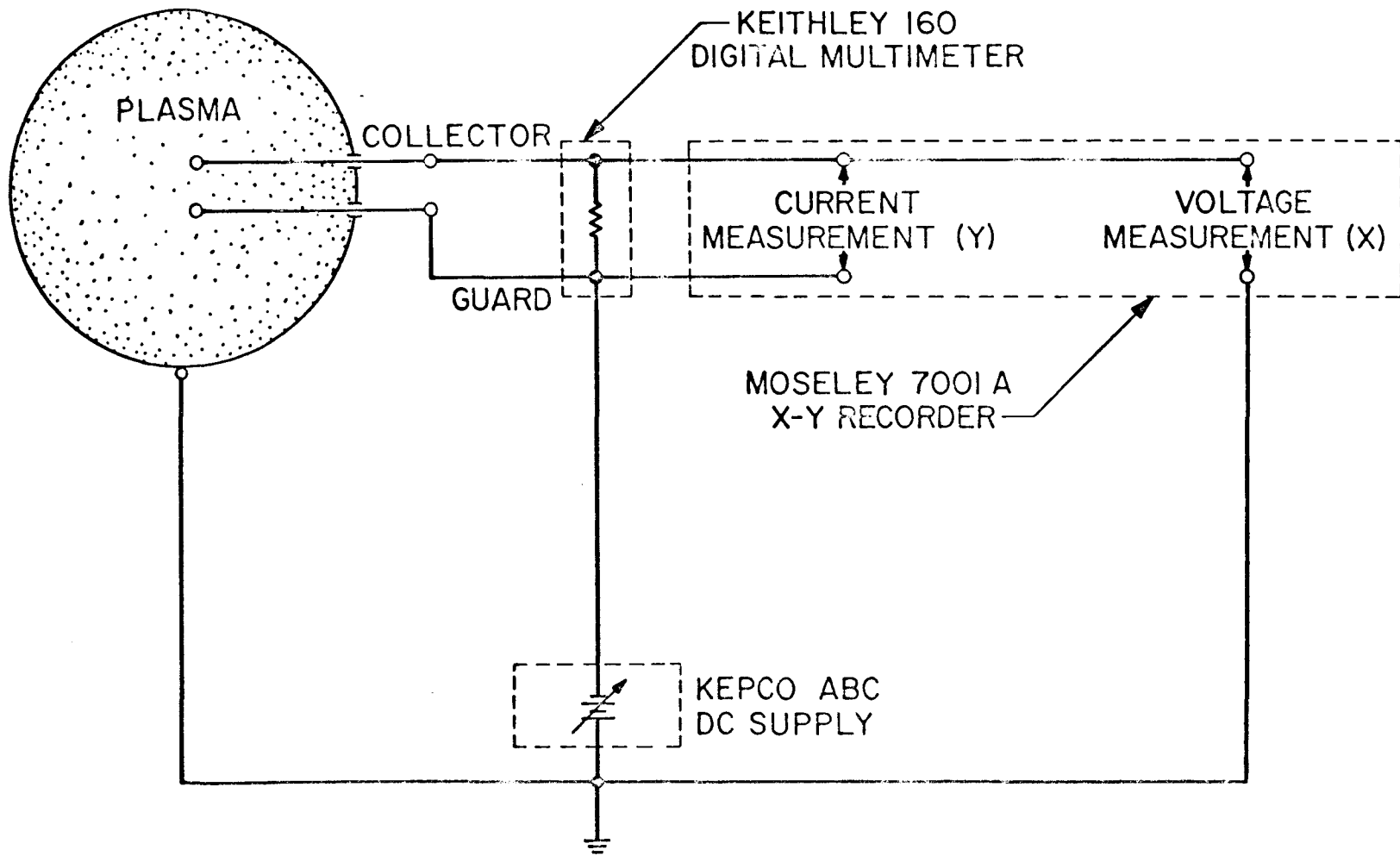


FIG. 2.5 EXPERIMENTAL CONFIGURATION AND COORDINATE SYSTEM



2.6a SCHEMATIC OF PROBE CIRCUIT -
LANGMUIR MODE - PROBE CHARACTERISTIC

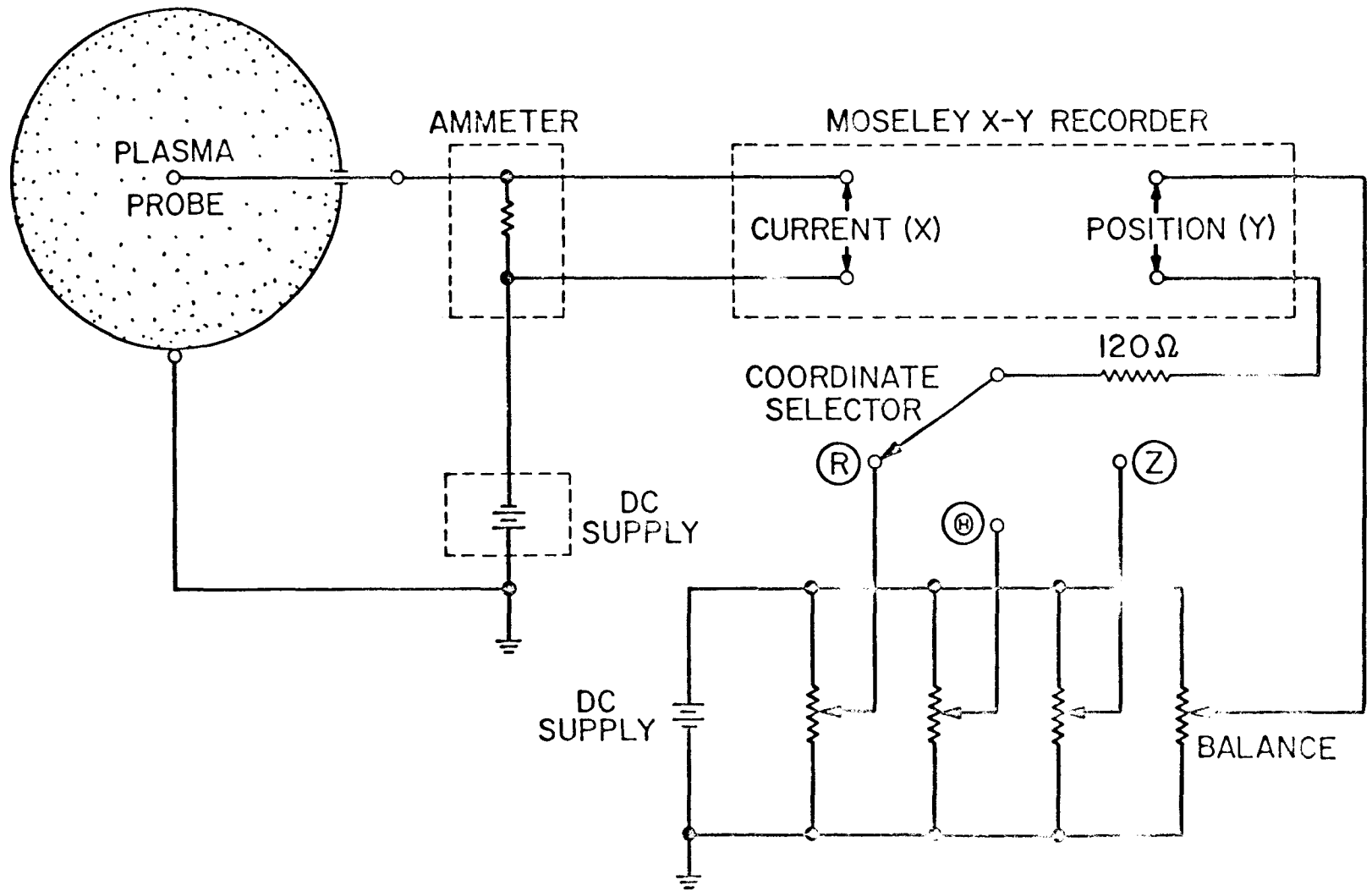
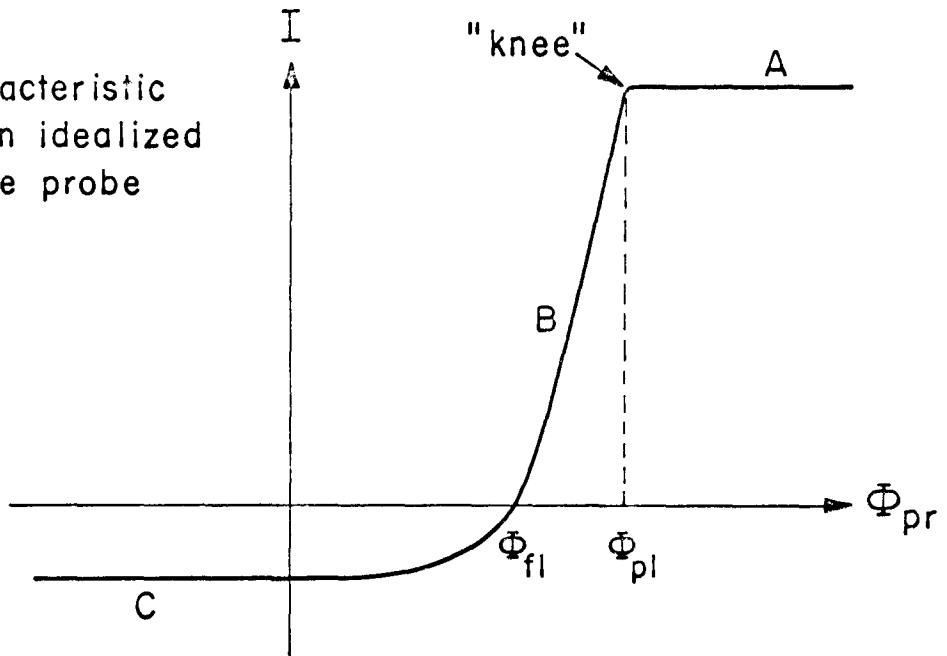


FIG. 2.6b SCHEMATIC OF PROBE CIRCUIT -
ION CURRENT MODE - RELATIVE MEASUREMENTS

a) Characteristic of an idealized plane probe



b) Definition of probe currents

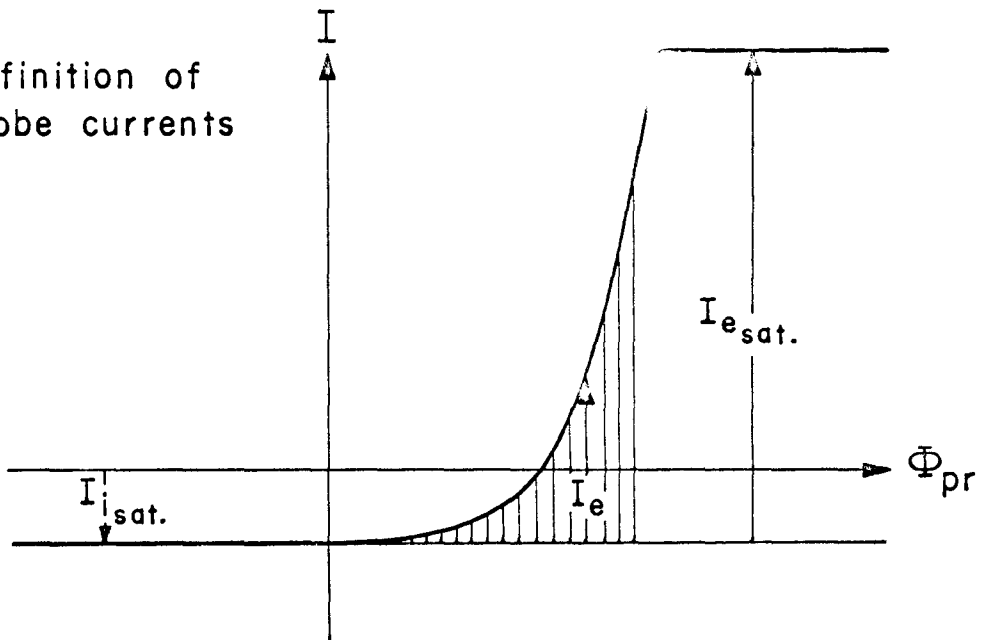


FIG. 2.7 LANGMUIR PROBE CHARACTERISTIC

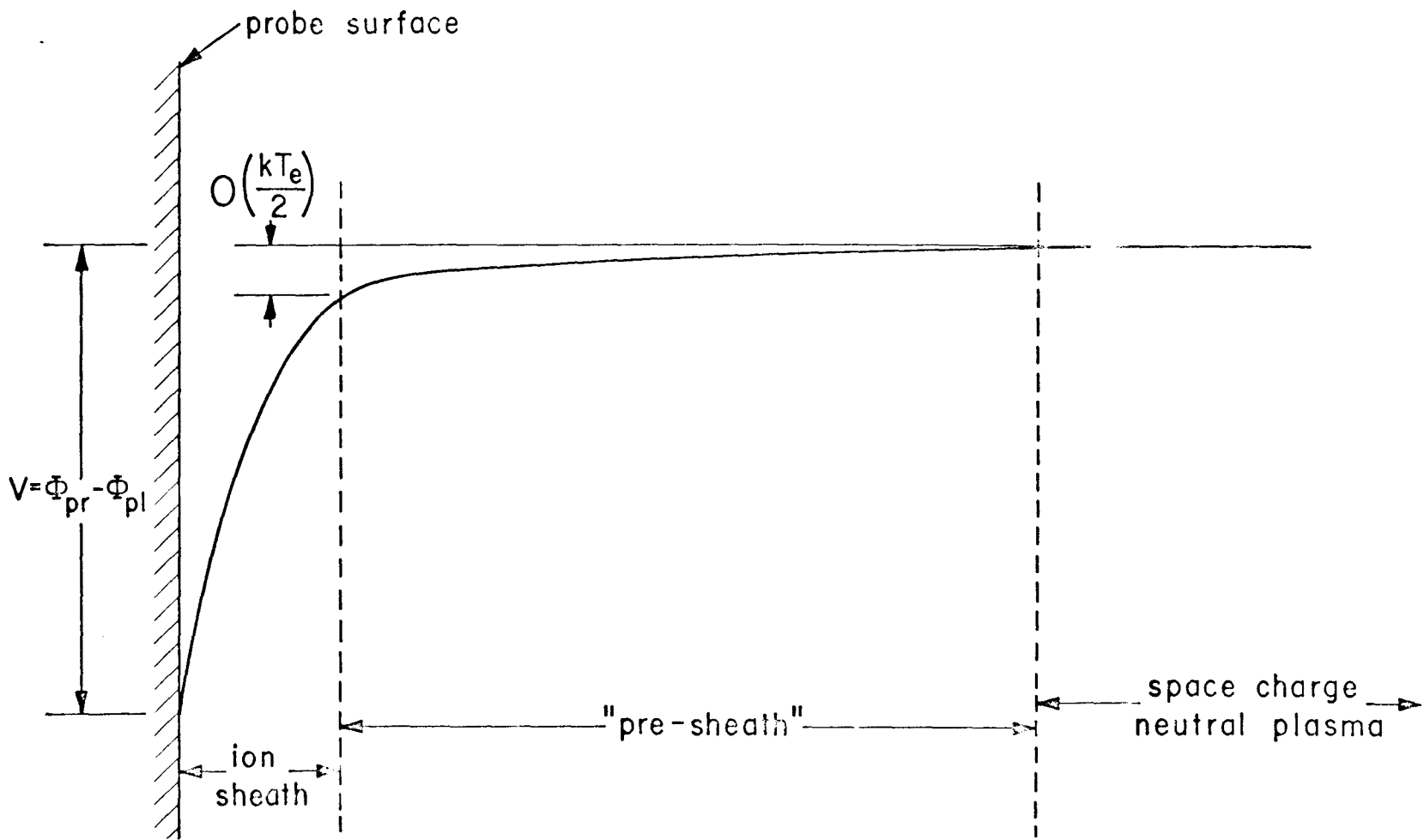
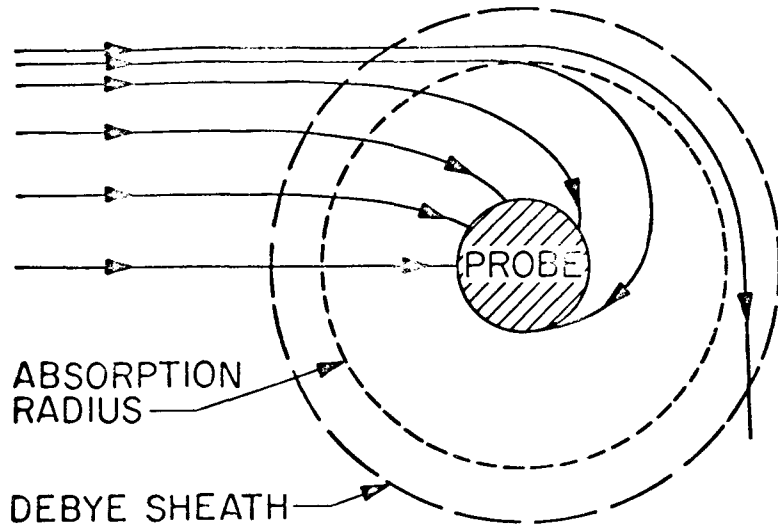


FIG. 2.8 SCHEMATIC OF THE PROBE POTENTIAL FIELD

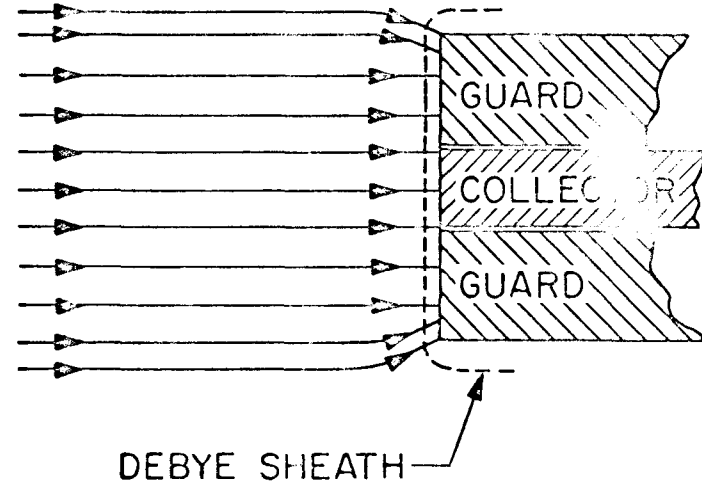
THICK SHEATH



$$I_{\perp} = NeUA_{\perp} \left[1 + \frac{e(\Phi_{pl} - \Phi_{pr})}{\frac{1}{2} m_i U^2} \right]^{1/2}$$

ORBITAL MOTION LIMITED
ION COLLECTION

THIN SHEATH



$$I_{\perp} = NeUA_{\perp}$$

"SWEEP AREA" CONCEPT
ION COLLECTION

FIG. 2.9 ION CURRENT COLLECTION OF LANGMUIR PROBES IN "HYPERSONIC" FLOWING PLASMA

Data 27-(3)-4

Probe position: $z = 45(\text{cm}), r = 0$

Source condition:

$\Phi_D = 60\text{V}$

$\Phi_A = 80\text{V}$

$\Phi_{N.F.} = 20.6\text{V}$

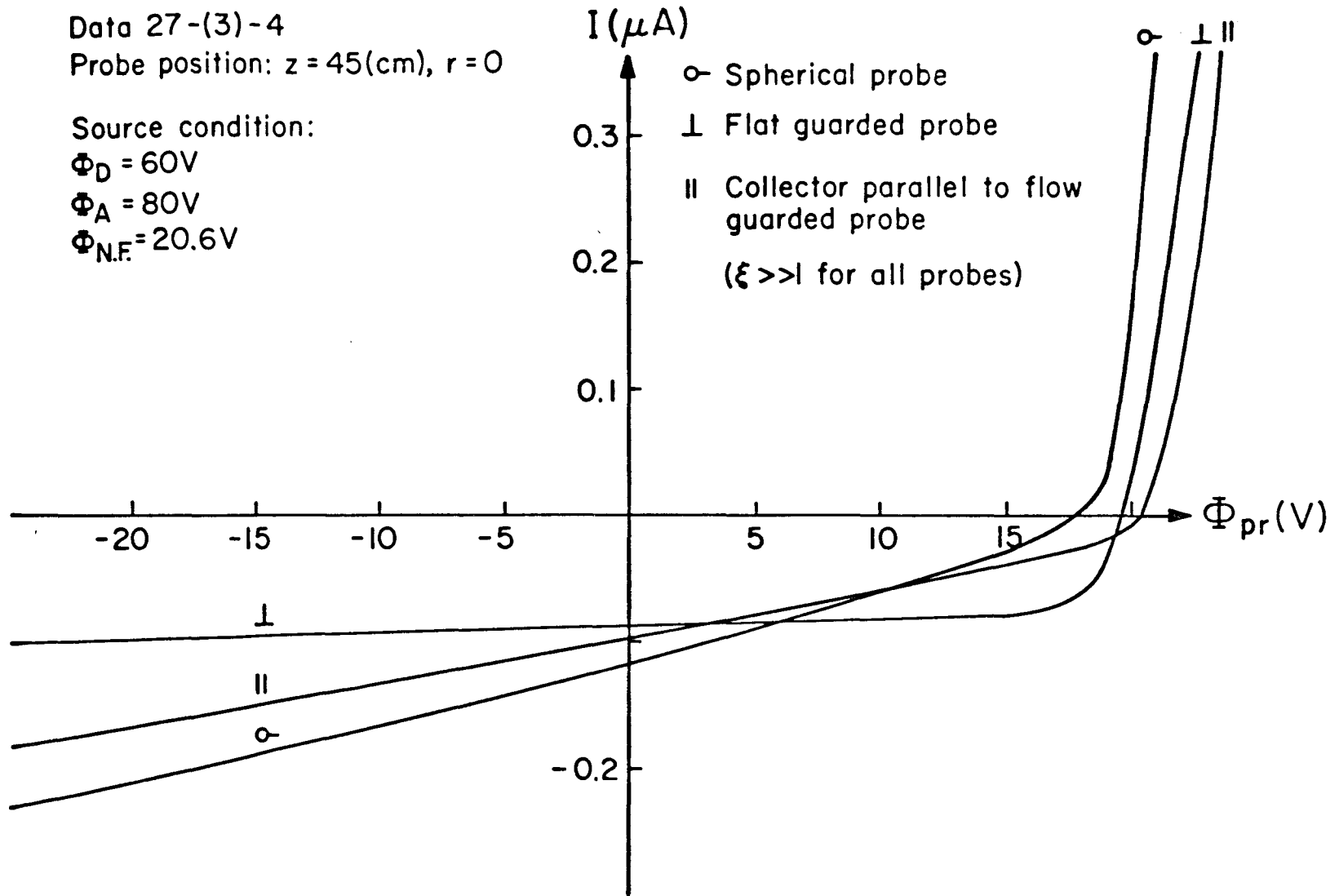


FIG. 2.10 COMPARISON OF PROBE CHARACTERISTICS IN THE THIN SHEATH CASE

Data: 34-2-(6)-2

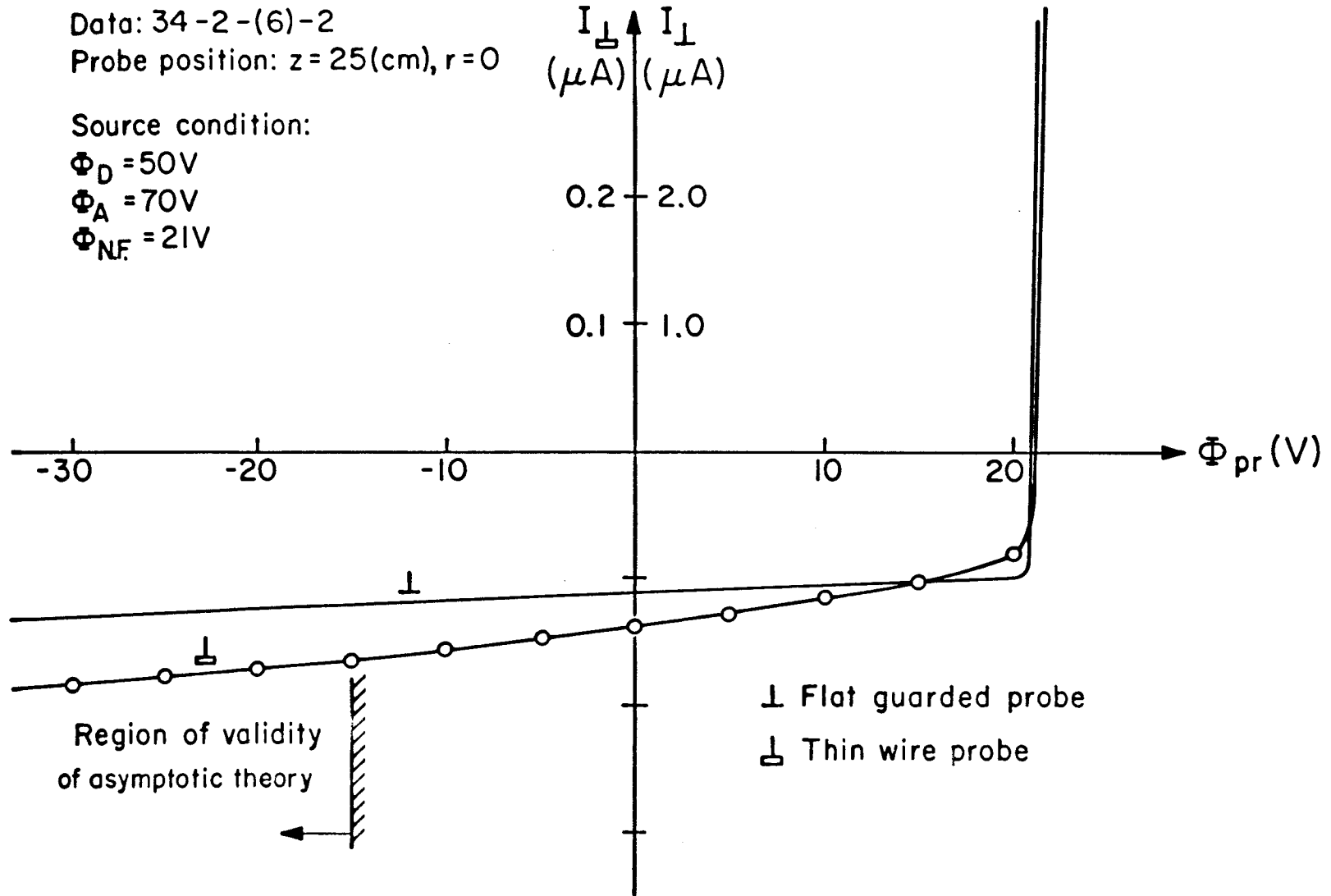
Probe position: $z = 25(\text{cm}), r = 0$

Source condition:

$\Phi_D = 50\text{V}$

$\Phi_A = 70\text{V}$

$\Phi_{NF} = 21\text{V}$



-107-

FIG. 2.11a PROBE CHARACTERISTIC OF FLAT GUARDED PROBE AND THIN WIRE PROBE ($\Phi_{N.F.} = 21\text{V}$)

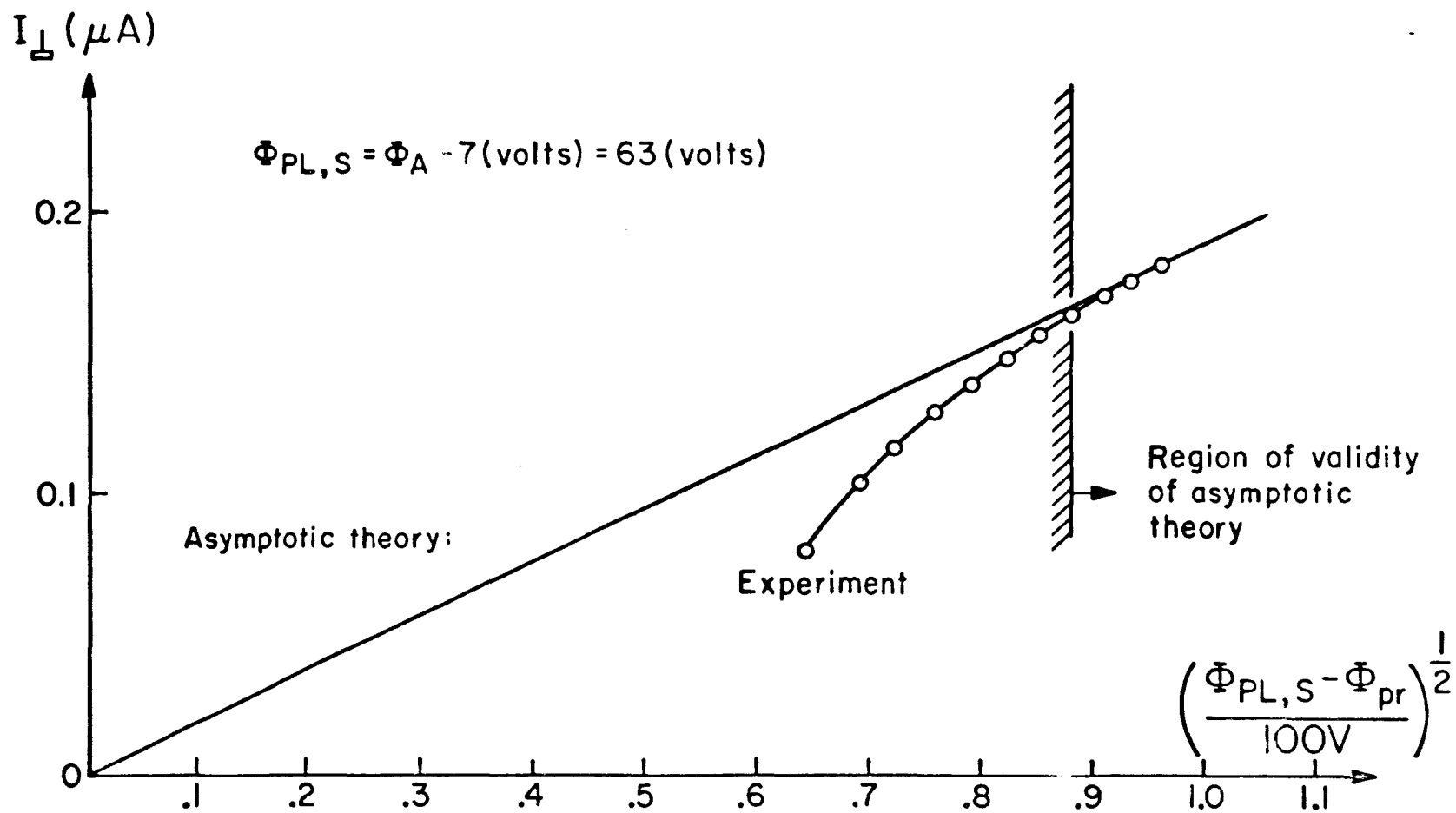


FIG. 2.11b THIN WIRE PROBE ION CURRENT vs. $(\Phi_{PL,S} - \Phi_{pr})^{\frac{1}{2}}$

Data: 34-2-(7)-2

Probe position: $z=25(\text{cm}), r=0$

Source condition:

$\Phi_D = 50\text{V}$

$\Phi_A = 80\text{V}$

$\Phi_{NF} = 31\text{V}$

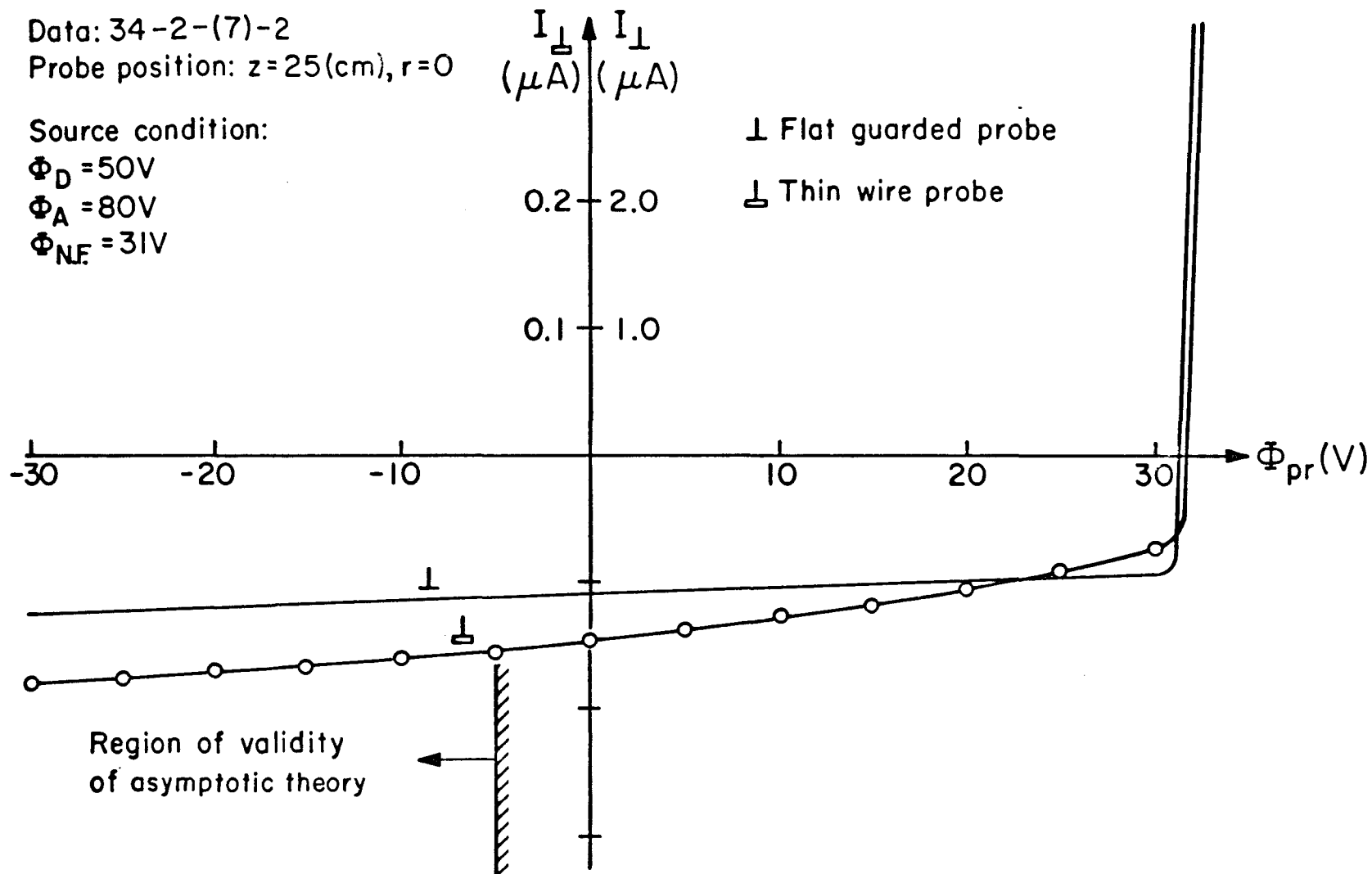


FIG. 2.12a PROBE CHARACTERISTICS OF FLAT GUARDED PROBE AND THIN WIRE PROBE ($\Phi_{N.F.} = 31\text{V}$)

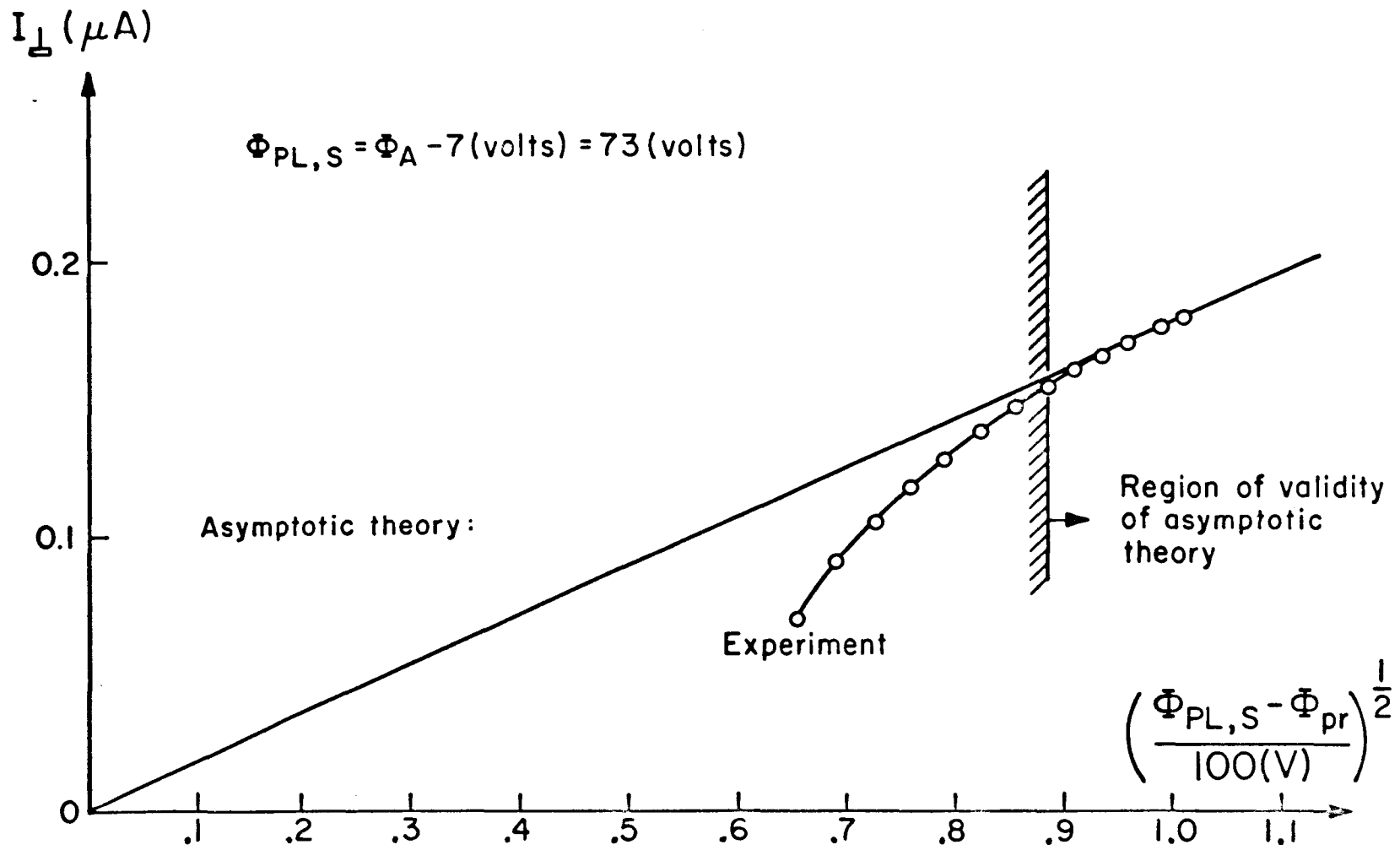


FIG. 2.12b THIN WIRE PROBE ION CURRENT vs. $\left(\frac{\Phi_{PL,S} - \Phi_{pr}}{100(\text{V})} \right)^{\frac{1}{2}}$

Data (8-1)

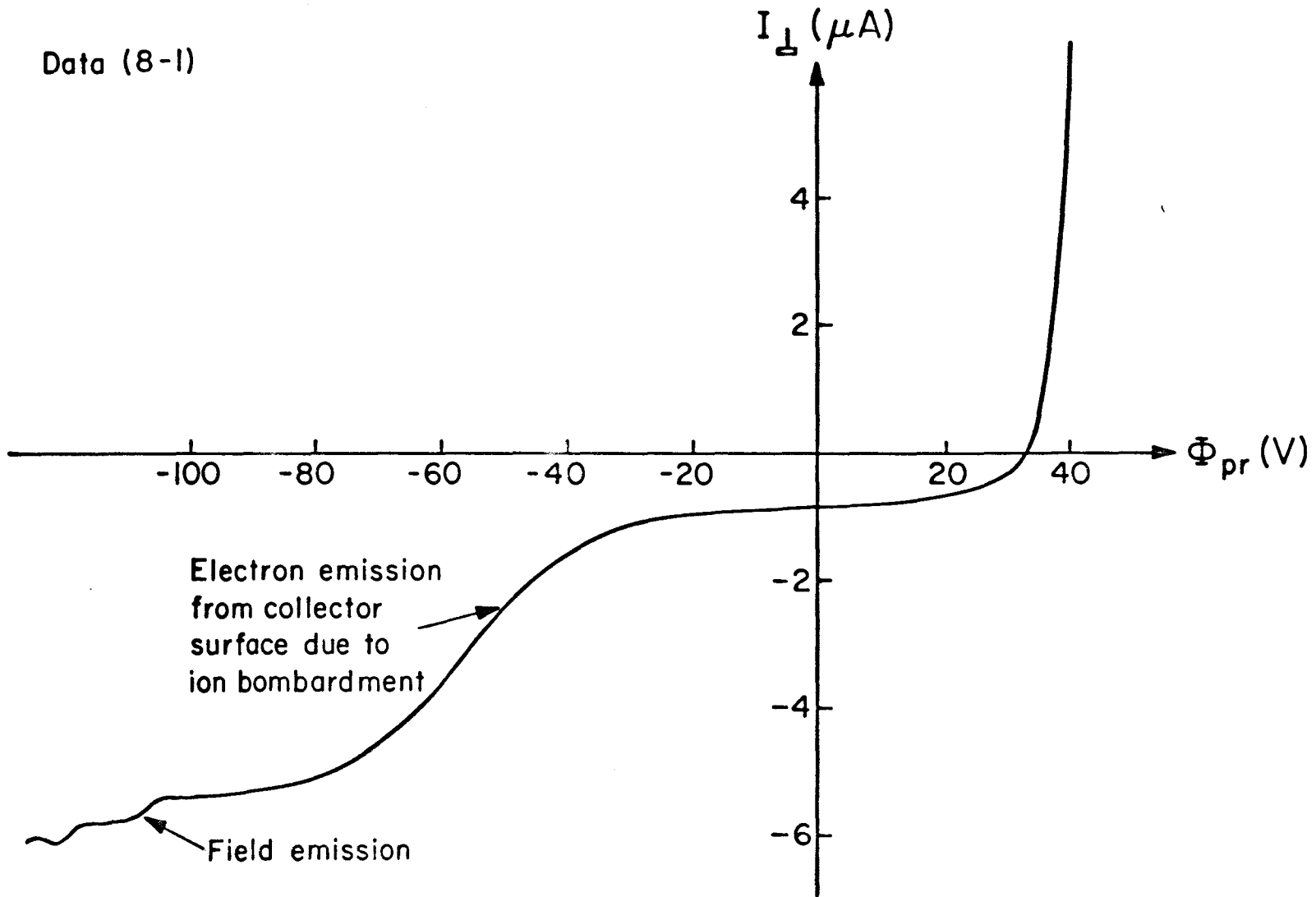


FIG. 2.13 PROBE CHARACTERISTIC OF THIN WIRE PROBE FOR LARGE NEGATIVE PROBE BIAS

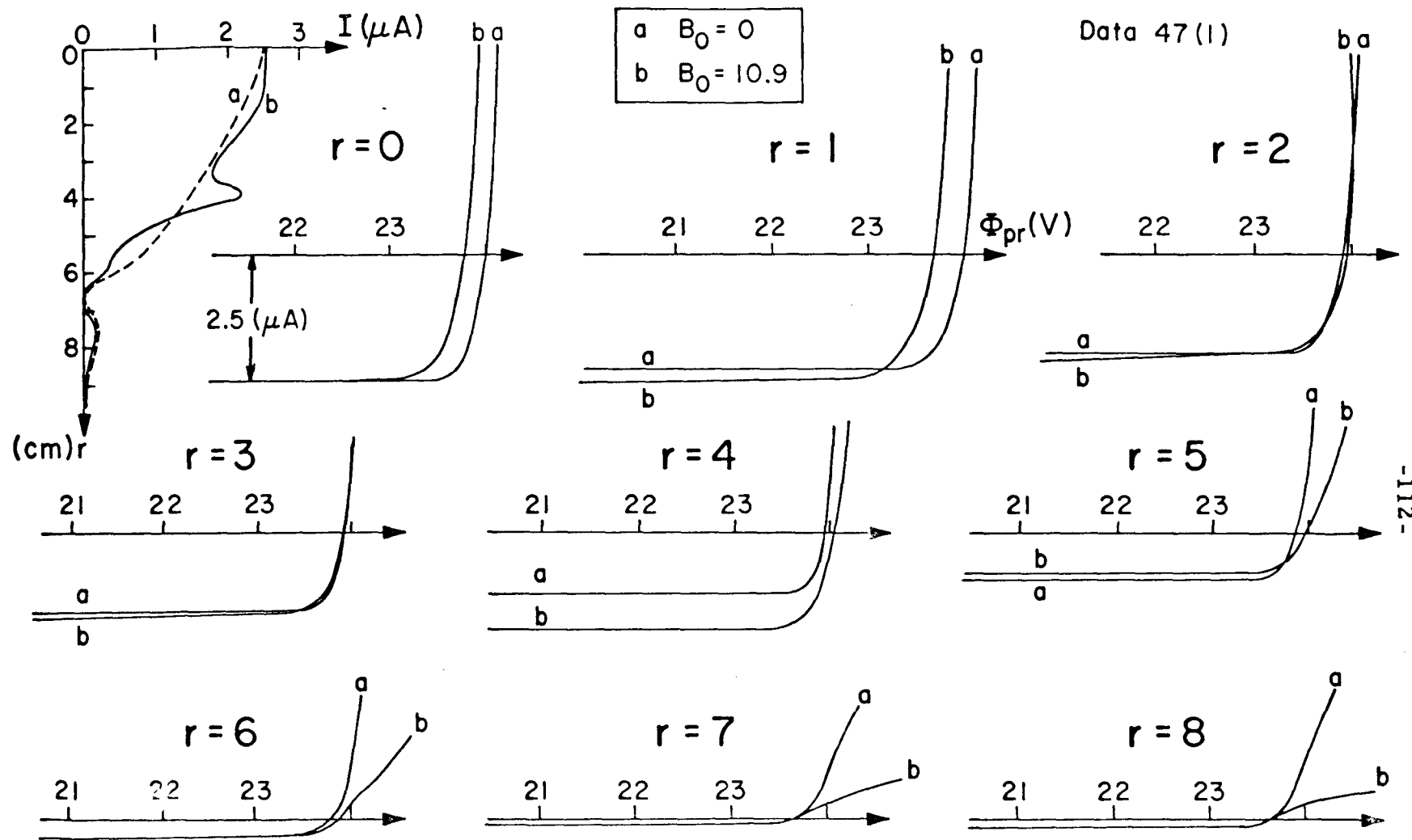
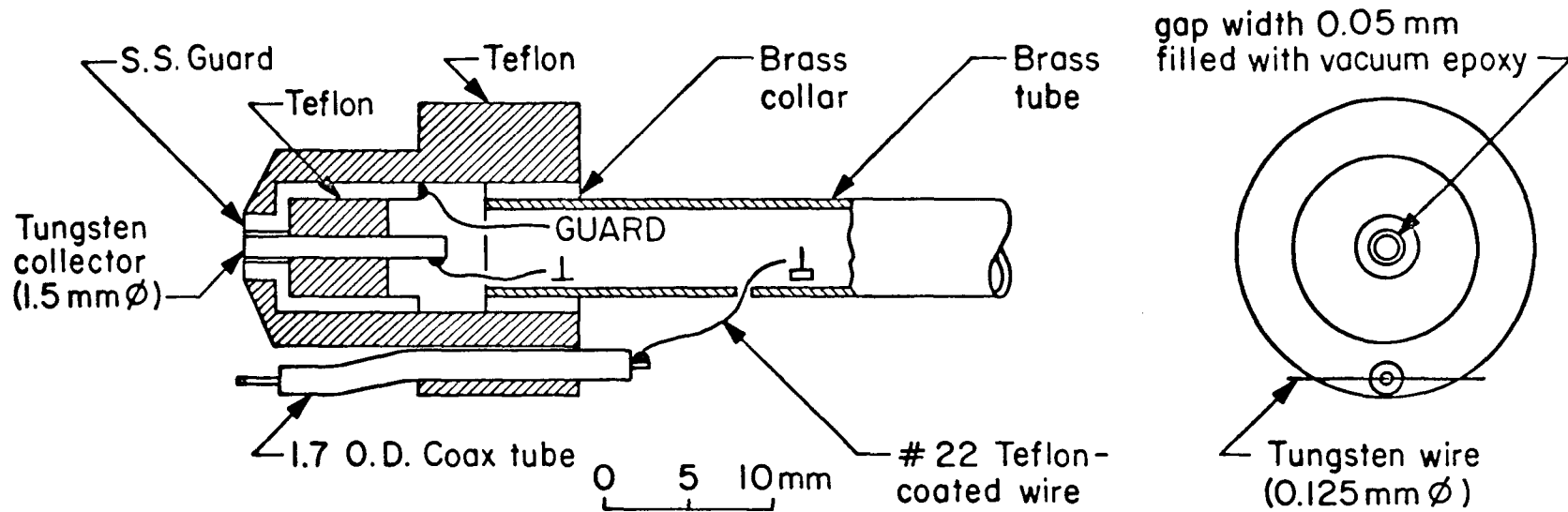


FIG. 2.14 INFLUENCE OF NON-HOMOGENEOUS MAGNETIC FIELD ON THE PROBE CHARACTERISTIC



DETAILS OF PROBE CONSTRUCTION

COLLECTION AREAS

$A_{\perp} = 1.75 \text{ (mm}^2\text{)}$
 $A_{\perp} = 1.44 \text{ (mm}^2\text{)}$

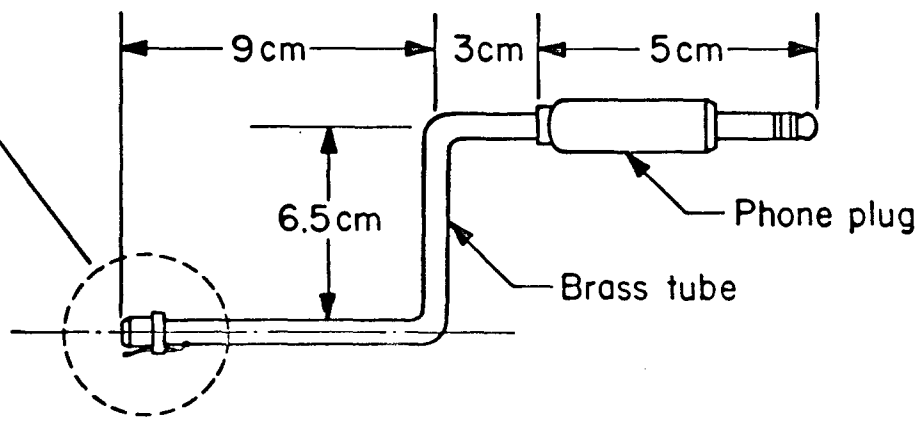


FIG. 2.15 THE HYBRID PROBE

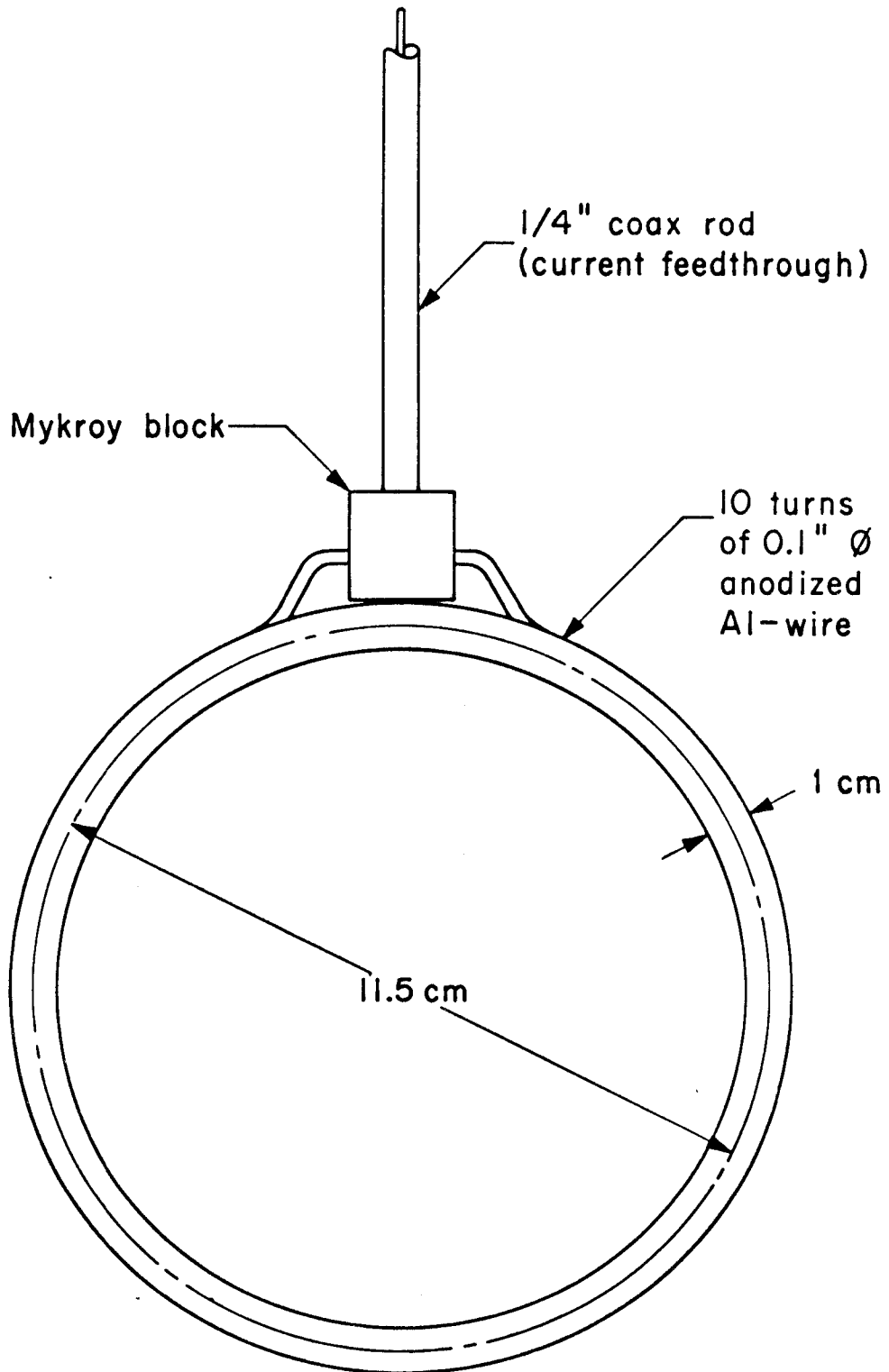


FIG. 2.16 SCHEMATIC OF THE CURRENT LOOP

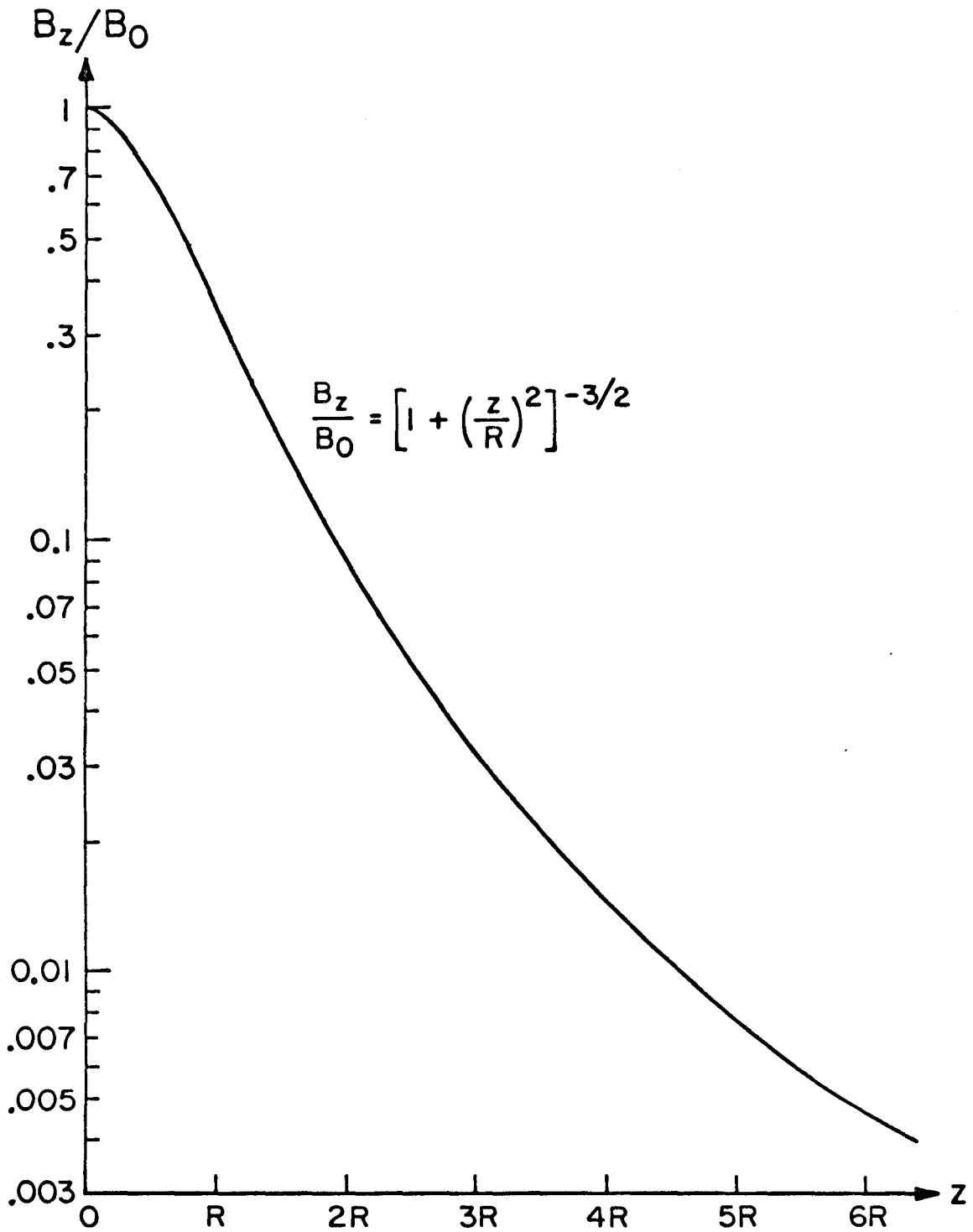


FIG. 2.17 CALIBRATION OF AXIAL FIELD STRENGTH OF CURRENT LOOP

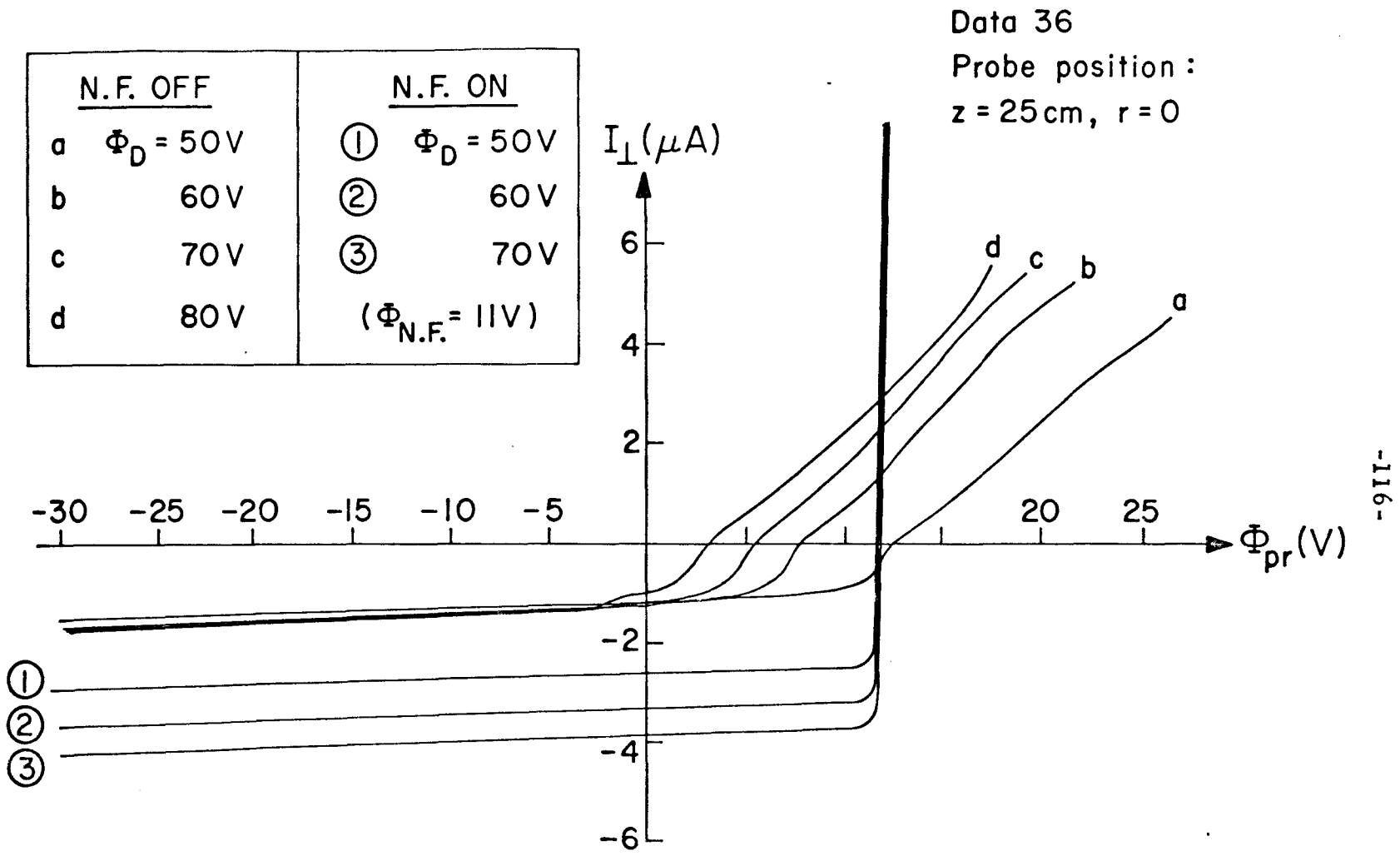


FIG. 3.1 EFFECT OF NEUTRALIZER FILAMENT ON PROBE CHARACTERISTIC

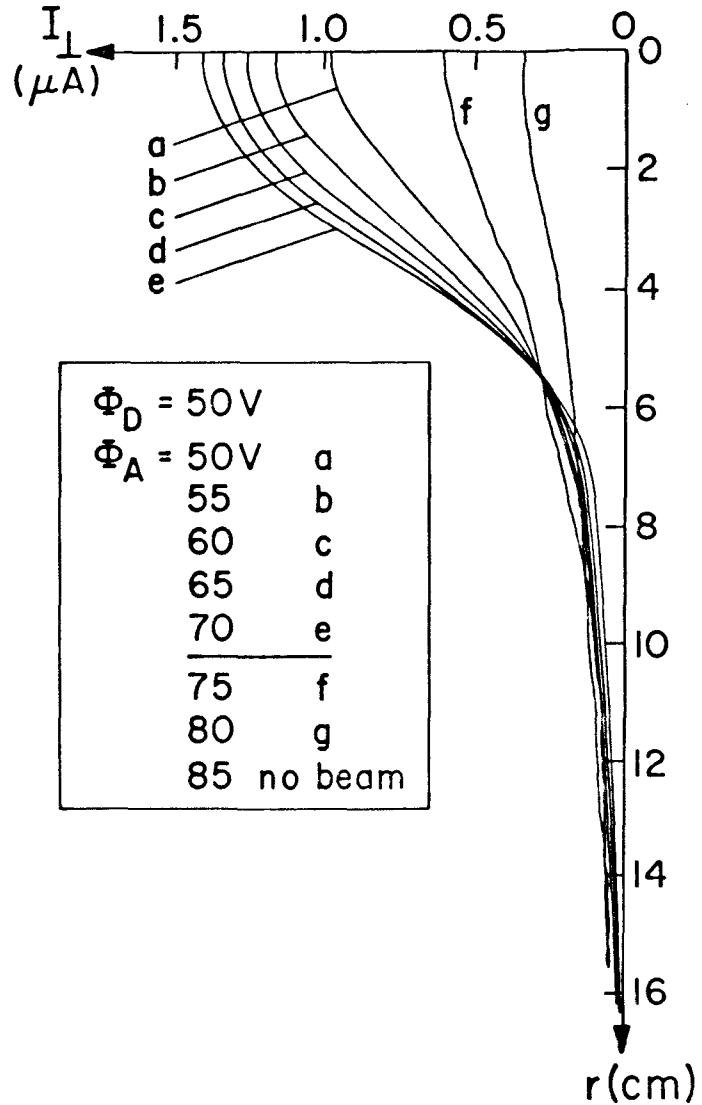
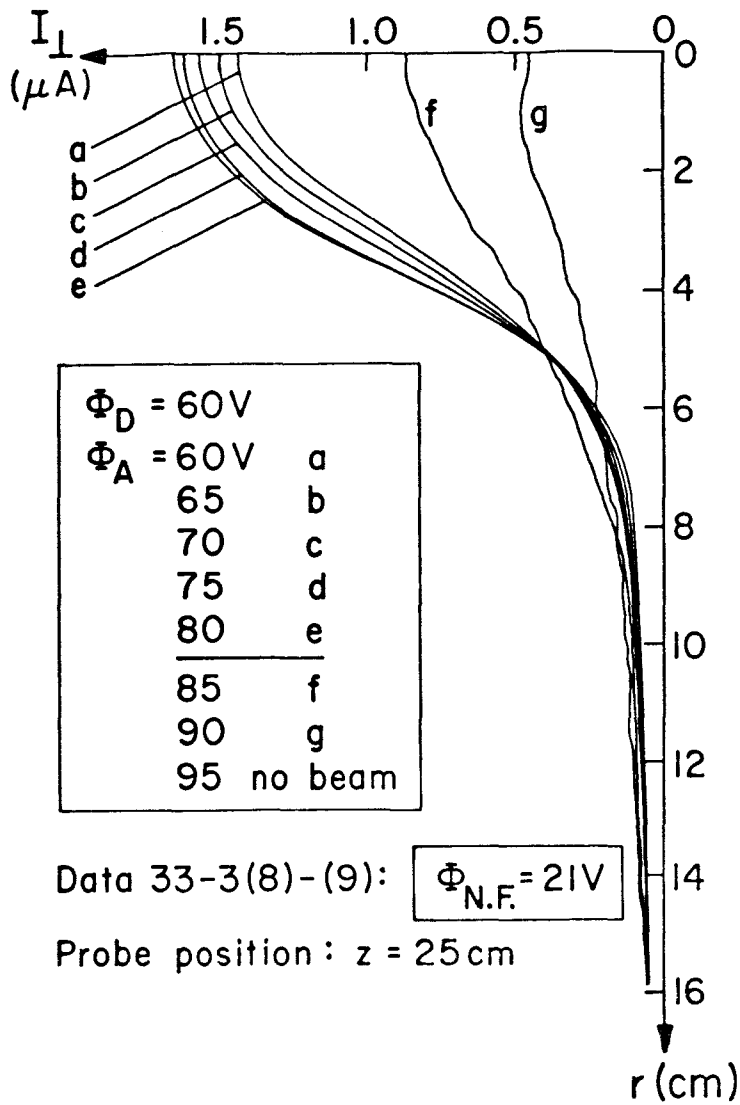


FIG. 3.2a CONDITION FOR "OPTIMUM" PLASMA BEAM: ($\Phi_A - \Phi_D \leq \Phi_{N.F.}$)
 $\Phi_{N.F.} = 21V$

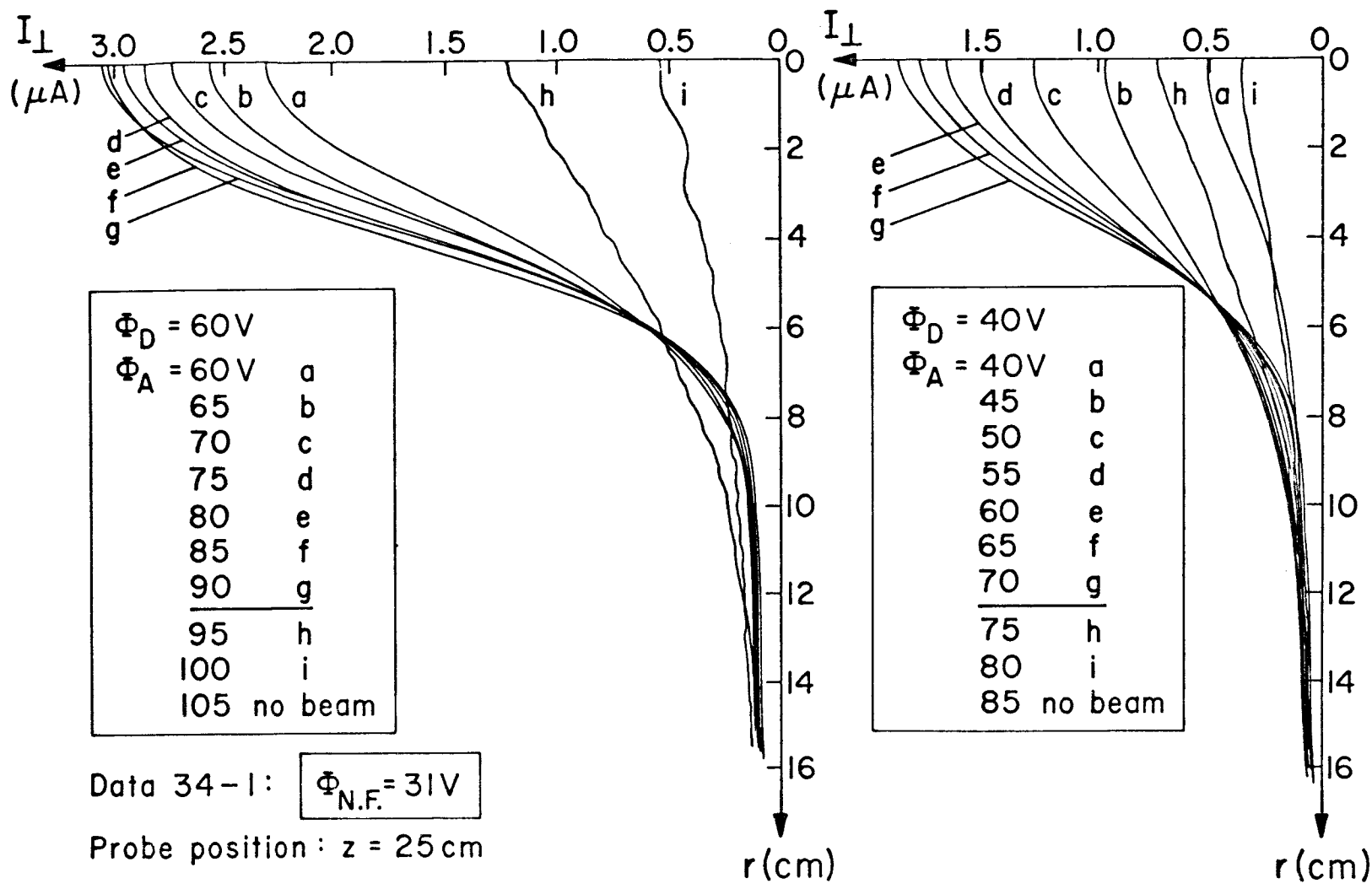


FIG. 3.2b CONDITION FOR "OPTIMUM" PLASMA BEAM: ($\Phi_A - \Phi_D \leq \Phi_{N.F.}$)
 $\Phi_{N.F.} = 31V$

Data 38-3

$\Phi_D = 40V$

$\Phi_A = 60V$

$\Phi_{N.F.} = 24V$

Probe position:

$z = 26 \text{ cm}, r = 0$

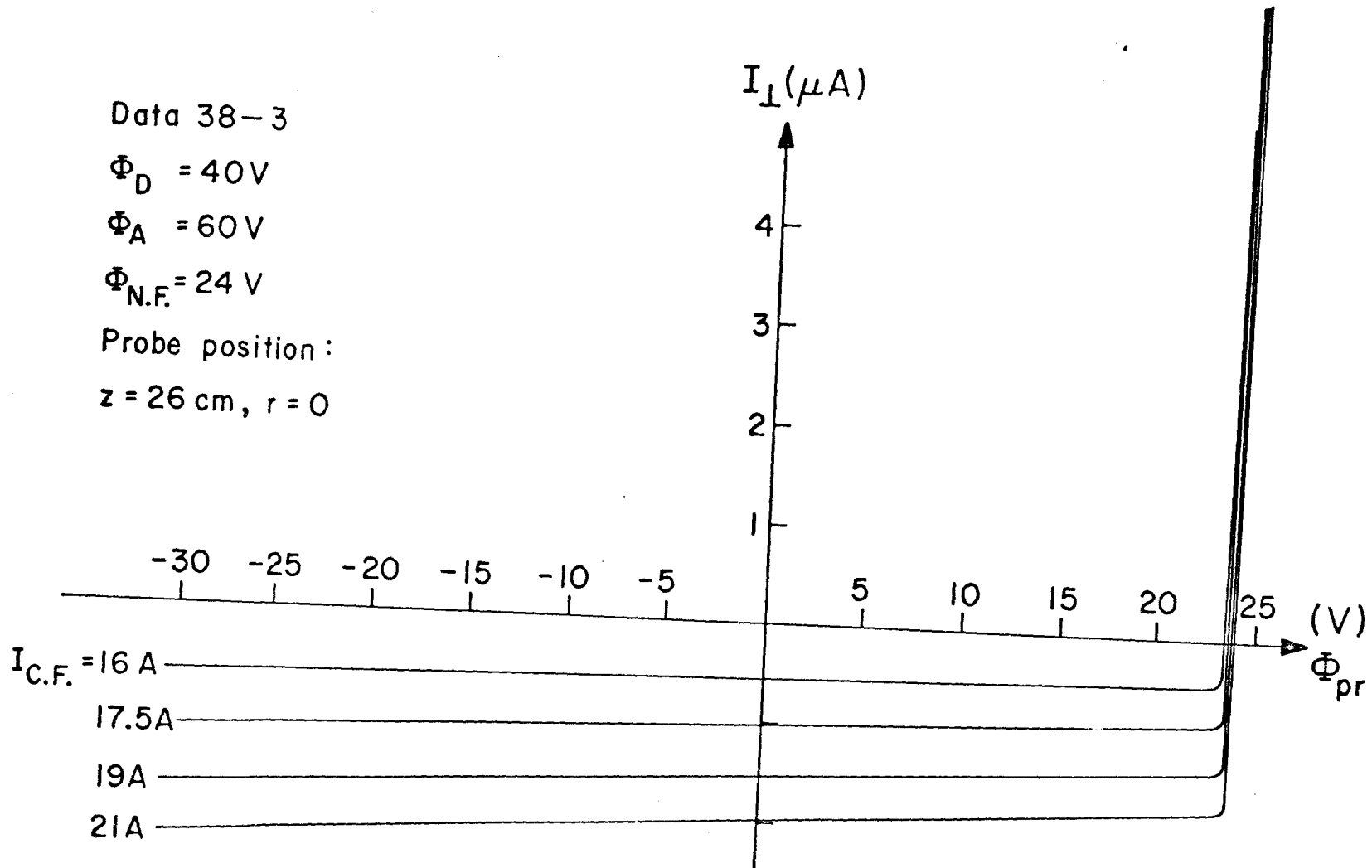


FIG. 3.3 EFFECT OF NEUTRALIZER FILAMENT BIAS ON FLOATING POTENTIAL (VARIABLE CATHODE FILAMENT CURRENT)

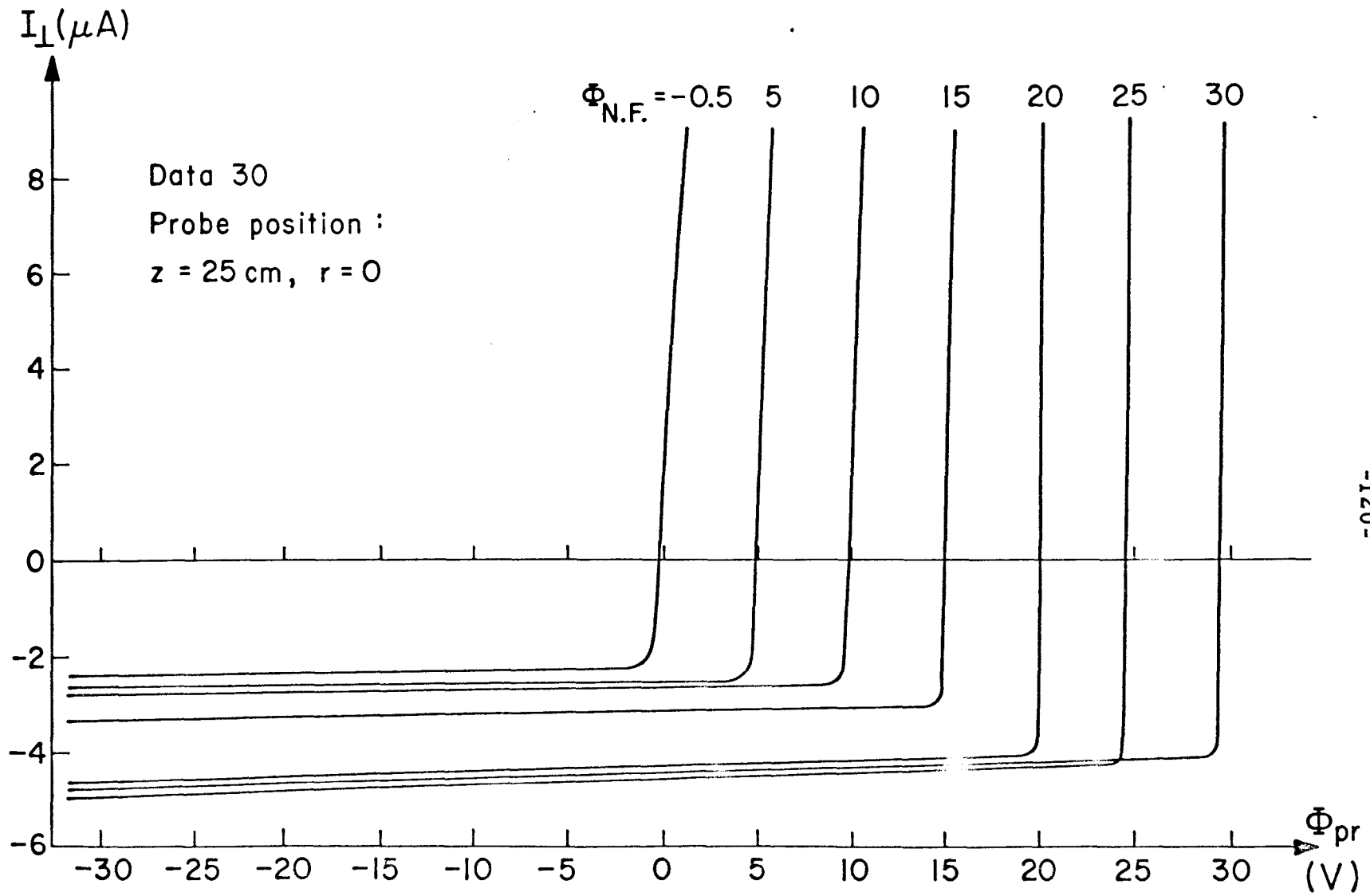


FIG. 3.4 EFFECT OF NEUTRALIZER FILAMENT BIAS
 ON FLOATING POTENTIAL (VARIABLE $\Phi_{N.F.}$)

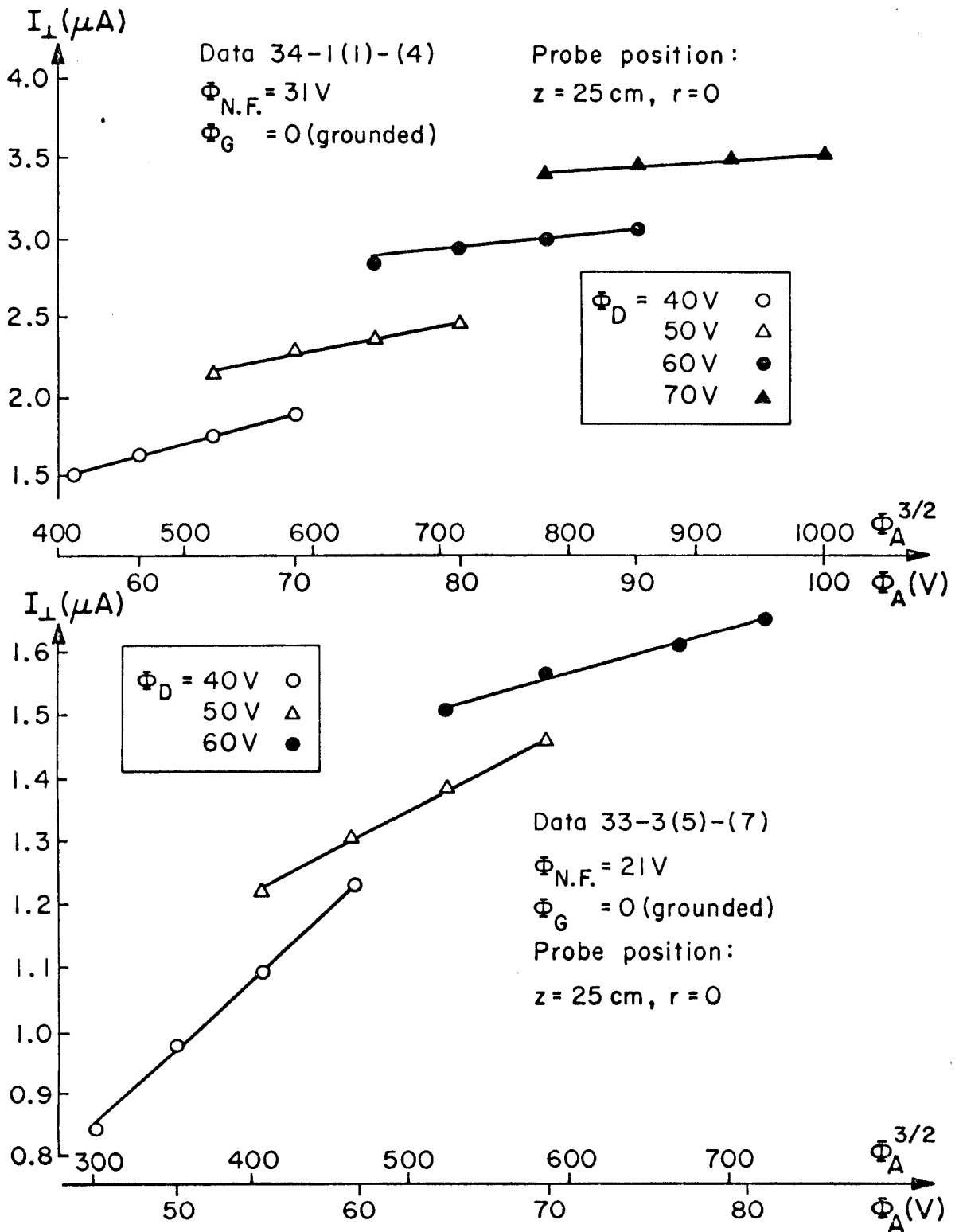


FIG. 3.5 EFFECT OF SOURCE ANODE POTENTIAL ON BEAM ION CURRENT

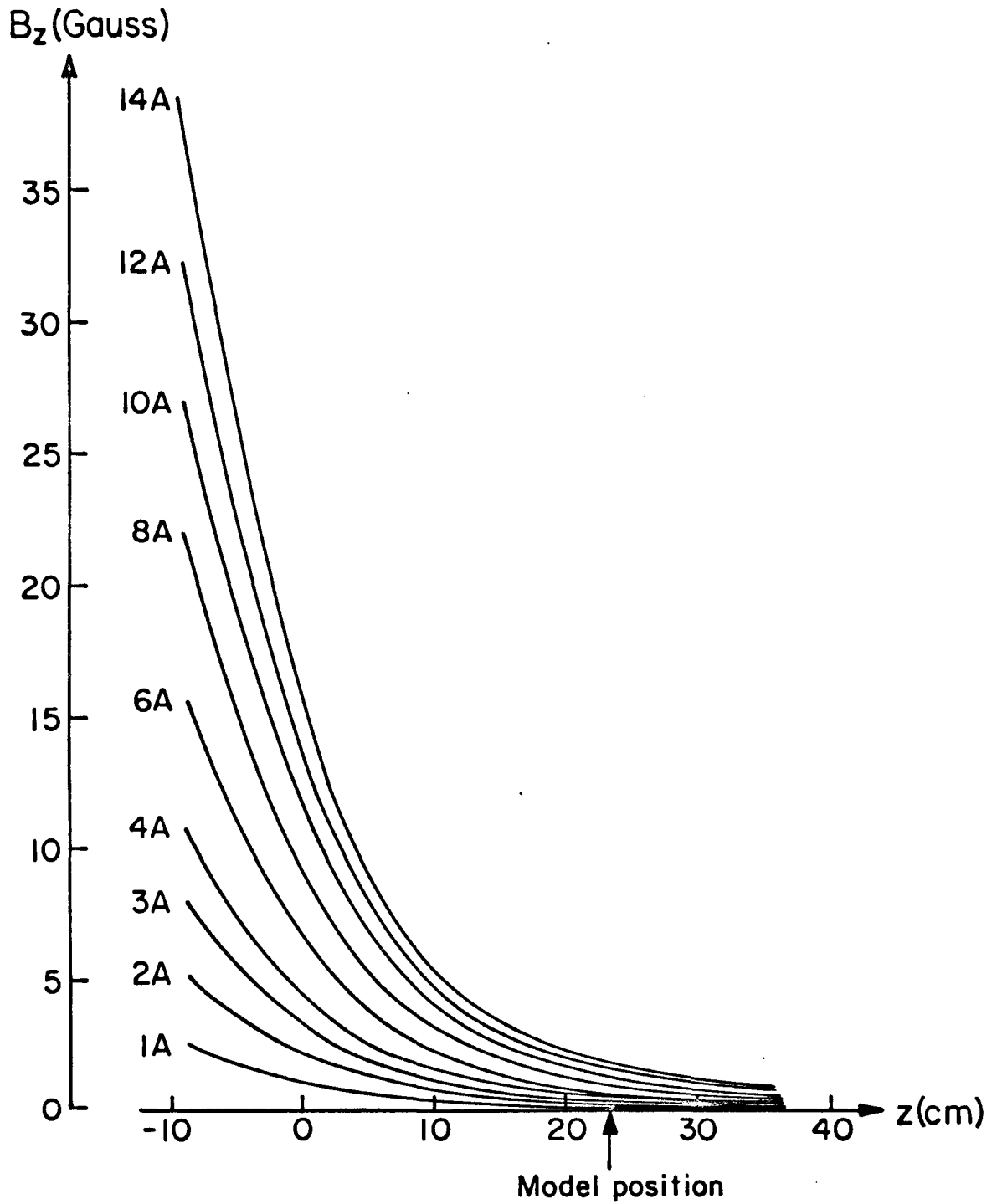


FIG. 3.6 AXIAL FIELD OF THE CONFINING MAGNET
IN THE TEST SECTION

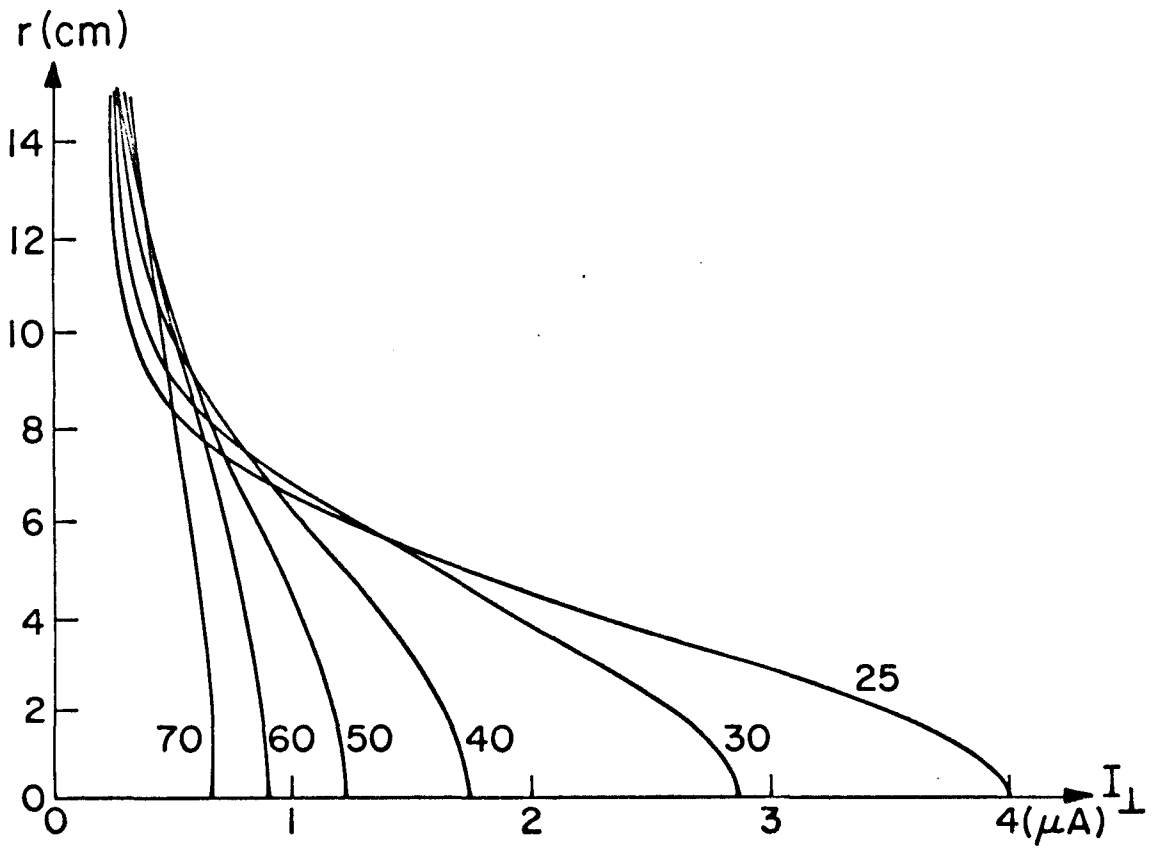
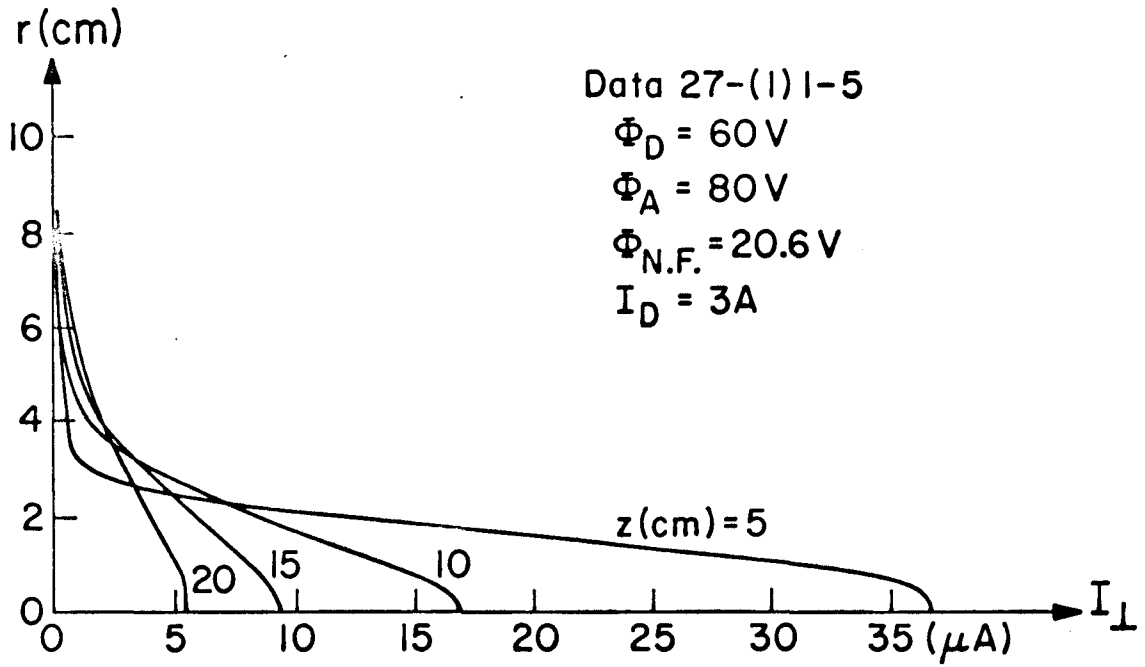


FIG. 3.7 RADIAL PROFILES OF PROBE ION CURRENT

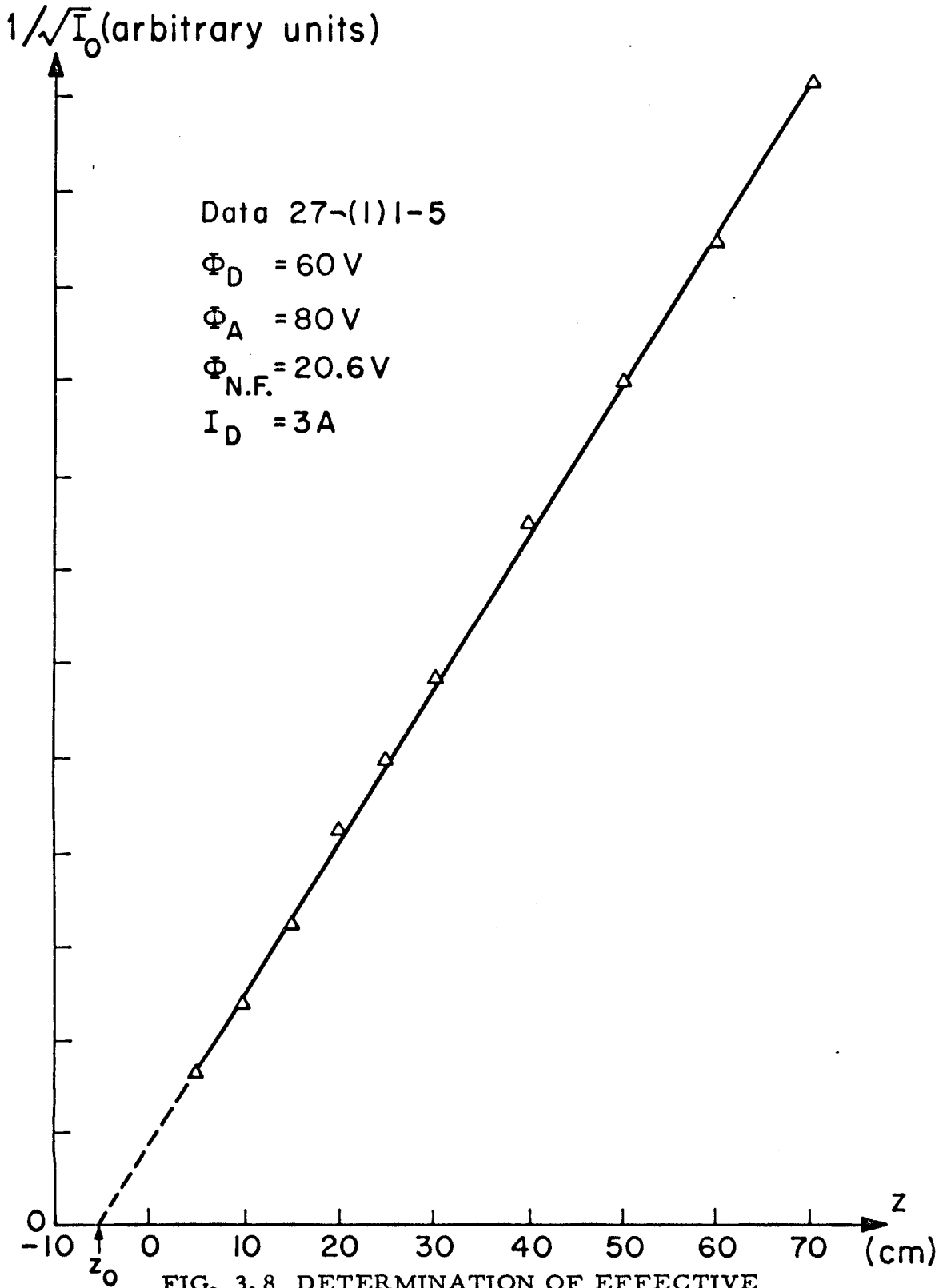


FIG. 3.8 DETERMINATION OF EFFECTIVE ORIGIN OF SOURCE-LIKE FLOW

$I_{\perp}[(z-z_0)^2+r^2]$ (arbitrary units)

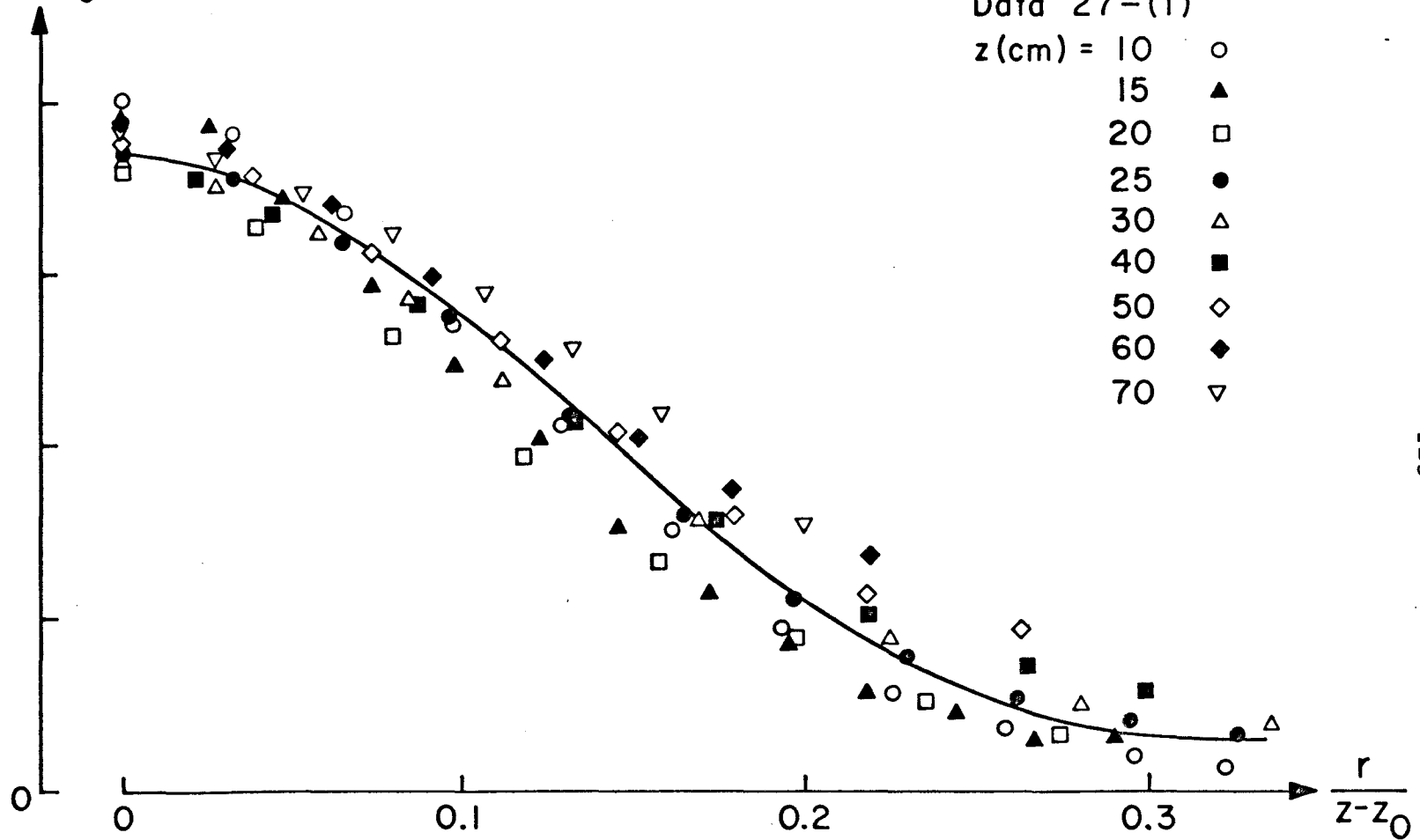


FIG. 3.9 SOURCE-LIKE NATURE OF FLOW

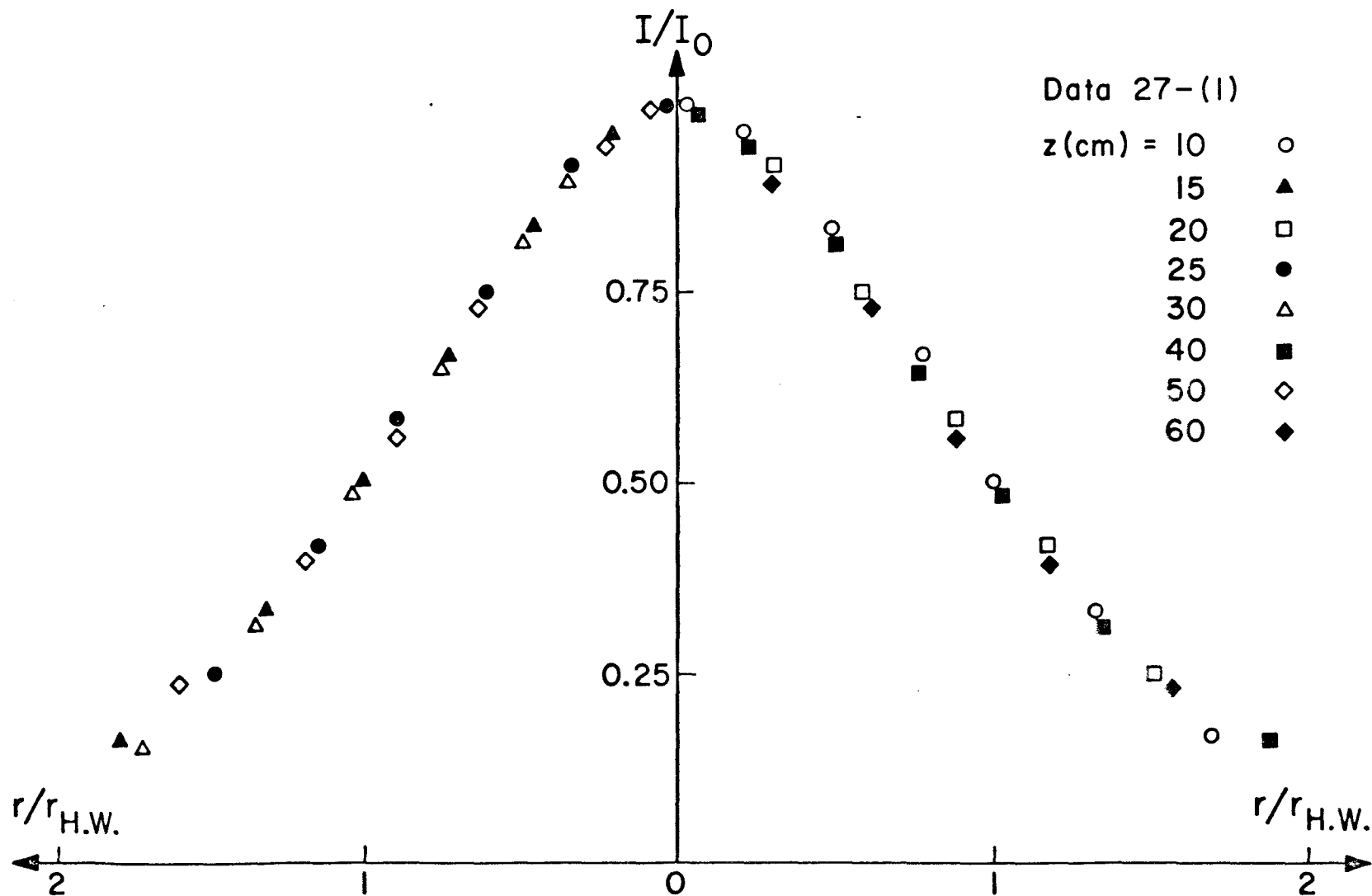


FIG. 3.10 "SIMILARITY" OF PROFILES

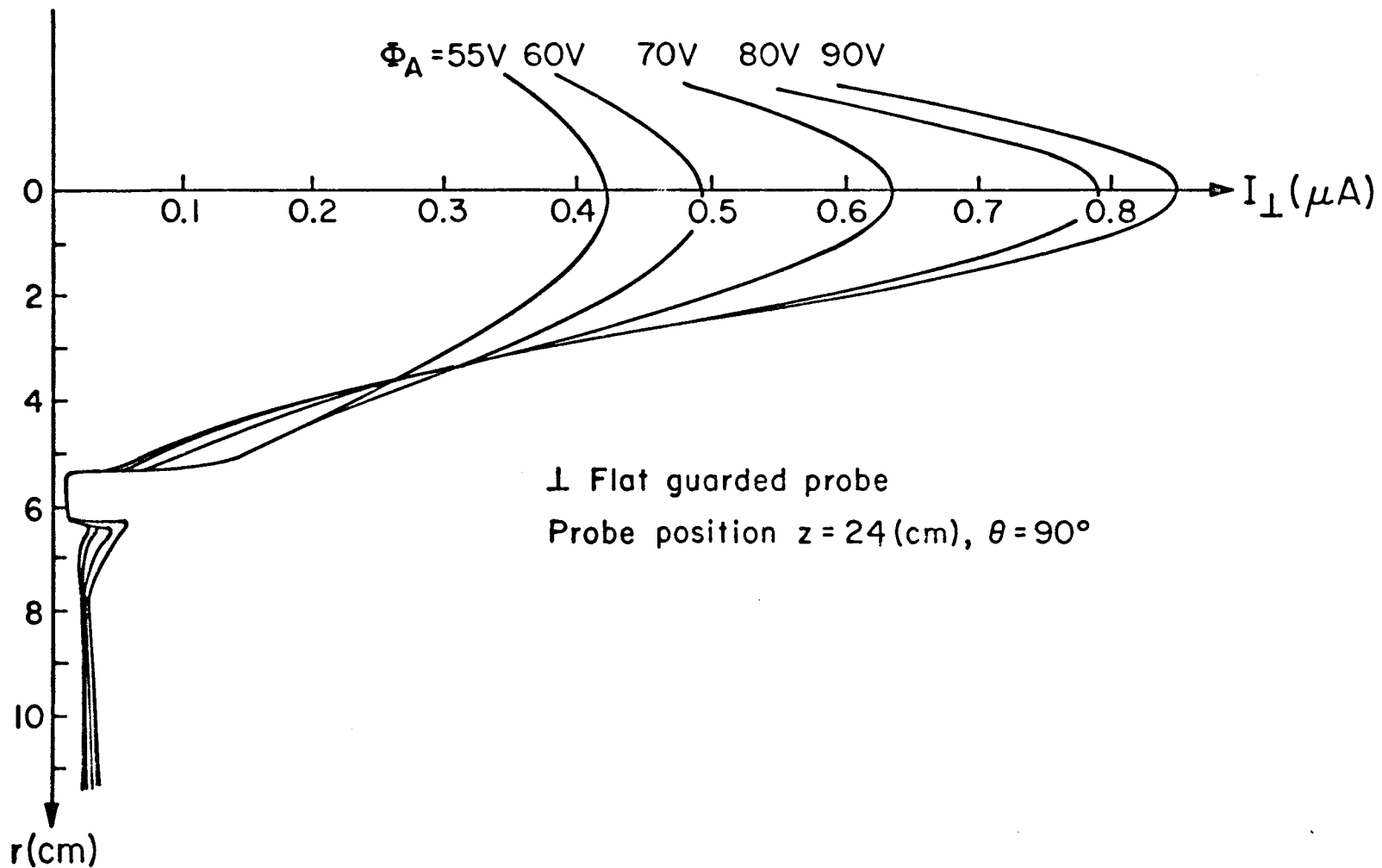


FIG. 3.11 EFFECT OF ANODE POTENTIAL ON BEAM SPREAD
 AND BLOCKING EFFECT OF MODEL

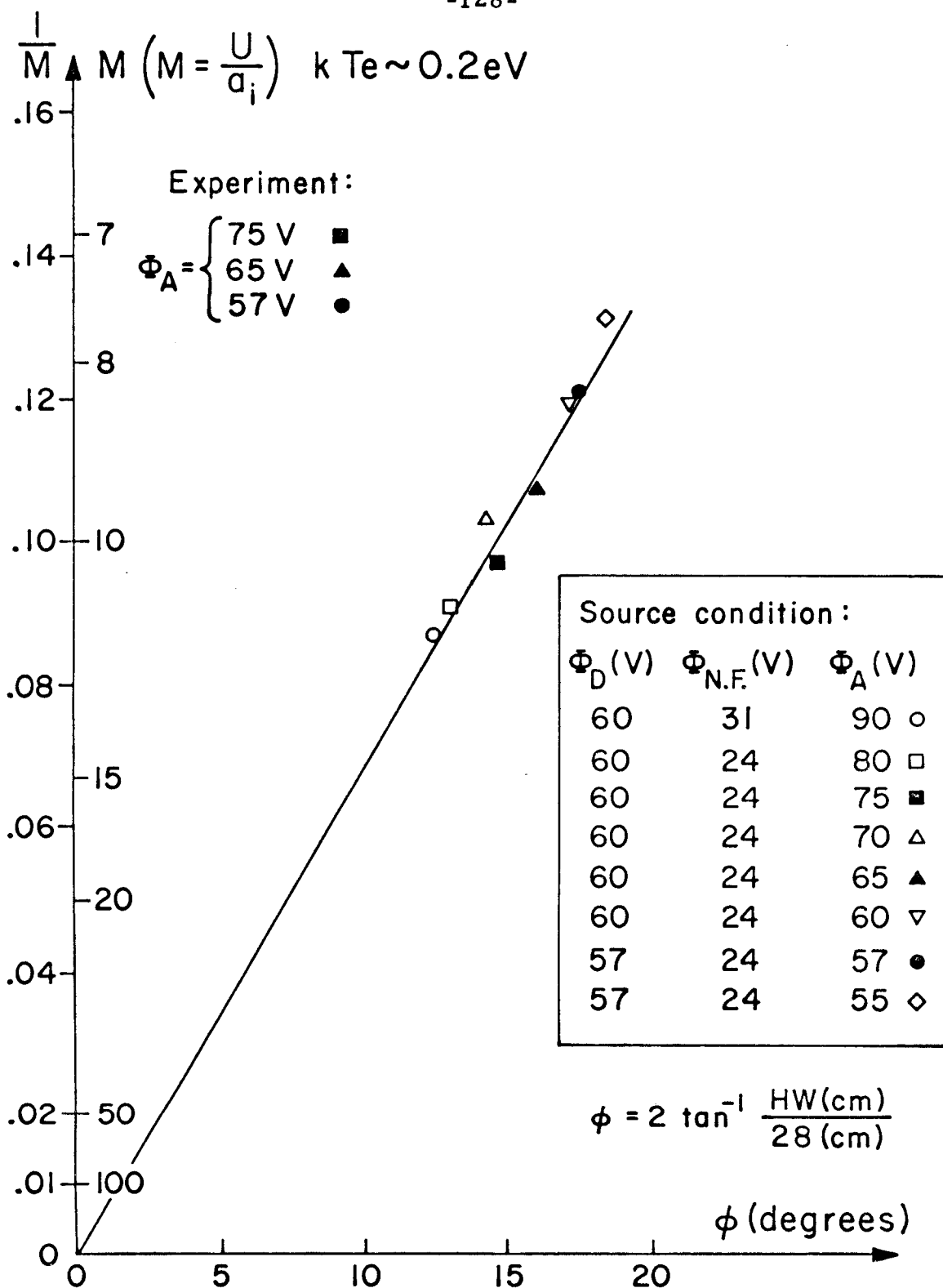
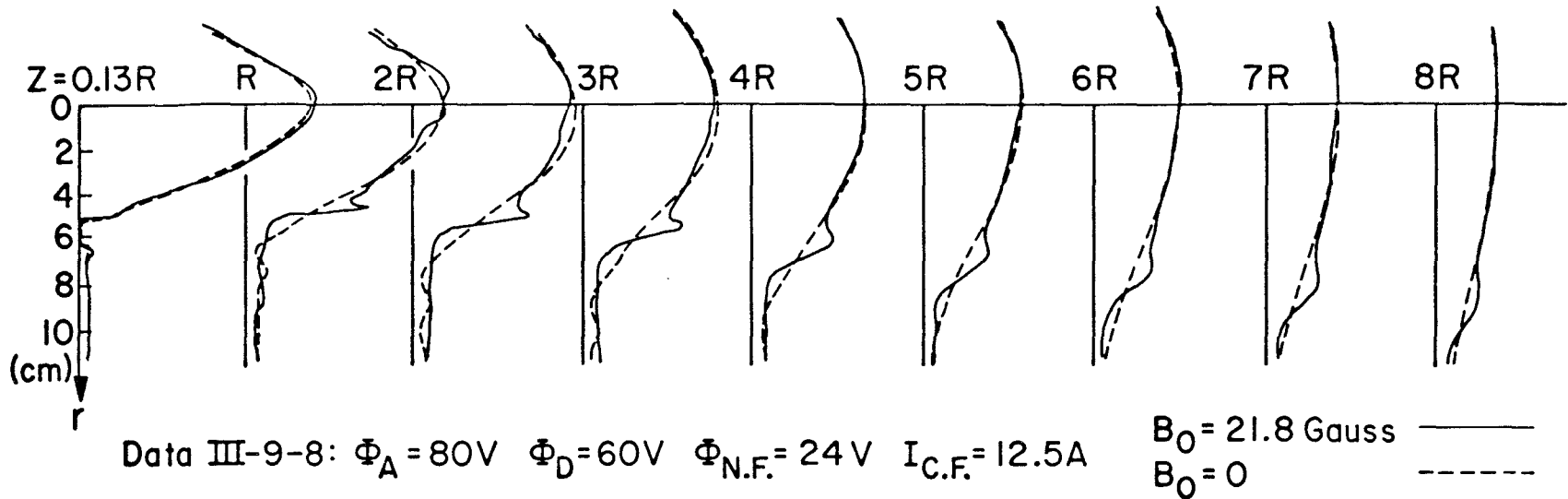


FIG. 3.12 BEAM SPREAD vs. MACH NUMBER

Radial Profiles of Flat Guarded Probe



Radial Profiles of Thin-Wire Probe

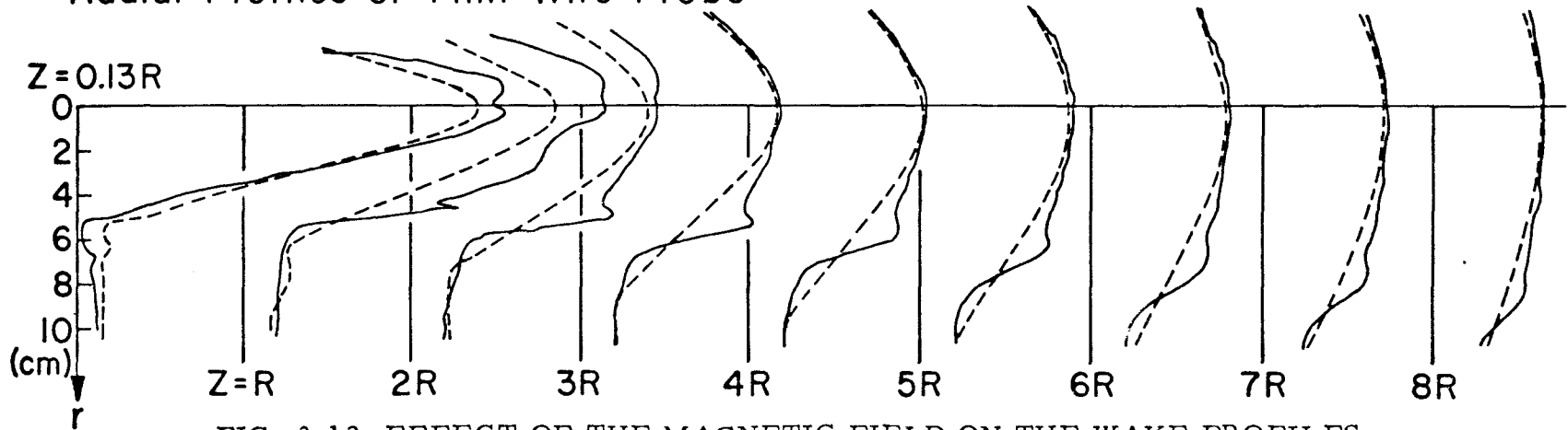


FIG. 3.13 EFFECT OF THE MAGNETIC FIELD ON THE WAKE PROFILES

Data 41-2-1 $\Phi_A = 80V$ $\Phi_D = 60V$ $\Phi_{N.F.} = 24V$

$B_0 = 10.9$ Gauss ———
 $B_0 = 0$ - - - - -

Radial Profiles of Flat Guarded Probe ($A_{\perp} = 18.8 \text{ mm}^2$)

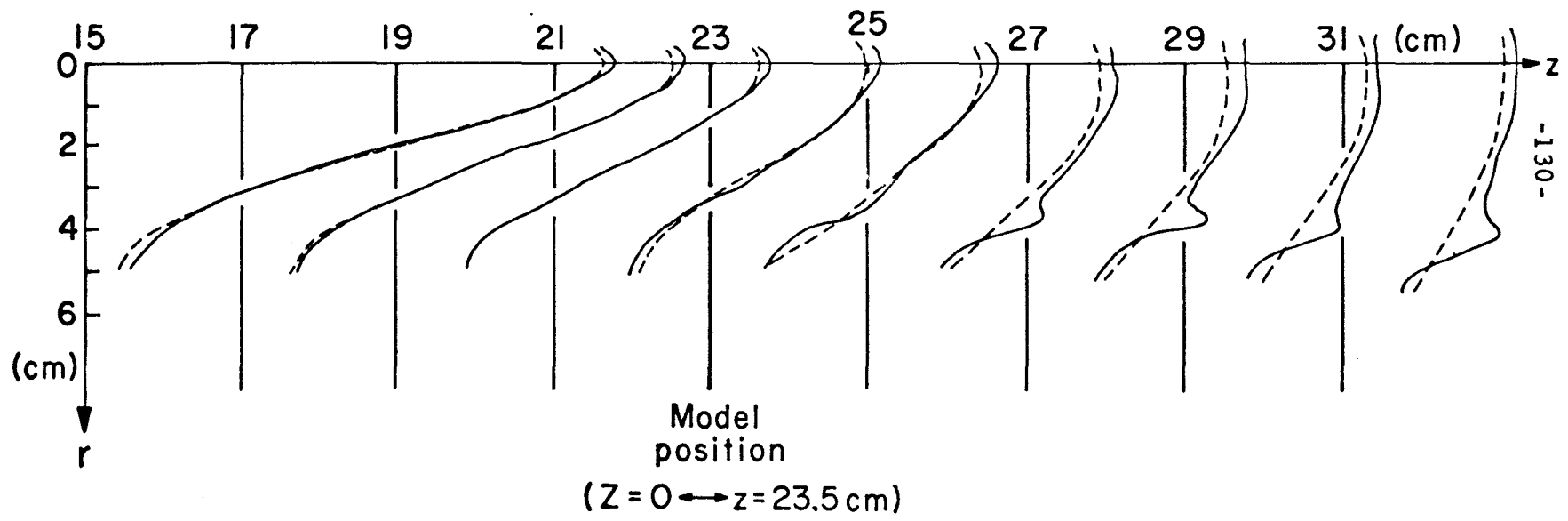


FIG. 3.14 UPSTREAM PROFILES

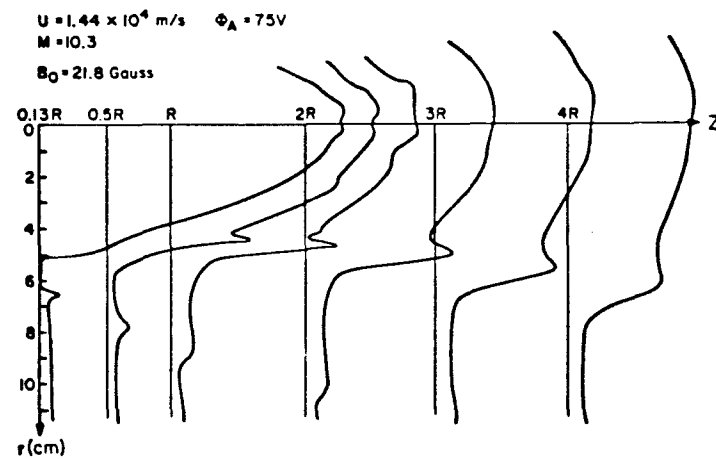
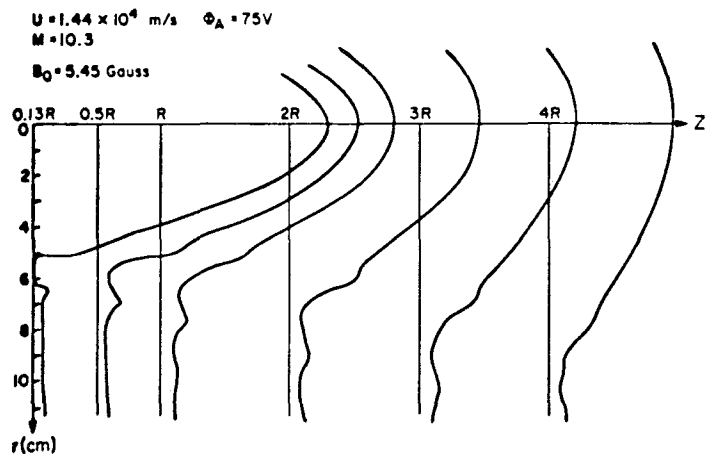
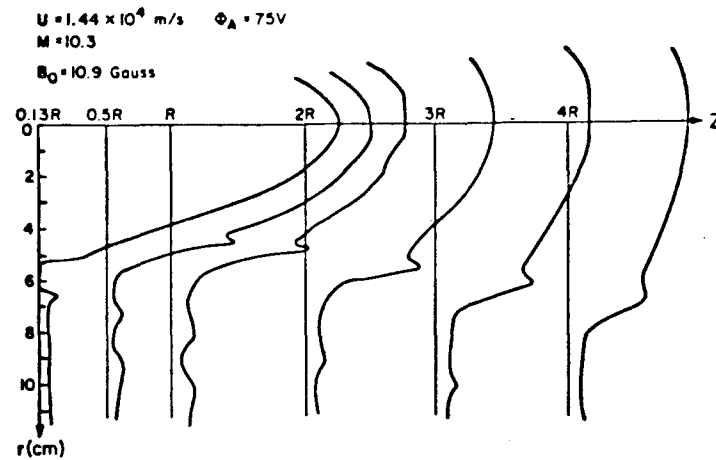
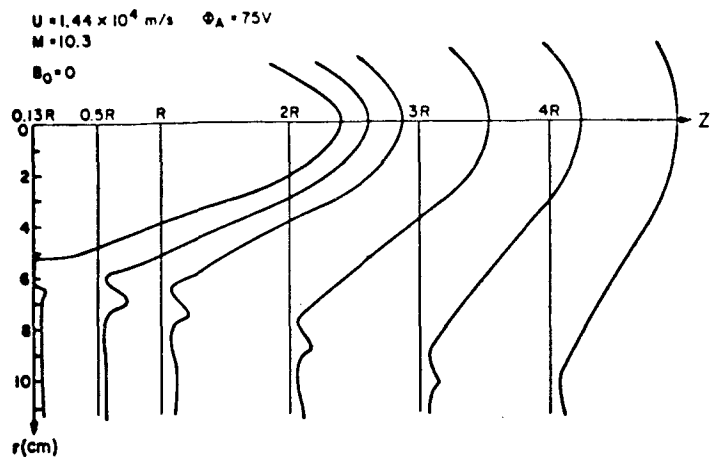


FIG. 3.15a "PINCH" EFFECT IN THE NEAR WAKE ($M = 10.35$)

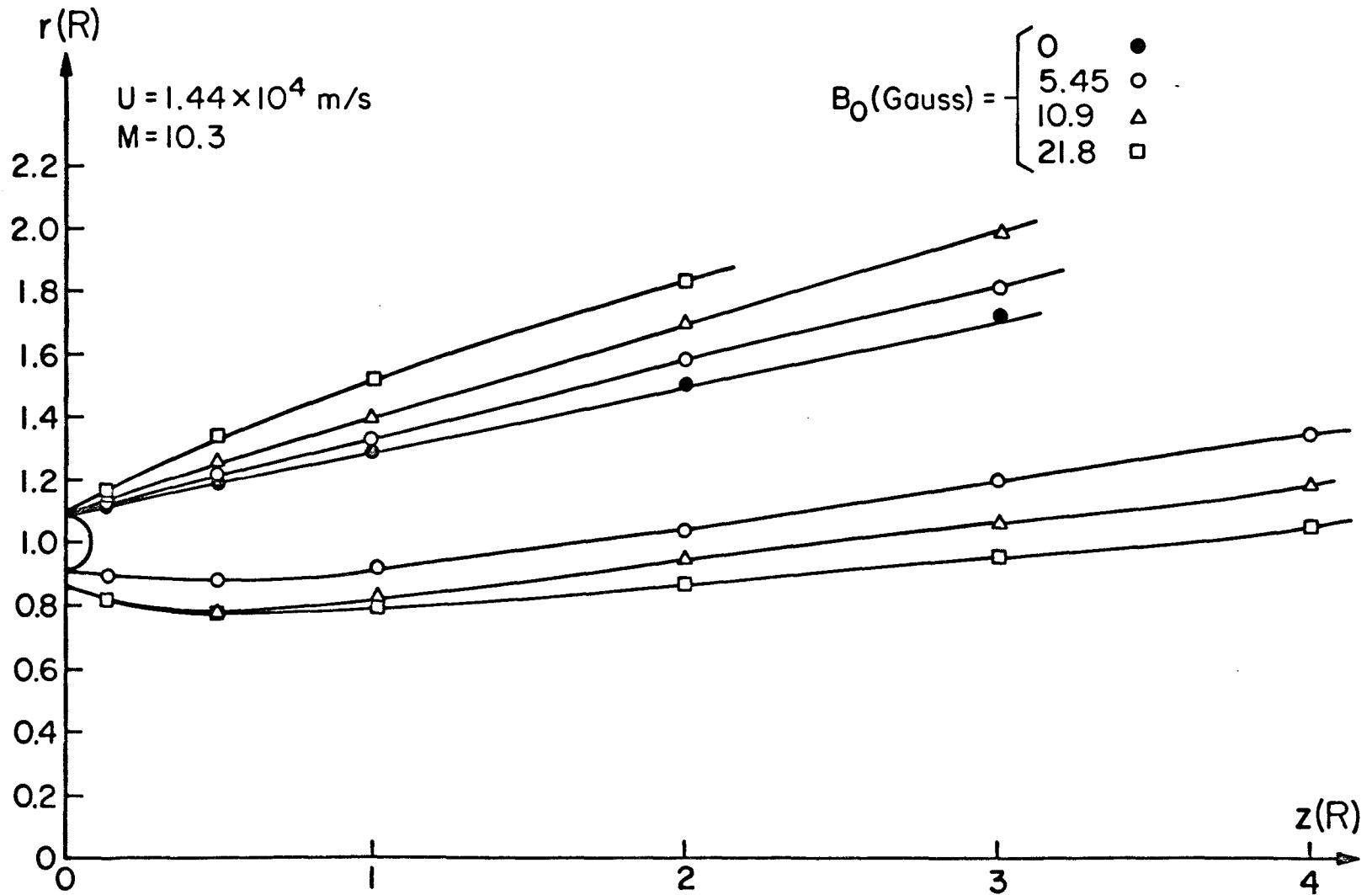


FIG. 3.15b POSITION OF THE ION DENSITY "PEAK" ($M = 10.35$)

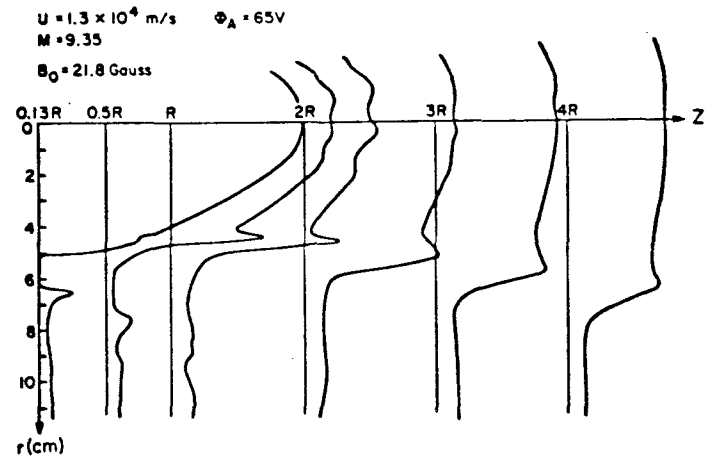
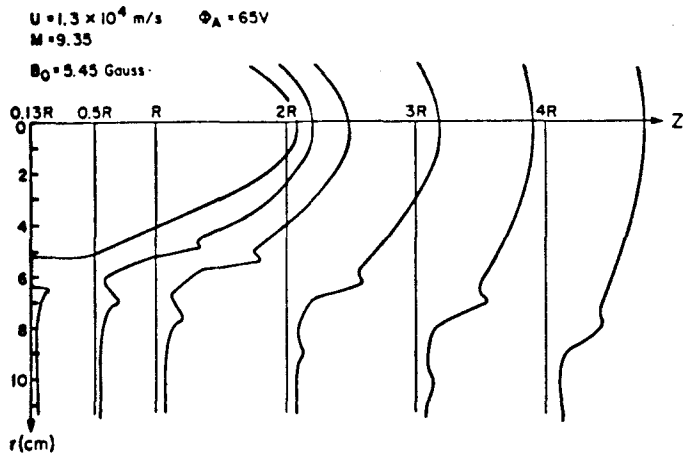
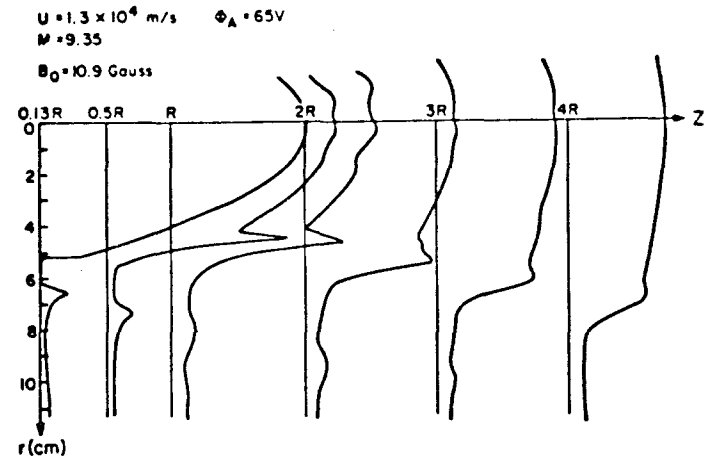
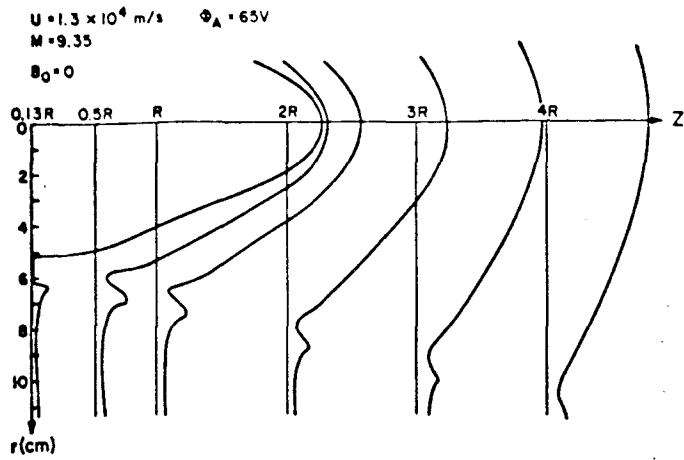


FIG. 3.16a "PINCH" EFFECT IN THE NEAR WAKE ($M = 9.35$)

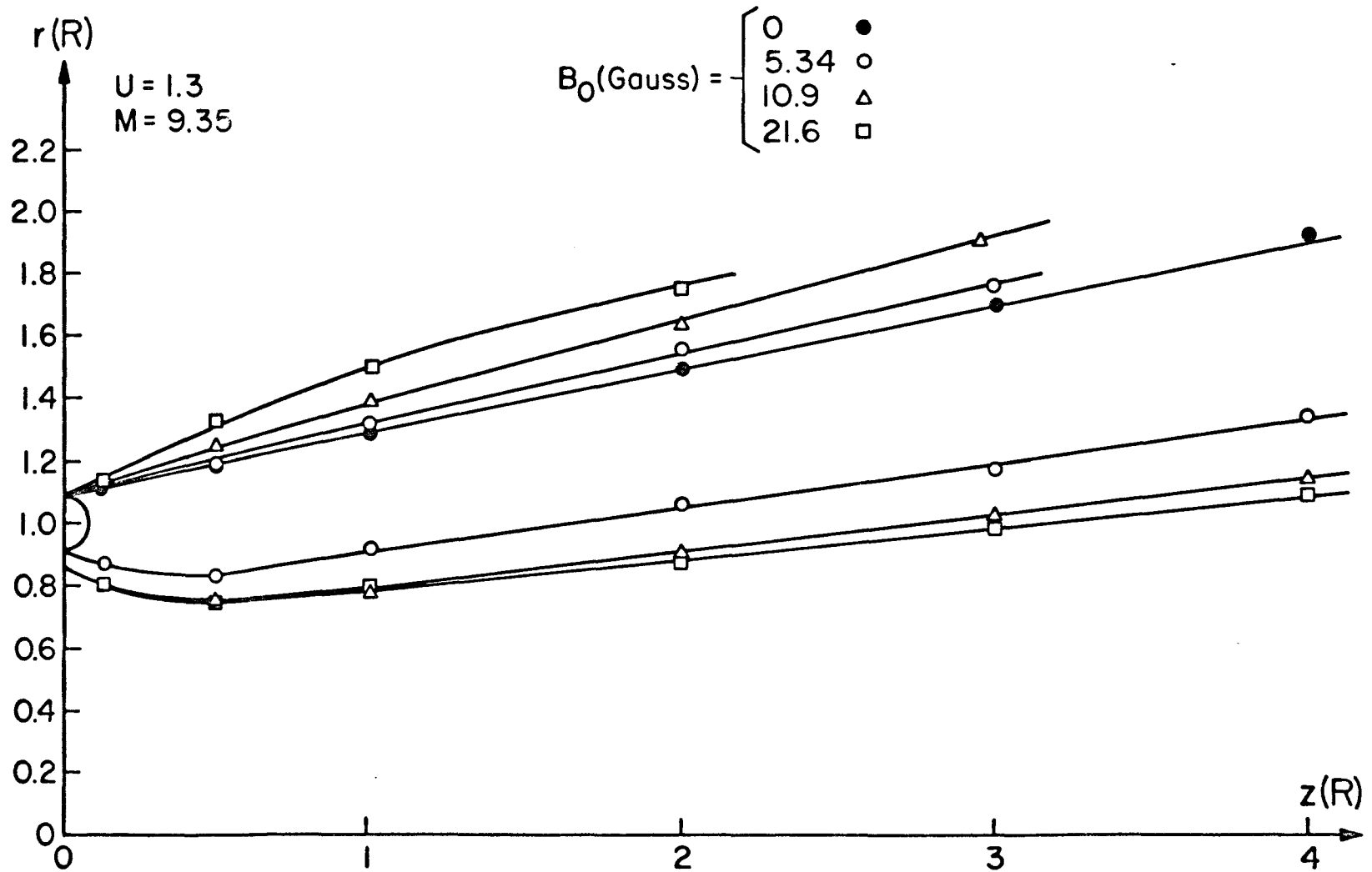


FIG. 3.16b POSITION OF THE ION DENSITY "PEAK" ($M = 9.35$)

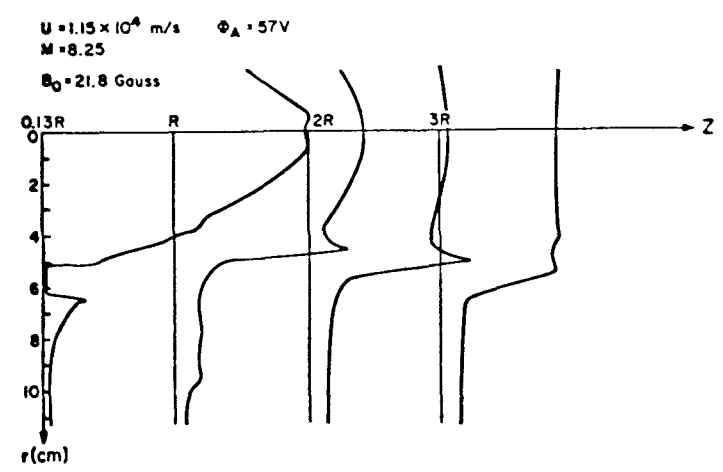
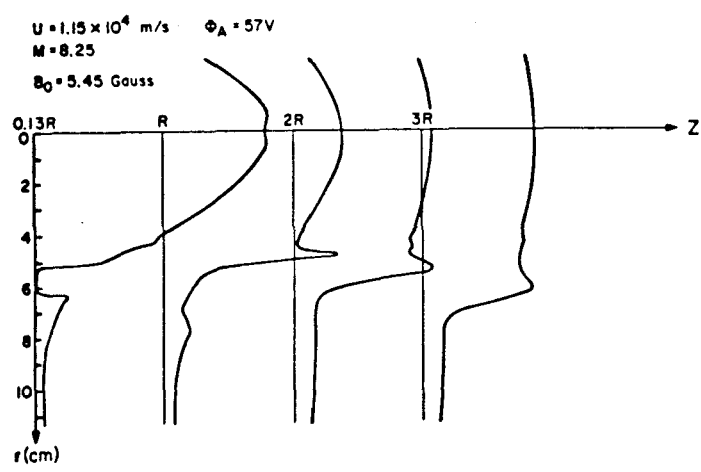
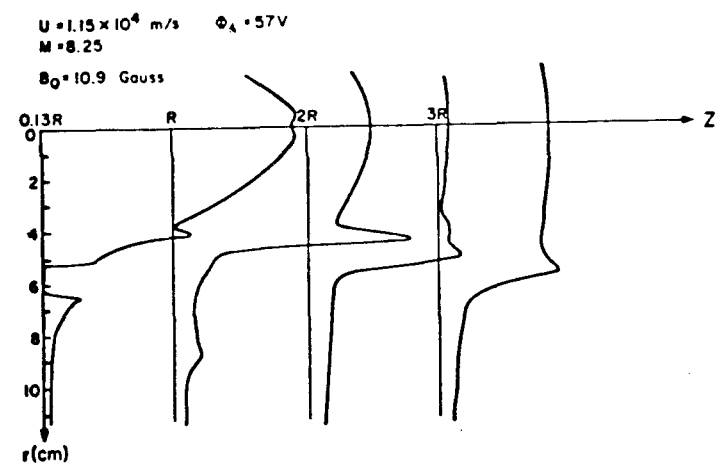
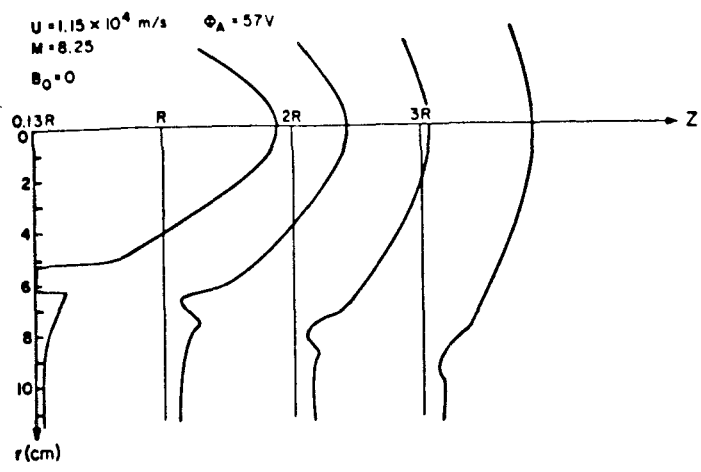


FIG. 3.17a "PINCH" EFFECT IN THE NEAR WAKE ($M = 8.25$)

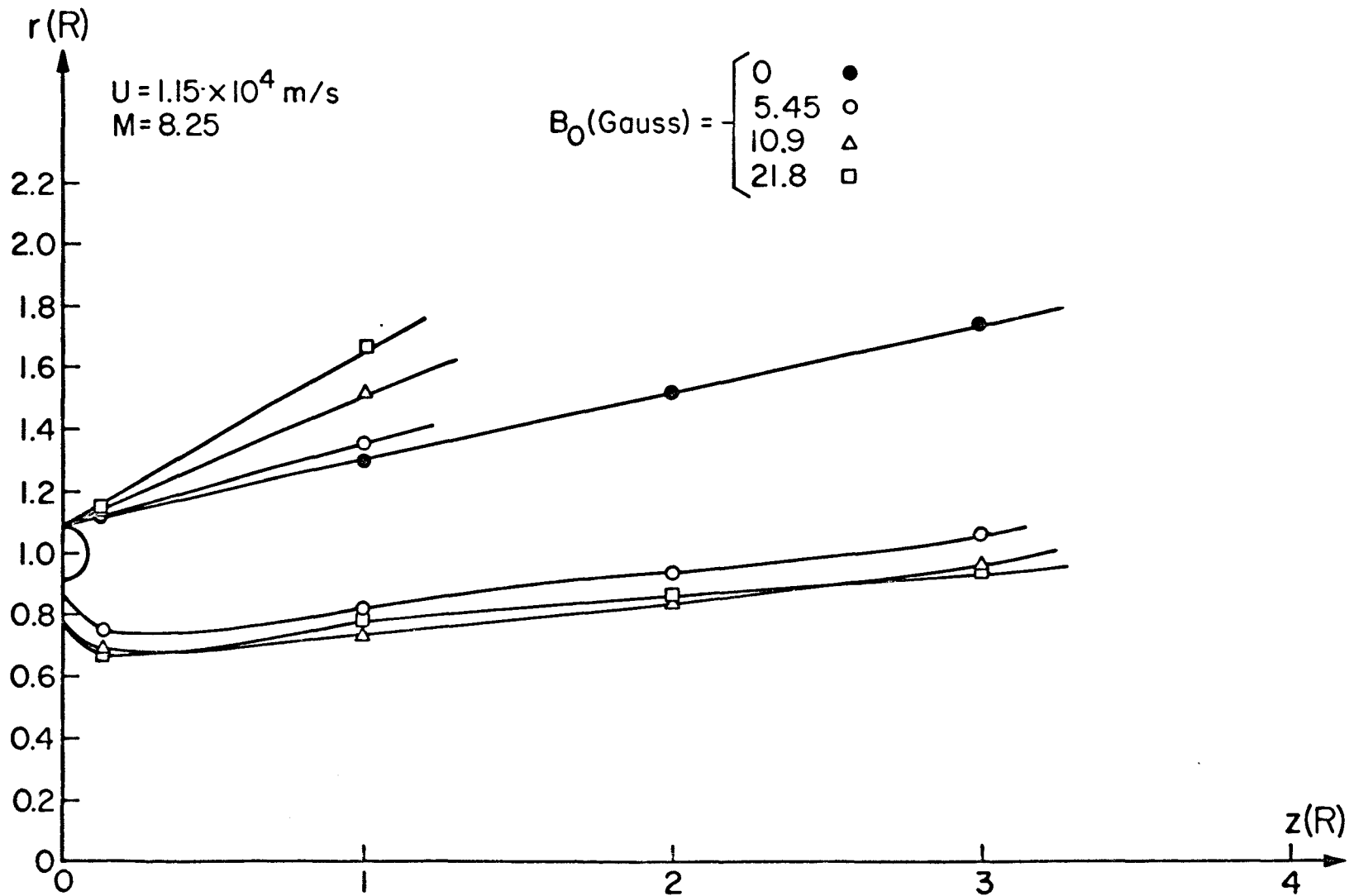


FIG. 3.17b POSITION OF THE ION DENSITY "PEAK" ($M = 8.25$)

Data III-3 $\Phi_A = 80V$ $\Phi_D = 60V$ $\Phi_{N.F.} = 24V$

Nozzle Aperture : 0.5 cm \emptyset

$B_0 = 10.9$ Gauss ————

$B_0 = 0$ - - - - -

Radial Profiles of Thin-Wire Probe

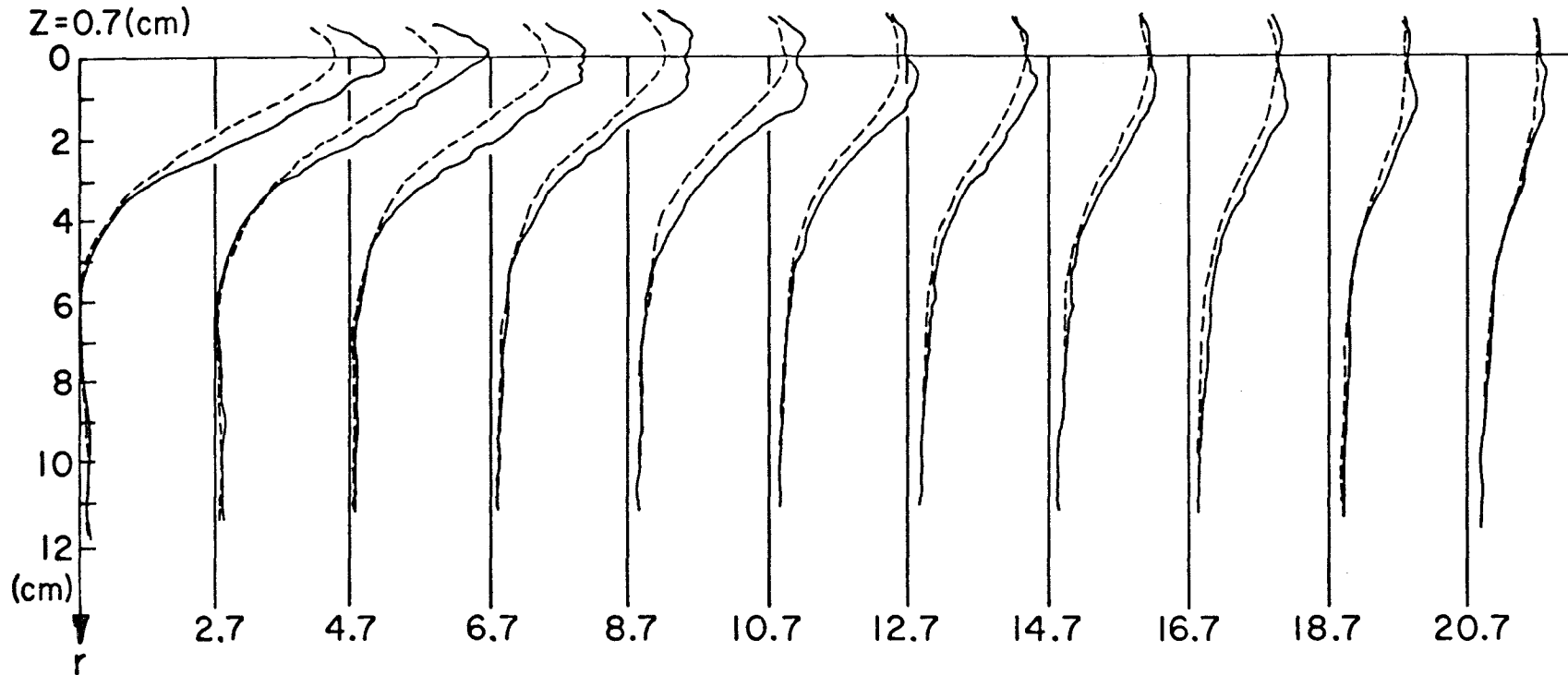


FIG. 3.18 WAKE OF A NARROW BEAM (NO BLOCKING)

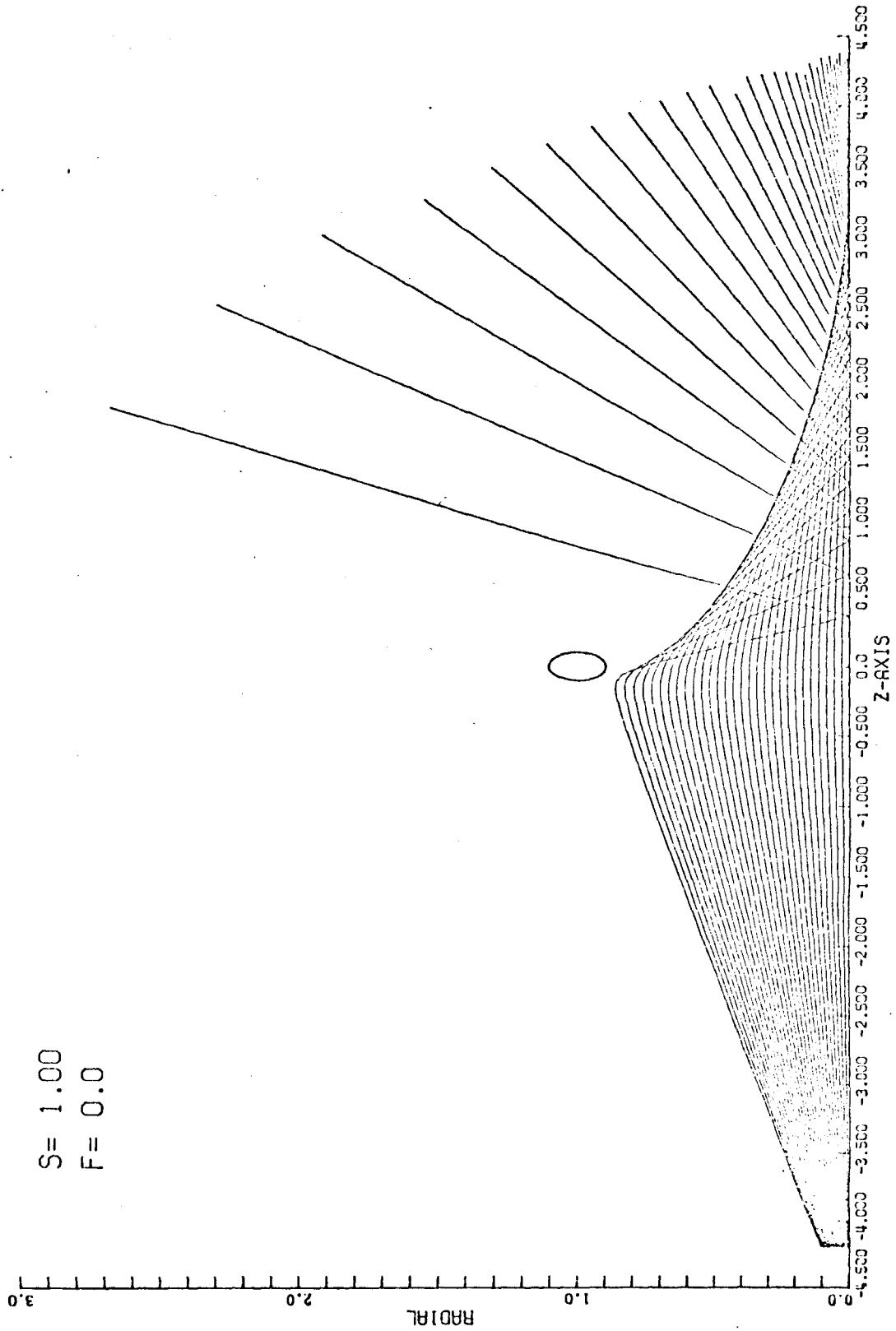
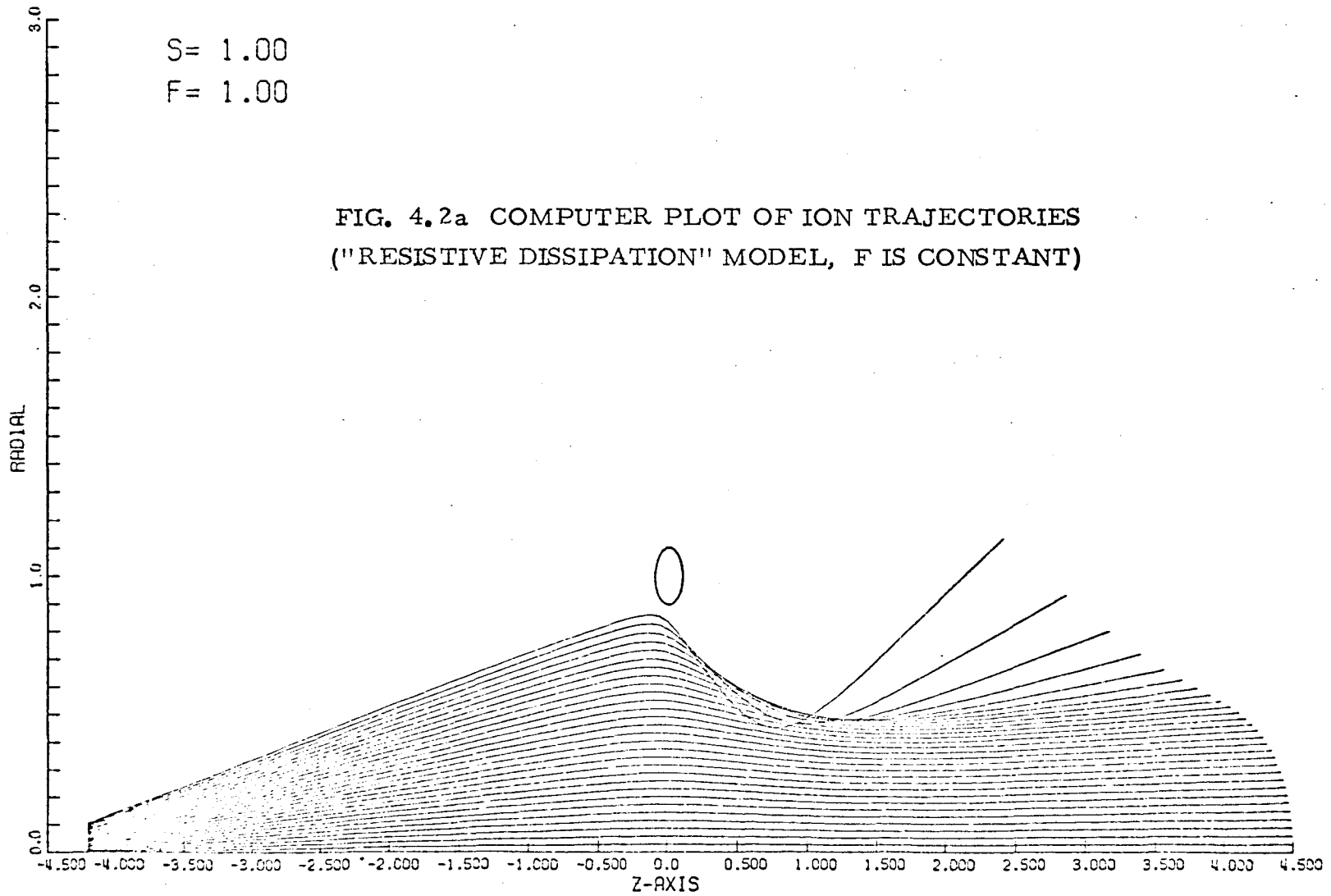


FIG. 4.1 COMPUTER PLOT OF ION TRAJECTORIES (COLLISIONLESS THEORY)

S = 1.00
F = 1.00

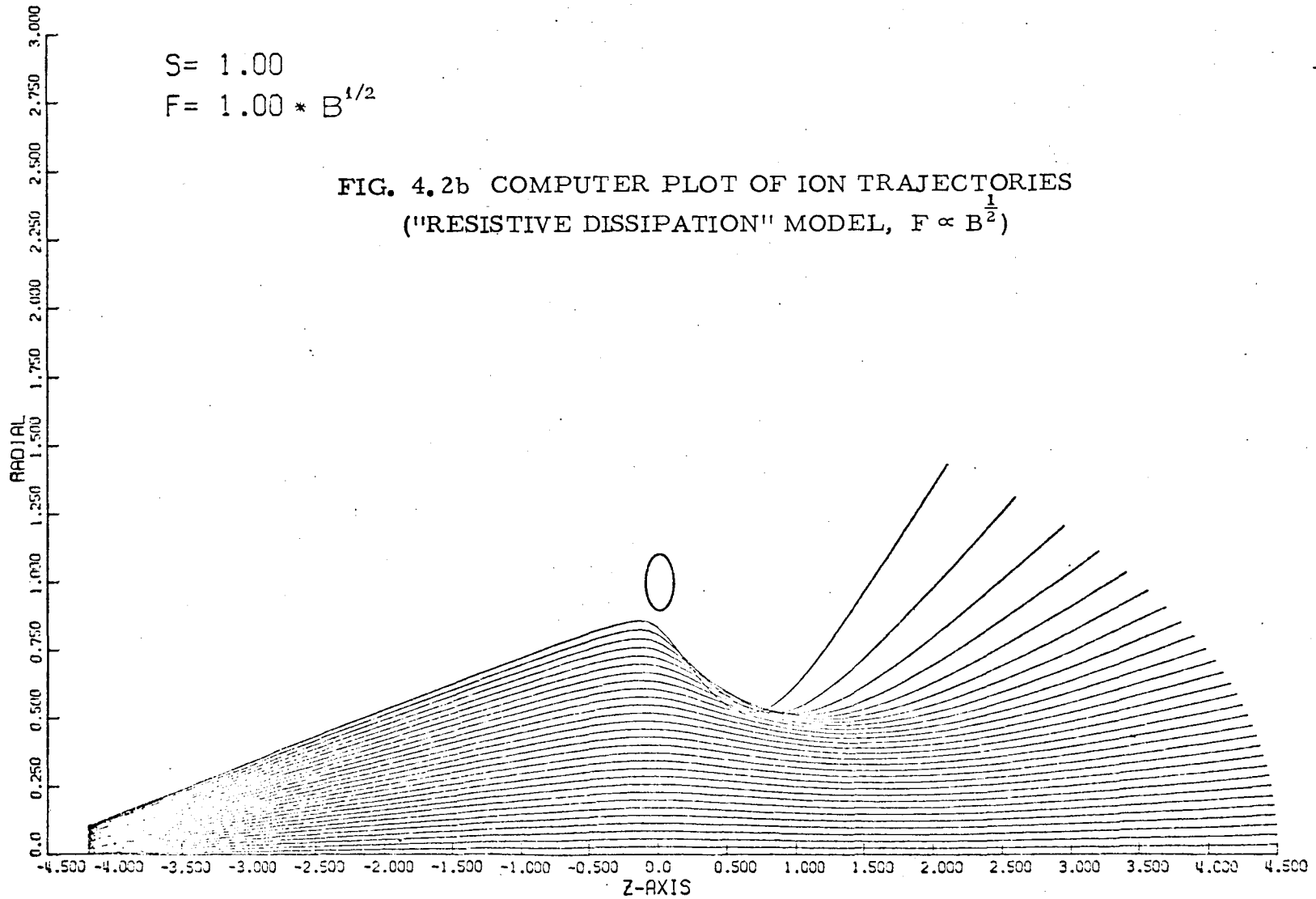
FIG. 4.2a COMPUTER PLOT OF ION TRAJECTORIES
("RESISTIVE DISSIPATION" MODEL, F IS CONSTANT)



$$S = 1.00$$

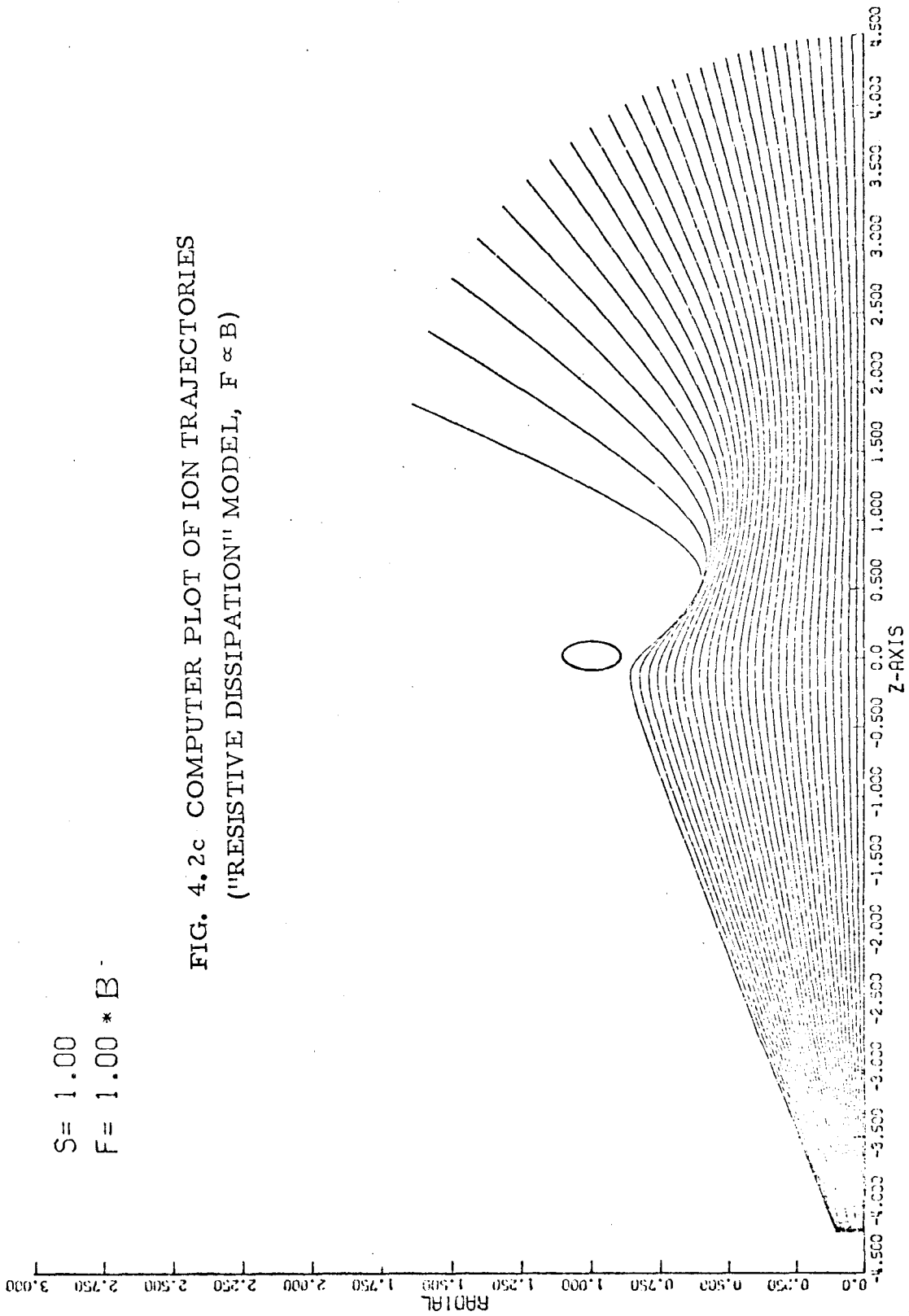
$$F = 1.00 * B^{1/2}$$

FIG. 4.2b COMPUTER PLOT OF ION TRAJECTORIES
("RESISTIVE DISSIPATION" MODEL, $F \propto B^{1/2}$)



S= 1.00
F= 1.00 * B

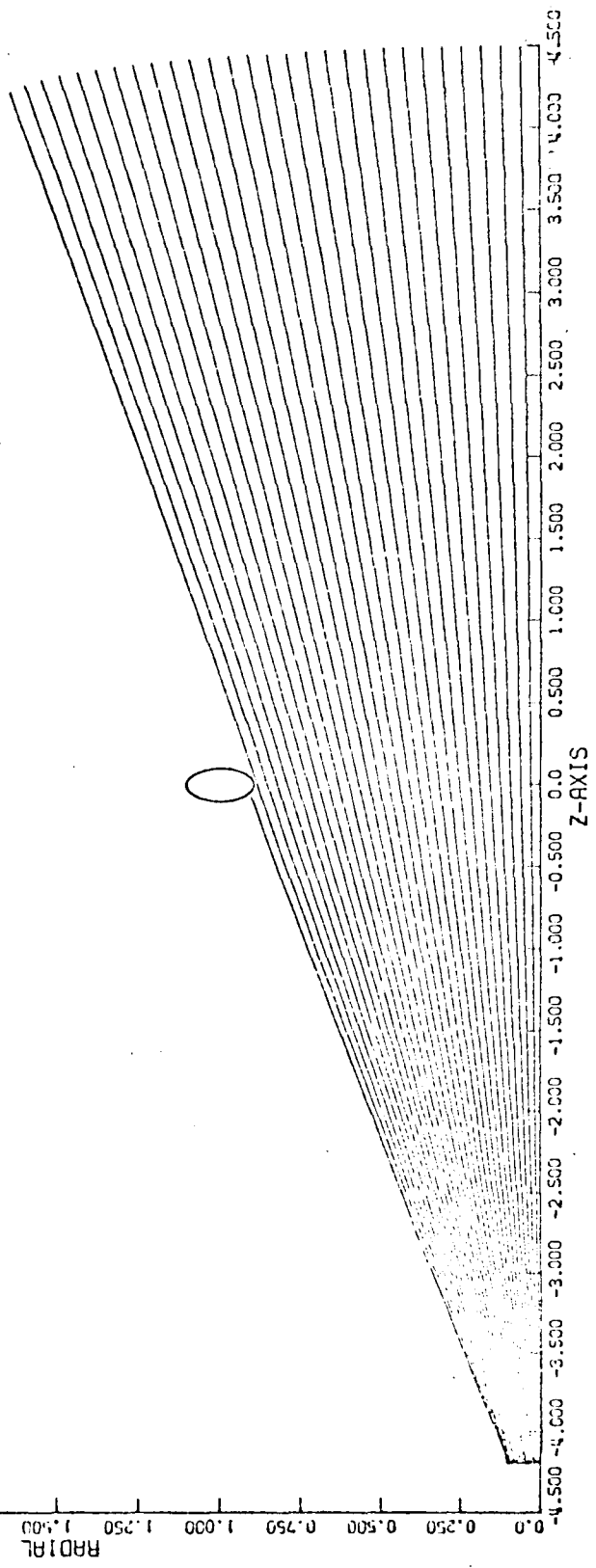
FIG. 4.2c COMPUTER PLOT OF ION TRAJECTORIES
("RESISTIVE DISSIPATION" MODEL, $F \propto B$)

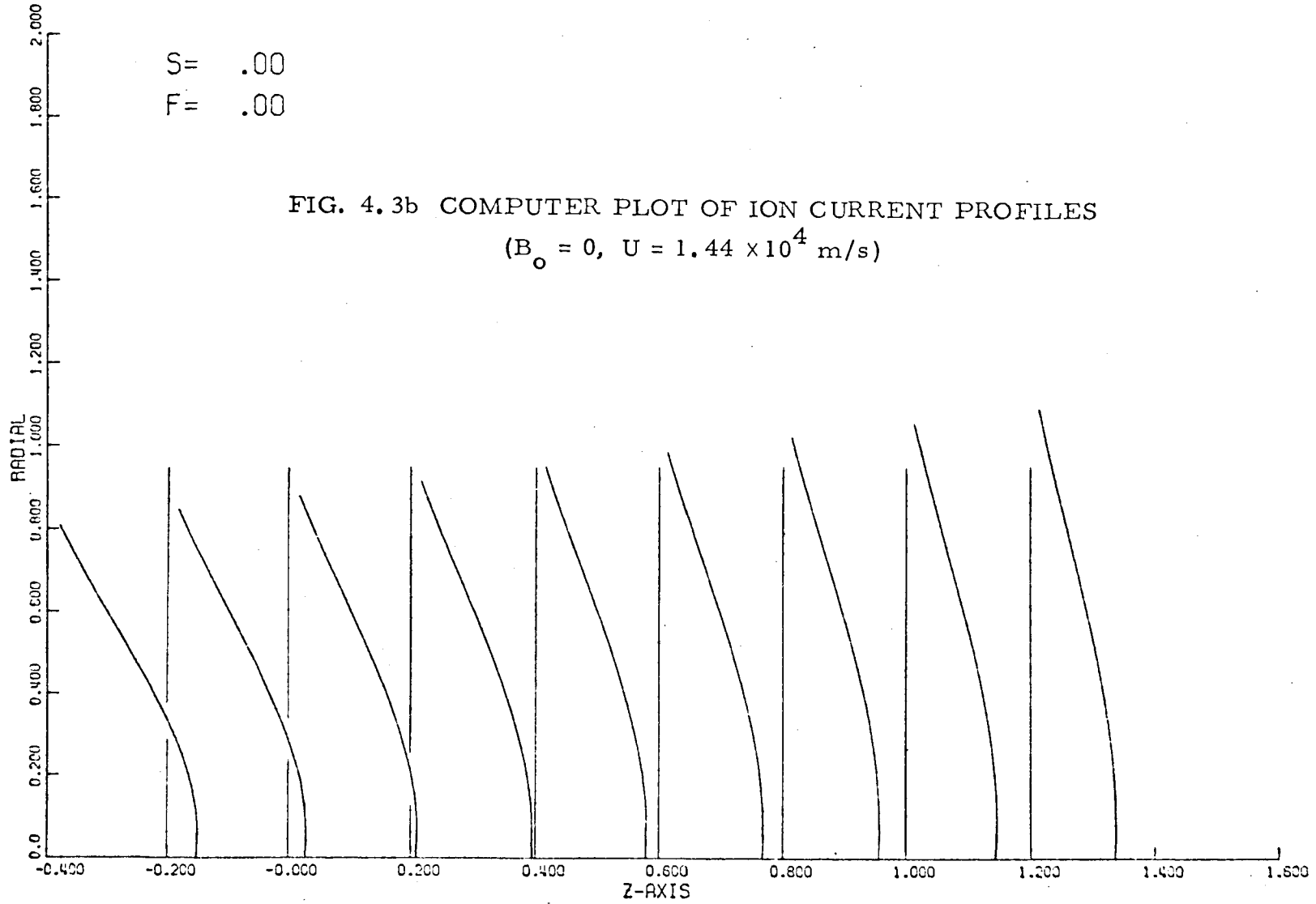


3.000
2.750
2.500
2.250
2.000
1.750
1.500
1.250
1.000
0.750
0.500
0.250
0.0

S= .00
F= .00

FIG. 4.3a COMPUTER PLOT OF ION TRAJECTORIES ($B_0 = 0$)

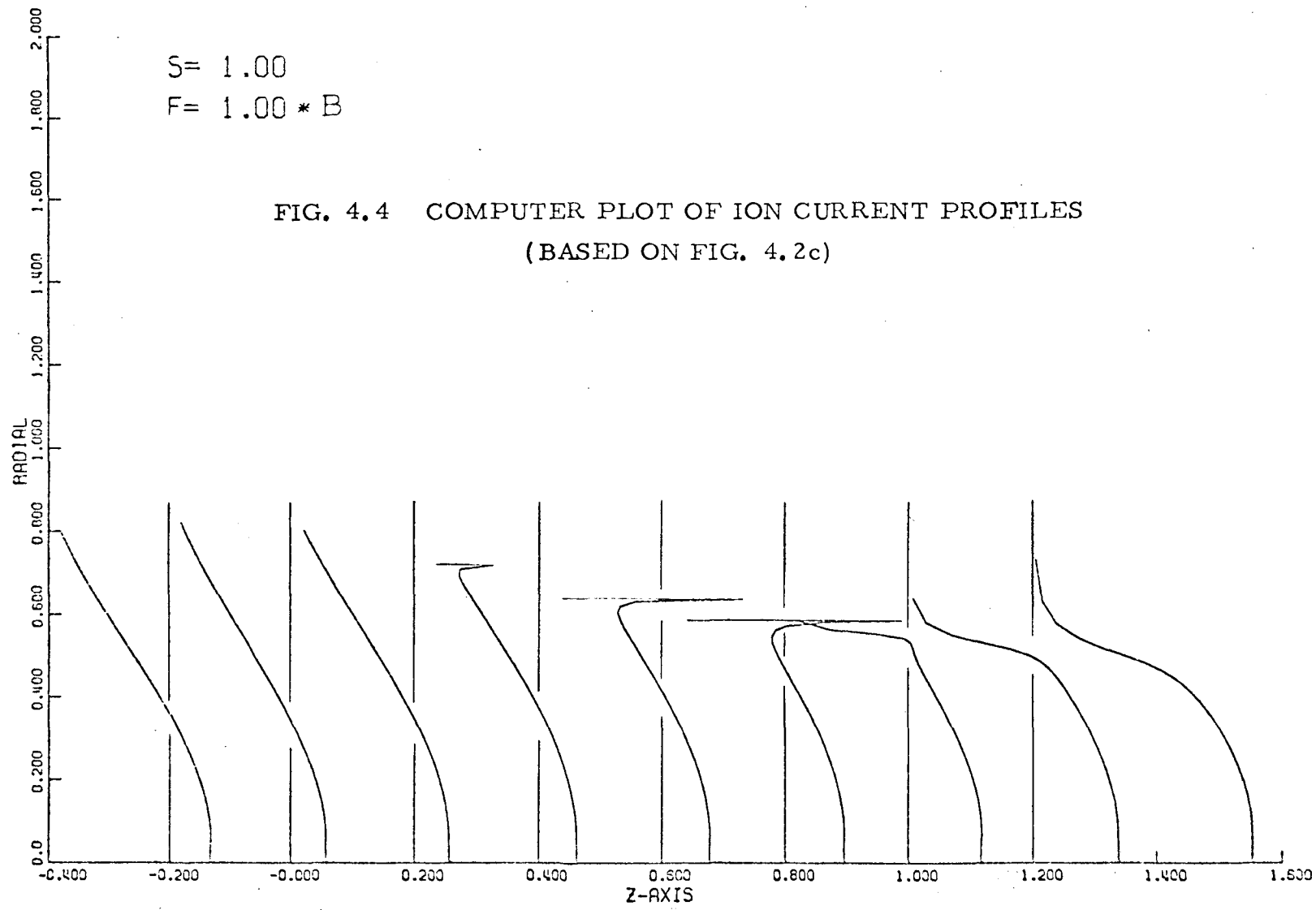




S= 1.00

F= 1.00 * B

FIG. 4.4 COMPUTER PLOT OF ION CURRENT PROFILES
(BASED ON FIG. 4.2c)



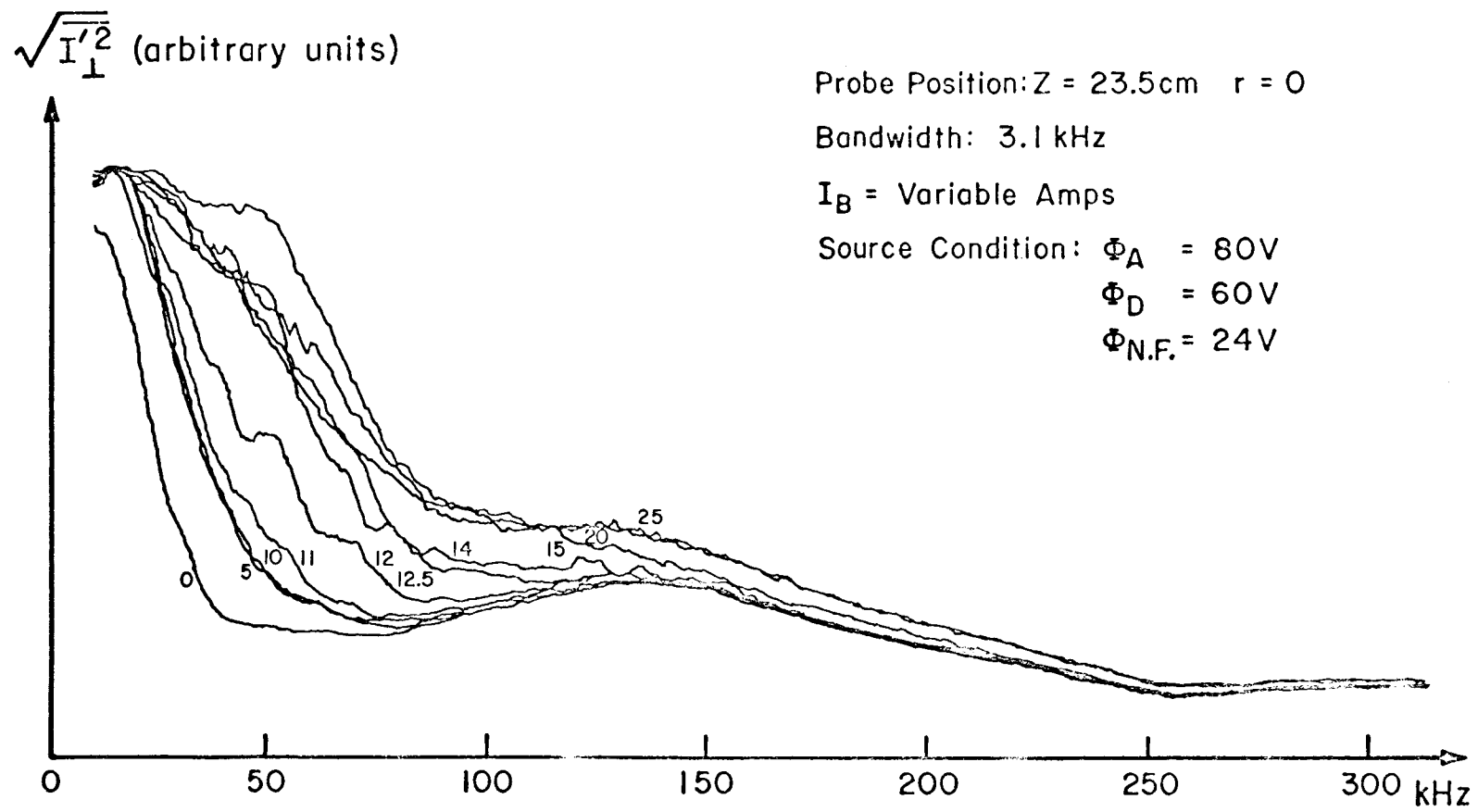


FIG. 4.5 SPECTRUM OF RMS FLUCTUATING PROBE CURRENTS
 (VARIABLE MAGNETIC FIELD)

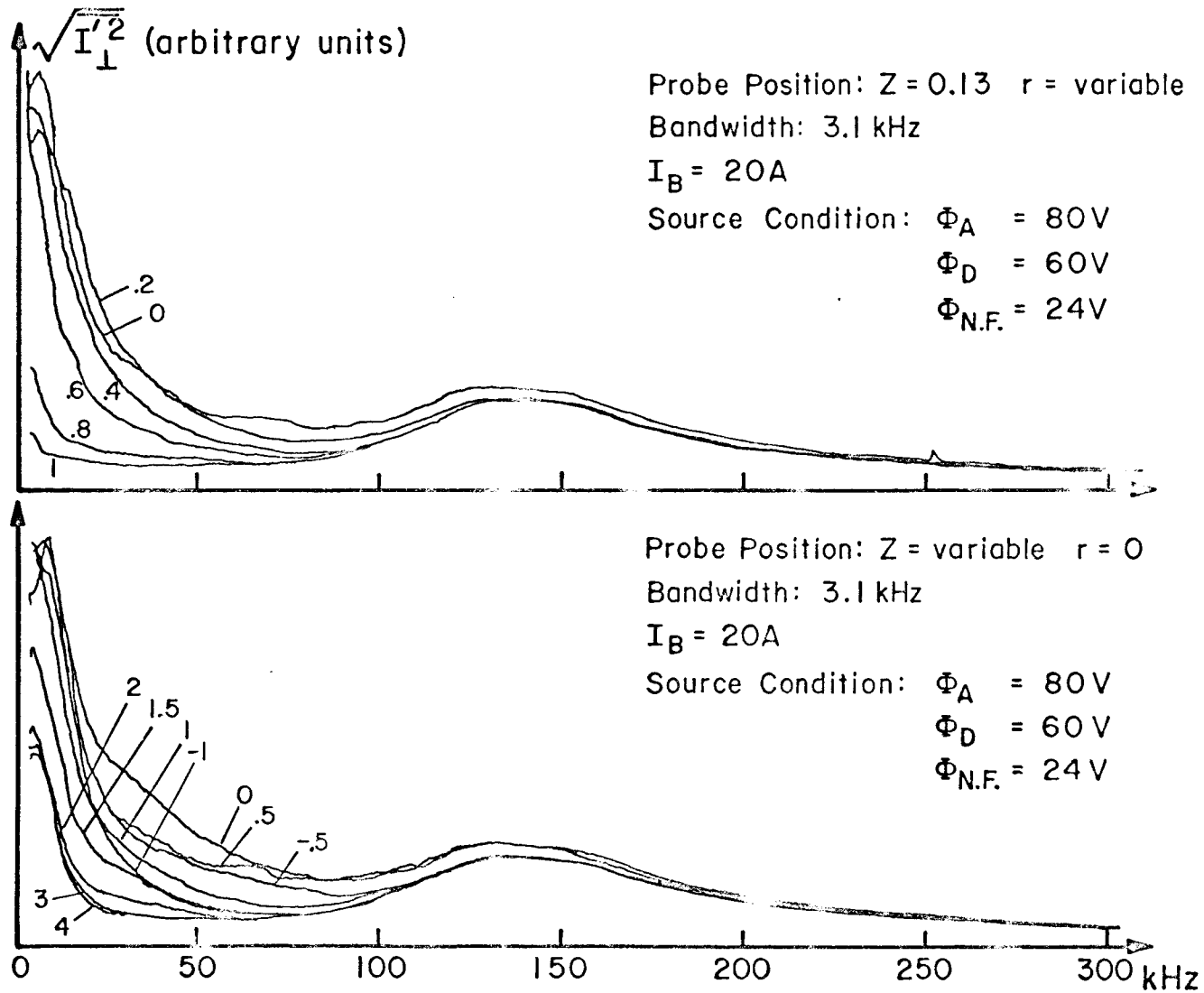


FIG. 4.6 SPECTRUM OF RMS FLUCTUATING PROBE CURRENTS

- a. VARIABLE RADIAL PROBE POSITION
- b. VARIABLE AXIAL PROBE POSITION